Characterizing Cortical Responses Evoked by Robotic Joint Manipulation after Stroke

Vlaar, Martijn

Important note
To cite this publication, please use the final published version (if applicable).
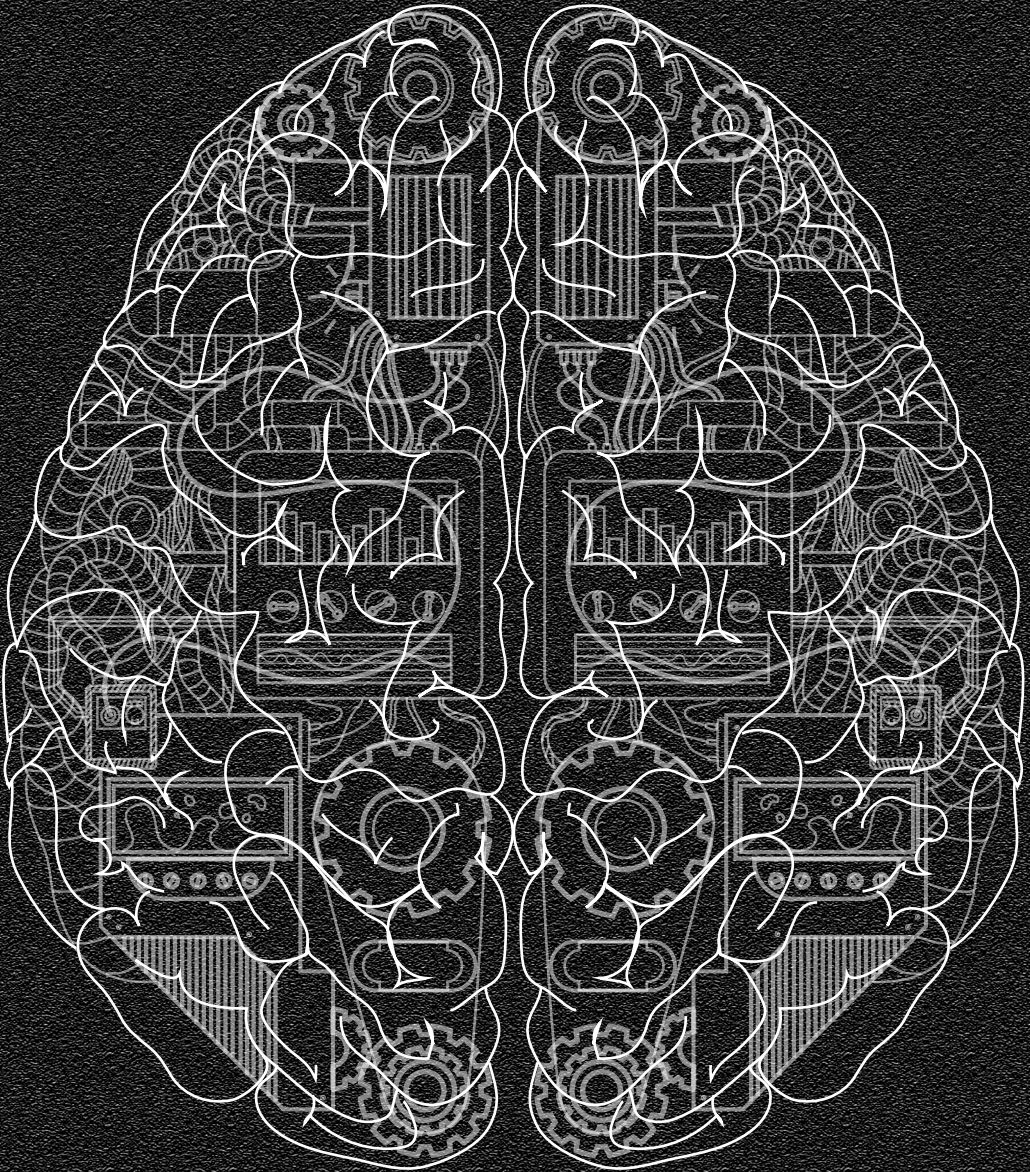Please check the document version above.

Characterizing Cortical Responses Evoked by Robotic Joint Manipulation after Stroke

Martijn P. Vlaar

Characterizing Cortical Responses Evoked by Robotic Joint Manipulation after Stroke

Martijn P. Vlaar

Characterizing Cortical Responses Evoked by Robotic Joint Manipulation after Stroke

Proefschrift

ter verkrijging van de graad van doctor
aan de Technische Universiteit Delft,
op gezag van de Rector Magnificus prof. ir. K.C.A.M. Luyben;
voorzitter van het College voor Promoties,
in het openbaar te verdedigen op
donderdag, 28 september, 2017
om 10:00 uur

door

Martijn Pieter VLAAR
Master of Science in Biomedical Engineering
geboren te Rheden

Dit proefschrift is goedgekeurd door de promotor:

Prof. dr. F.C.T. van der Helm

Copromotor:

Dr. ir. A.C. Schouten

Samenstelling promotiecommissie:

Rector Magnificus	voorzitter
Prof. dr. F.C.T. van der Helm	Technische Universiteit Delft, promotor
Dr. ir. A.C. Schouten	Technische Universiteit Delft, copromotor
Prof. dr. G. Kwakkel	Vrije Universiteit Amsterdam

Onafhankelijke leden:

Prof. dr. D.P. Ferris	University of Florida
Prof. dr. G.M. Ribbers	Erasmus MC Rotterdam
Prof. dr. ir. R. Pintelon	Vrije Universiteit Brussel
Prof. dr. ir. M. Mulder	Technische Universiteit Delft
Prof. dr. H.E.J. Veeger	Technische Universiteit Delft, reservelid

Table of Contents

Chapter 1

Introduction

Cortical damage after a stroke often affects movement control, resulting in impairments such as paresis and synergies. Although some recover, most stroke survivors are left with reduced function of the upper limb, which has a severe impact on their activities of daily living. People who have suffered a stroke demonstrate heterogeneous impairments due to large variability in lesion location and extent; thus, rehabilitation should be tailored to each individual. Design and evaluation of rehabilitation programs requires a thorough understanding of the healthy and the impaired sensorimotor system. Impairments to the motor system have been extensively investigated. On the contrary, the sensory aspects of impaired motor control have received less attention. This thesis intends to characterize the relation between sensory information from the periphery and the corresponding cortical responses using quantitative measurement techniques. The introductory chapter provides the reader with the required background on the topic of movement control, electroencephalographic recordings and stroke, before presenting the problem and aim of the thesis.

1.1 Movement control

Humans plan and execute complex movements, and have the ability to correct for disturbances while doing so. This feedforward (i.e. voluntary motor drive) and feedback control (i.e. reflexes) is facilitated by the central nervous system (controller), in conjunction with muscles (actuators) and mechanoreceptors (sensors). Together, these components form a closed loop control system: the sensorimotor system (see **Figure 1.1**).

The sensorimotor system

To enable feedback control and the optimization of internal models for feedforward control, sensors are essential. The human body is equipped with many types of sensory systems, such as the vision system, auditory system, vestibular system and somatosensory system (Kandel et al., 2000). This thesis focuses on the somatosensory system, and specifically on the mechanoreceptors. Mechanoreceptors, comprising proprioceptive and tactile sensors, facilitate feedback control of limbs due to their ability to communicate quickly with the central nervous system. There are several types of afferent fibers, which can be classified according to the type of mechanoreceptors they connect to, and to their conduction speed. Ordered from high to low conduction speed, the fibers are defined as Aα, Aβ, Aδ, and C fibers, where the conduction speed is directly related to their cross-sectional area and amount of myelination.

The proprioceptive system consists of muscle spindles, Golgi tendon organs, joint capsules, and stretch sensitive free endings. Muscle spindles are located within the muscle, parallel to the extrafusal muscle fibers. Thus, when the muscle is stretched, the muscle spindles are concurrently stretched, sensing both muscle length and rate of change in muscle length. Length information is transmitted through II-afferent (i.e. Aβ) fibers. Ia-afferent (i.e. Aα) fibers transmit either length or change in muscle length information. Nonlinear velocity dependence in the response of the muscle spindle has been experimentally observed (Houk et al., 1981), and has also been incorporated into a mathematical model of the muscle spindle (Mileusnic et al., 2006). The sensitivity of the muscle spindles can be altered through the activation of gamma motor neurons. Golgi tendon organs sense muscle tension and are connected to the CNS via Ib-afferent (i.e. Aα) fibers. There is a linear relation between firing rate and muscle force (Crago et al., 1982). Muscle force is mainly sensed during active

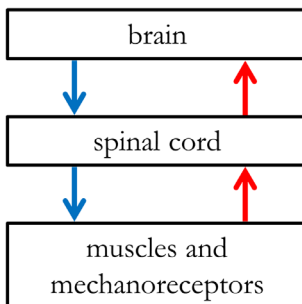**Figure 1.1.** Scheme of the elements of movement control. The brain and spinal cord constitute the central nervous system, which controls the muscles in the periphery through voluntary or reflexive activation. This efferent information is indicated by the blue arrows. Sensory (or afferent) information is passed from the mechanoreceptors to the spinal cord and subsequently to the brain, as indicated by the red arrows.

contraction of the muscle, and less during passive stretch. Joint capsule mechanoreceptors provide information on joint angle via II-afferent (i.e. Aβ) fibers. Stretch-sensitive free endings register excess stretch and muscle force and transmit through the slower III-afferent (i.e. Aδ) fibers.

The tactile system encompasses many types of sensors in the skin, including Meissner's corpuscles, Merkel disk receptors, Pacinian corpuscles and Ruffini endings. These sensors vary in the size of their receptive field, their bandwidth, and their sensitivity to transient or sustained stimulation. Tactile sensors enable the sensing of (for example) pressure, texture, vibration, and skin stretch; these sensors are connected to the CNS through Aβ afferent fibers. Additionally, there are sensors in the skin for registration of pain and temperature which connect to the CNS through the slower Aδ and C afferent fibers.

The actuators of the sensorimotor system are the muscles, which consist of muscle fibers grouped into motor units. These motor units are activated by alpha motor neurons in the spinal cord; alpha motor neurons can be excited or inhibited both by spinal reflexes and by supraspinal input. When a motor unit is innervated, the potential travelling across the unit can be noninvasively recorded from the skin using electromyography (EMG).

The sensory neurons from the mechanoreceptors are connected to the spinal cord. From there, the proprioceptive and tactile sensory information reaches the brain. Information first arrives in the thalamus, and is subsequently conveyed to the primary somatosensory cortex; this cortex has a somatotopic organization (see **Figure 1.2**), in which body parts for fine motor control have a large representation. From the primary somatosensory cortex, sensory information is distributed to the posterior parietal cortex and the secondary somatosensory cortex, where the information is further processed and integrated. The motor cortex, consisting of the primary motor cortex, premotor cortex and supplementary motor area, is responsible for the planning and execution of motor commands. The primary motor cortex has a somatotopic organization similar to that of the primary somatosensory cortex. Motor commands are sent down to the alpha motor neurons in the spinal cord through the corticospinal tract. Although there are other tracts through which muscles can be activated, these do not allow for such fine motor control as does the high-resolution corticospinal tract. The ascending sensory tracts and most fibers of the descending corticospinal tract cross sides in the medulla (i.e. undergo sensory and motor decussation), and as a consequence the right hemisphere controls the left side of the body and vice versa.

Impaired movement control: stroke

The malfunctioning of one of the components of the sensorimotor system can lead to functional impairments. Impaired movement control can, for example, be caused by movement disorders such as essential tremor and Parkinson's disease, or by damage to the central nervous system due to a stroke.

Chapter 1

Stroke is a major cause of acquired disability in developed countries (Mendis, 2013), with an incidence of around 1.5 million per year in Europe (Wilkins et al., 2017). Due to the aging population, this number is expected to increase over the coming years (Truelsen et al., 2006). Upper limb paresis after stroke has significant consequences for autonomy during activities of daily living (ADL) (Veerbeek et al., 2011) and occurs in about 80% of stroke survivors. Only around one third of those people will regain some dexterity (Kwakkel et al., 2003).

Stroke occurs when the blood supply to the brain is disturbed, leading to the death of brain cells. There are two main types of stroke, namely ischemic and hemorrhagic. An ischemic stroke occurs when a blockage in a blood vessel interrupts the blood supply to a brain region. A hemorrhagic stroke occurs when there is bleeding inside the brain or in the space surrounding the brain, causing, besides a lack of blood supply, swelling and pressure. Hemorrhagic strokes are less common, as 87% of strokes are classified as ischemic (Benjamin et al., 2017).

Even though all strokes result in damage to the brain, the consequences of this damage vary greatly among individuals due to differences in affected brain region and tracts. Therefore, the population of individuals who suffer a stroke is very heterogeneous with respect to initial impairments and functional outcomes after recovery. In addition to impairments that affect cognition (e.g. aphasia, problems with attention and neglect) and emotions, motor impairments are very common. Motor impairments after stroke have a huge impact on an individual's independence during activities of daily living (ADL), and thus on their quality of
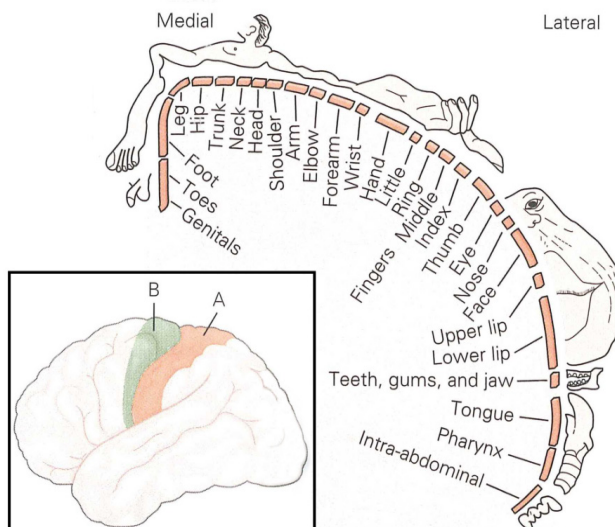

Figure 1.2. Sensory homunculus. Figure depicts the primary somatosensory cortex of one hemisphere. Size of the body parts shown on the cortex indicates the relative size of cortical representation for that body part. Insert shows the location of the primary somatosensory cortex (A) and the primary motor cortex (B). Adapted from Kandel et al. (2000).

life. There are many different types of motor impairment associated with stroke, such as (hemi)paresis, spasticity and synergisms (Krakauer, 2005).

Studying movement control of the upper limb

Humans can generate movements and forces in many ways due to the redundancy of the musculoskeletal system (Franklin and Wolpert, 2011), which challenges the consistent and unambiguous study of movement control. This redundancy can be mitigated by presenting a person with a functionally-relevant upper limb control task and by constraining the limb under study, as with a robotic manipulator; robotic manipulators ensure well-conditioned experiments and they provide a quantitative way of assessing movement control.

The sensorimotor system consists of multiple control loops, in which the controller performance is largely dependent on the inherent time delays in the system. Due to its closed loop nature, discerning cause and effect in the sensorimotor system requires an external stimulus (van der Kooij et al., 2005). System identification techniques can be employed to model the dynamics between the different components of the sensorimotor system. This modeling can be nonparametric or parametric, where the former has the advantage of requiring little a priori knowledge about the system and the latter has the advantage of requiring a limited set of parameters to describe the system.

Two main strategies can be employed to perform movement control tasks, namely voluntary muscle (co-)contraction (feedforward) and reflexes (sensory feedback). The latter is crucial for disturbance rejection during movement control, which can be internal (e.g. variability in muscle output force [Faisal et al., 2008]) or external (e.g. the train movements when standing in a train). The intrinsic properties of a limb (i.e. viscoelasticity and inertia of tissues), together with the reflexive activity, govern the dynamic relation between joint angle and joint torque, which is defined as mechanical impedance. Unimpaired individuals can adapt their mechanical impedance to the task at hand by modulating voluntary muscle contraction and reflexes (Mugge et al., 2010), while impaired individuals might not adapt properly (Meskers et al., 2009, Mugge et al., 2016). Unambiguous task instruction (e.g. "maintain position" or "maintain force") and extensive training prevent adaptation of sensory feedback during an experiment.

During the execution of an upper limb control task, several mechanical and physiological signals can be noninvasively recorded, all of which provide information on task execution. These signals include the position of and the force on the joint, the activity of the muscles controlling the joint, and the activity in the brain. There are several methods that allow for the noninvasive recording of cortical signals, such as electromagnetic measurements (e.g. electroencephalography [EEG] or magnetoencephalography [MEG]) and measurements related to metabolism (e.g. functional magnetic resonance imaging [fMRI], positron emission tomography [fMRI] or functional near-infrared spectroscopy [fNIRS]). Electromagnetic measurements provide a direct measure of brain activity by recording electromagnetic signals generated by neuronal populations with high temporal resolution (< 1 ms). These signals can

only be recorded if many aligned neurons fire synchronously, and they are most detectable in the superficial cortical areas. Metabolic measurement techniques such as fMRI and PET, can detect activity in deeper regions of the brain; however, they measure an indirect effect of brain activity, i.e. energy consumption. Therefore, the temporal resolution with which changes in brain activity can be detected is slow, i.e. on the order of seconds. EEG is highly suitable for studying movement control due to its high temporal resolution and its mild experimental restrictions with regard to movement and presence of a robotic manipulator.

Due to volume conduction effects in EEG (see **Figure 1.3**), the signals generated in the brain are spread to all recording electrodes on the scalp. The cortical areas responsible for generating the activity observed at the scalp have to be identified through a procedure called source localization. Due to the high sensitivity of EEG to artifacts coming from muscle activity, eye movements and line noise, as well as to the ongoing cortical activity that is not necessarily related to the response of interest, the signal-to-noise ratio in EEG is poor. Consequently, a proper estimate of the evoked response is only obtained after applying many (typically >100) stimuli and averaging the recorded responses.

1.2 Stroke recovery

Recovery after stroke can be classified as restitution, substitution or compensation. Recovery is most likely to occur within six months after the stroke (defined here as the sub-acute phase) (Cramer, 2008, Langhorne et al., 2011), after which the chronic phase is reached. Restitution entails the regain of function of damaged brain areas. Substitution comprises the use of anatomically different brain areas or pathways to achieve pre-stroke function. Compensation strategies involve the use of other joints or muscles to perform movements that can no longer be performed using regular strategies due to the stroke. Compensation can restore independence during ADL; however, it may further reduce the capabilities of the affected joints due to non-use (Krakauer, 2006). Although the types of recovery that can occur are known, the mechanisms that drive this recovery are presently not well understood (Buma et al., 2013). As a result, rehabilitation programs are currently not achieving maximal
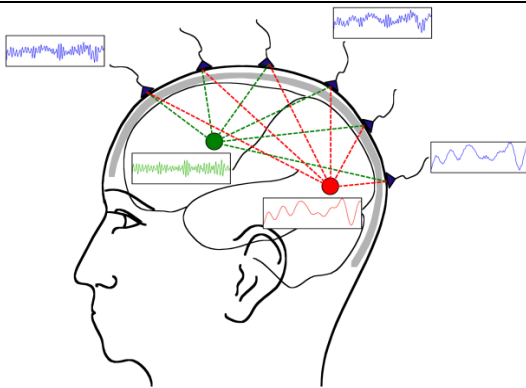

Figure 1.3. Volume conduction in EEG. Green and red dot represent a source inside the brain, of which the signal is picked up at all electrodes on the scalp. The signals recorded at the scalp electrodes are therefore a mix of all signals generated in the brain, as well as sources of artifacts such as muscle activations and eye blinks. Figure by R. Oostenveld, reprinted with permission.

outcome.

Impairments of motor function after stroke have been extensively studied, and their course during recovery in relation has been studied in relation to cortical activity (Kim and Winstein, 2017). The study of impaired sensory function, along with its relation to motor recovery, has received less attention. Control of movement is facilitated by both feedforward control and feedback control, which require sensory information to form proper internal models and correct for internal and external disturbances. Therefore, it is important to design appropriate experimental methodologies that specifically allow to study the sensory system.

1.3 The 4D-EEG project

The 4D-EEG project is a collaboration among Delft University of Technology, VU University Medical Center, VU University, and Northwestern University, and is funded by the European Research Council (Advanced ERC grant, n. 291339). The 4D-EEG project studies the cortical involvement in motor control in unimpaired individuals and in individuals who suffered a stroke. The application of system identification techniques on the sensorimotor system generates quantitative descriptions of the dynamic relations between the different components of the sensorimotor system. Such descriptions are particularly interesting when obtained from a sensorimotor system which is engaged in a meaningful control task. Different research activities within the project include the development of: system identification techniques on signals recorded from the brain, source localization techniques, and diffusion tensor imaging (DTI). Combining the results from these different lines of research increases our understanding of the sensorimotor system; for individuals who suffered a stroke, the obtained understanding may aid setting therapeutic goals and select particular rehabilitation programs (Stinear, 2010), with improving functional outcome as the final objective.

1.4 Research approach

This thesis studies the cortical involvement in sensorimotor control by examining the responses to robotic proprioceptive stimulation of the wrist as recorded using EEG (a typical experimental setup is shown in **Figure 1.4**). The wrist stimulation serves two purposes. Firstly, it challenges individuals to control their wrist, thus engaging the sensorimotor system in control. Secondly, this stimulation generates responses in the sensorimotor system, which can be recorded using noninvasive measurement techniques. The responses from the muscles can be recorded using EMG, whereas the cortical responses can be recorded using EEG. The cortical responses have two particularly interesting aspects: the location (i.e. which brain region is involved in processing the sensory signal) and the time course, which reveals information about the dynamic relation between the stimulus and the cortex. As excess muscle stretch and muscle force, pain, and changes in temperature are avoided, the evoked cortical responses are assumed to origin from mechanoreceptors which connect to CNS through Aα and Aβ afferent fibers. First exploring cortical involvement in movement control in unimpaired individuals, makes it possible to determine how this cortical involvement is

altered after stroke. Importantly, experimental paradigms for studying the restitution or substitution aspects of recovery after stroke should ensure that compensation strategies are reduced to a minimum (Buma et al., 2010), which is achieved by the use of the robotic manipulator.

Many nonlinearities are present in human movement (e.g. nonlinear behavior of sensors, nonlinear force-length and force-velocity relationships of muscles, and changing geometry of limbs leading to changes in lever arms). In a nonlinear system, the superposition principle does not hold, which means that the output is not proportional to the input; in other words scaling the amplitude of the input signal does not necessarily mean that the output signal scales the same amount. Many methods and techniques implicitly assume linearity. When repeatedly using the same somatosensory stimulus in combination with linear analysis techniques, as is often done when studying cortical evoked responses, possible nonlinear behavior is easily overlooked and might be assumed absent. Herein lies the danger of neglecting nonlinear behavior: the obtained model (i.e. description of the relation between sensory stimulus and cortical response) will only be valid for that specific stimulus, and can therefore only be descriptive. Previous studies have revealed that the relation between sensory stimulus and recorded cortical response is nonlinear to some extent (e.g. Snyder, 1992, Tobimatsu et al., 1999, Jamali and Ross, 2013). Therefore, the applicability of linear analysis techniques in the study of somatosensory evoked cortical responses needs to be investigated.

Perturbing the sensorimotor system using an intermittently applied brief stimulus reveals the response to an abrupt change in the system, whereas the use of continuous stimulation allows to study the sensorimotor while it is constantly and consistently engaged in performing a control task; the initial transient response can be omitted from the analysis and the steady
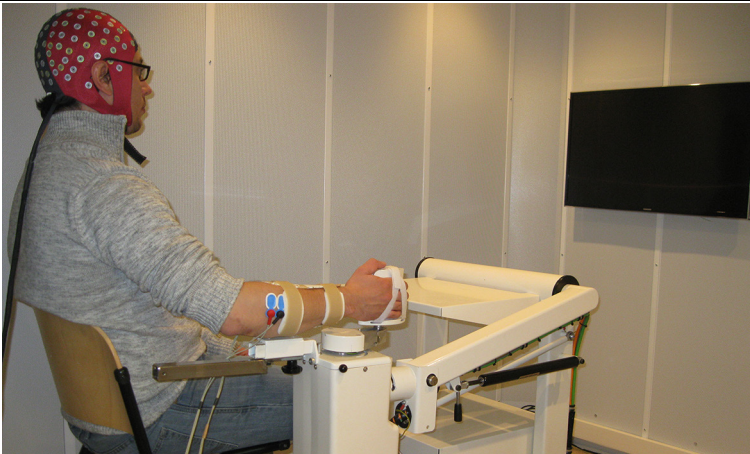

Figure 1.4. Experimental setup. The right forearm of the participant is strapped into an armrest and the right hand is strapped to the handle, requiring no hand force to hold the handle. Both angle of and torque at the axis of the motor are recorded.

state behavior of the system can be studied. Many types of continuous stimulation signals have been used in the study of movement control, including white (or colored) noise, pseudo-random binary sequences (Kearney et al., 1997) and multisine signals (Schouten et al., 2008a, Meskers et al., 2009, Mugge et al., 2010). Multisine signals are generated by summing multiple sinusoids; they have a fully customizable frequency content, allowing for increased signal-to-noise ratio (SNR) per frequency, leakage-free analysis and the ability to detect and quantify nonlinear distortions (Pintelon and Schoukens, 2012). These advantages make the multisine signal a good candidate for use in the investigation of a noisy and potentially nonlinear system, as it allows to quantify and characterize both noise and nonlinear behavior.

1.5 Problem statement

Most recovery after stroke occurs within the first six months and varies widely: some people regain full function, while others are left with severe disabilities. Increased insight in neurological recovery patterns after stroke will enable the development of more effective and patient-tailored rehabilitation programs, and of methods to test the effectiveness of these programs. Comprehension of neurological recovery can be enhanced by studying cortical involvement in sensorimotor control, with a focus on the processing of sensory information; the problem is that this requires carefully designed experiments and analysis techniques, which specifically take into account the possibly nonlinear behavior of the sensorimotor system.

1.6 Aim and outline

The overall objective is to enhance the understanding of the sensorimotor system in both unimpaired individuals and individuals who have suffered a stroke. The goal of this thesis is to characterize the cortical responses evoked by robotic joint manipulation in unimpaired individuals, and to establish how it is altered during and after stroke recovery.

Chapters two to six have been written as journal articles and are therefore considered autonomous chapters.

Chapters 2 to 4 explore the characteristics of the cortical evoked responses in unimpaired individuals. The aim of **Chapter 2** is to determine the appropriate analysis tools for characterizing the cortical evoked responses to robotic joint manipulation. The obtained findings are applied in **Chapter 3**, which quantifies the linear and nonlinear contributions to the cortical responses obtained from continuous somatosensory stimulation. Chapter 3 reveals that the response is dominated by nonlinear behavior, such that application of linear system identification tools is not appropriate. Therefore, in **Chapter 4** the relation between stimulus at the wrist and the response in the cortex is modeled using novel nonparametric nonlinear modeling techniques.

The last chapters study the cortical evoked responses in individuals who have suffered a stroke. Measurements are performed during both the subacute and the chronic phases of stroke. In **Chapter 5** the differences in cortical evoked responses are explored between

individuals with different levels of impairment who are in the chronic phase after stroke and unimpaired age-matched individuals to investigate if cortical evoked responses relate to level of impairment. **Chapter 6** presents a measurement protocol and analysis strategies to track the location and intensity of the responses in longitudinal recordings. These recordings take place during four measurement points from the subacute to the chronic phase of stroke, allowing for the study of recovery mechanisms and the development of predictive models. Preliminary findings are presented and a relation between these findings and the levels of sensory and motor impairment is explored, with improving prediction of functional outcome as the ultimate goal.

Finally**, Chapter 7** discusses and connects the main conclusions, and reflects on the research approach by discussing limitations and future directions.

Chapter 2

Frequency Domain Characterization of the Somatosensory Steady State Response using Electroencephalography

Martijn P. Vlaar, Frans C.T. van der Helm, and Alfred C. Schouten

A continuous somatosensory stimulation evokes a steady state response in the cortex, which can be measured using electroencephalography. Studying somatosensory evoked cortical responses can increase our understanding of cortical involvement in movement control. Previous studies reported a cortical response with power at frequencies that were not in the stimulation signal, indicating nonlinear behavior. The goal of this study was to characterize the cortical evoked response and establish the type of system identification tools that can be used to study the relation between applied stimulus and evoked response. Wrist joint manipulation using a multisine signal was applied to unimpaired individuals to investigate the properties of the steady state response in the frequency domain. The results showed a response in the contralateral sensorimotor cortex at the stimulated frequencies, yet with more power at their even harmonics, indicating substantial nonlinear behavior. It was concluded that the observed cortical response to a mechanical somatosensory stimulation is nonlinear; however, shows no time-variant behavior or subharmonics, allowing for the application of a broad range of (non)linear system identification tools.

2.1 Introduction

Movement control entails the feedforward and feedback control of posture. The central nervous system uses information from sensors (proprioceptors) to control actuators (muscles). Movement disorders cause erroneous control and often have an unknown pathophysiology (Obeso et al., 2014, Smith et al., 2014b). By studying movement control we can increase our understanding of the pathophysiologies of movement disorders. Much work has been done regarding movement control with respect to reflexive feedback (e.g. Kearney et al., 1997, Schouten et al., 2008a, Lewis et al., 2010). These studies use system identification techniques to assess joint and muscle dynamics, and focus on short latency reflexive feedback, which is believed to originate from the spinal cord.

The use of system identification techniques to assess the cortical involvement in movement control is currently underexplored. Cortical activity can be noninvasively recorded with a high temporal resolution and reasonable spatial resolution using electroencephalography (EEG). In this study we take a first step to explore the relationship between somatosensory input at the periphery and the response in the cortex, using system identification techniques.

Nevertheless, extracting information from cortical signals generated by external stimuli has been around for a long time. Cortical responses to sensory stimuli can be obtained by applying transient stimuli or repetitive stimulation (Capilla et al., 2011). Due to the poor signal-to-noise ratio of cortical signals recorded with EEG, many (in the order of hundreds) stimuli have to be applied to enable averaging and therewith sufficient noise reduction. An event related potential (ERP) can be obtained by averaging the cortical response to transient stimuli. Alternatively, by recording the cortical response to repetitive stimuli (such as a square wave or sinusoidal signal) and omitting the transient response, a steady state response (SSR) is obtained (Regan, 1966). SSRs are obtained from stimulating a specific sensory systems (e.g. visual or auditory system). In the visual system SSRs have been obtained for clinically related purposes, such as investigating migraine (Angelini et al., 2004) and schizophrenia (Clementz et al., 2004, Brenner et al., 2009) as well as to obtain an improved general understanding of the visual system (Narici et al., 1998, Herrmann, 2001). Similarly, SSRs have been obtained from the auditory system (Stapells et al., 1984).

SSRs from the somatosensory system can be studied for example by applying electrical stimulation over sensory nerves (Narici et al., 1998) or by applying mechanical stimuli. Due to our interest in movement control, we focus on mechanical stimuli as they are closest to disturbances we experience during daily tasks. The number of studies investigating mechanically evoked SSRs (MSSRs) in humans is limited; **Table 2.1** gives an overview of all published studies involving MSSR to the best of our knowledge. MSSRs are in most studies obtained using tactile stimulation, either using low frequencies (<40 Hz) signals (e.g. Giabbiconi et al., 2004, Nangini et al., 2006) or a high frequency carrier signal (128-200 Hz) which is amplitude modulated at lower frequencies (<40 Hz) (e.g. Tobimatsu et al., 1999, Müller-Putz et al., 2006). MSSRs have been obtained from stimulating the fingers, palm of the hand, sole of the foot and from the wrist, resulting in a response in the contralateral

sensorimotor area. MSSRs are not often obtained using joint manipulation (Campfens et al., 2013, Piitulainen et al., 2013), yet are most relevant when interested in studying movement control. Interestingly, previous studies reported a response at harmonics of the stimulated frequency, while other studies did not. One study even reports the presence of subharmonics in the MSSR. Harmonics and subharmonics in the MSSR indicate nonlinear behavior of the system. Since (sub)harmonics will govern the type of usable analysis tools, it is important to establish their presence.

System identification techniques can be a valuable tool to investigate the cortical involvement during movement control. The goal of this study is to characterize the mechanically evoked steady state response (MSSR) at the cortex and therewith establish the type of system identification tools that can be applied to this type of signals.

2.2 Methods

Experimental protocol

To evoke a proprioceptive MSSR at the cortex, small rotations were imposed on the right wrist of the participant using a robotic manipulator (MOOG, The Netherlands), see **Figure 2.1**. EEG was recorded using a 128 channel EEG cap (ANT, The Netherlands) and amplifier (TMSi, The Netherlands) which acquired data at 2048 Hz. Three unimpaired volunteers participated in the experiment. The study was approved by the local research ethics committee. All participants gave written informed consent prior to participation. The participants performed a passive task in which they were instructed to relax and ignore the imposed movements of the wrist. The participants were furthermore instructed to gaze at the circle in the center of the screen and not to move during trials.
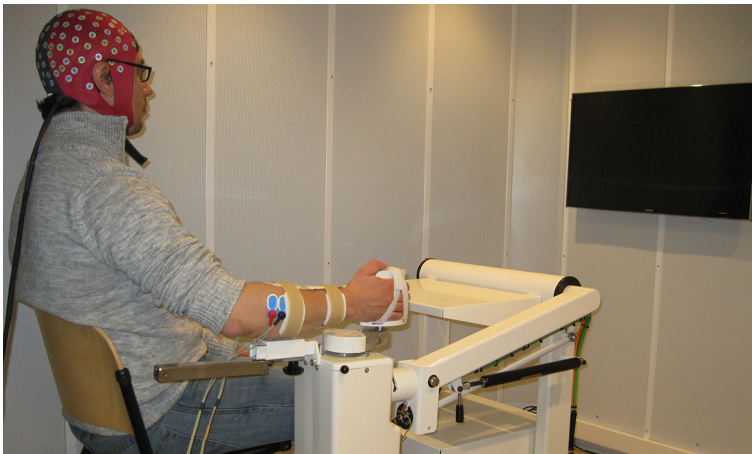

Figure 2.1. Experimental setup. The right forearm of the participant is strapped into an armrest and the right hand is strapped to the handle, requiring no hand force to hold the handle. Both angle of and torque at the axis of the motor are recorded.

Table 2.1. Literature on MSSR. Literature is categorized based if the authors reported on finding harmonics in the MSSR. Asterisk (*) indicates there was ambiguity about the presence of harmonics.

No harmonics	Weinberg et al. (1989), Kelly and Folger (1999), Müller et al. (2001), (Smith et al., 2014b), Giabbiconi et al. (2004), Müller-Putz et al. (2006), Nangini et al. (2006), Giabbiconi et al. (2007), Bardouille and Ross (2008), Adler et al. (2009), Bardouille et al. (2010), Severens et al. (2010), Spitzer et al. (2010), Spitzer and Blankenburg (2011), Voisin et al. (2011a), (Prochazka and Gorassini, 1998), Voisin et al. (2011b), Breitwieser et al. (2011), Breitwieser et al. (2012), Severens et al. (2013), Teale et al. (2013), Canizales et al. (2013), Marcoux et al. (2014), Ahn et al. (2014), Smith et al. (2014a), Pang and Mueller (2014), Pokorny et al. (2014)
Harmonics	Snyder (1992), Tobimatsu et al. (1999), Tobimatsu et al. (2000)*, Goto et al. (2003)*, Jamali and Ross (2012), Budd and Timora (2013), Campfens et al. (2013), Jamali and Ross (2013), Piitulainen et al. (2013), Porcu et al. (2013), Ross et al. (2013), Timora and Budd (2013)
Subharmonics	Langdon et al. (2011)

Sinusoidal stimulation signals with multiple excited frequencies (e.g. f_1 and f_2) allows for detection of nonlinear distortions at harmonics of these frequencies (e.g. $2f_1$ and $3f_2$) as well as at intermodulation frequencies (e.g. f_1+f_2 and $2f_1-f_2$). Intermodulation distortions and higher harmonics can reveal the order of the nonlinearity, where the higher harmonics might be attenuated by for example the presence of low pass characteristics. It is important to note that the use of square waves as stimulation signals will (unintentionally) include higher harmonics in the input signal (Teng et al., 2011) and will therefore hinder determining the origin of power at the harmonics in the recorded EEG signal.

In this study we applied a multisine signal as a periodic stimulus, which is defined as:

$$r(t) = \sum_{k=1}^{N-1} A_k \cos\left(2\pi f_0 k t + \phi_k\right) \tag{2.1}$$

where k is the frequency line (integer number), A_k and ϕ_k are the amplitude and phase at frequency line k, f_0 is the frequency resolution in hertz, N is the number of samples (as well as frequency lines) in one period and t is the time vector describing one period of the signal. Frequency line k corresponds to the Fourier coefficients, where $k = 0$ is the DC coefficient and is omitted to have a zero-mean signal. The multisine signal was designed at a sampling rate of 2048 Hz to match the sampling rate of the robotic manipulator and had a period duration of 1 s (i.e. $f_0 = 1$ Hz, $N = 2048$). The excited frequencies in the multisine signal were 3, 7 and 11 Hz. Phases were randomly selected from a uniform distribution between 0 and 2π rad. The amplitude of the excited frequencies decayed with -20 dB/dec by decreasing A_k for increasing values of k, so the spectrum of the velocity signal is flat (the stretch sensors in the muscles are thought to be primarily velocity sensitive). The amplitude of the time domain signal was set to have a maximum absolute amplitude 0.03 rad (~1.7 deg). An experiment consisted of twenty trials, where each trial is defined as 60 s consecutively recorded periods.

Between trials there was a small break. The first 5 periods of each trial were discarded to reduce transient effects. For each participant 1100 periods of 1 s were used for analysis.

Data processing

Data processing was performed using FieldTrip (Oostenveld et al., 2011) and MATLAB R2014a (The Mathworks, Inc., USA). Electrodes with poor connectivity to the scalp and therefore picking up large amounts of noise were removed from the analysis. All data were referenced to the common average and were high-pass filtered with a fourth order Butterworth filter (cut-off frequency 2 Hz). Due to the high electrical conductivity of the brain, a signal recorded at an EEG electrode contains contributions from multiple cortical sources. This volume conduction effect can be mitigated by separating the mixed signals at the electrodes into independent signals at separate sources using an independent component analysis (ICA) (Makeig et al., 1996a). ICA is a technique commonly used for neural signals and allows for blind source separation, meaning no prior knowledge is required on the signal mixing process. The number of obtainable components is one less than the number of recording channels; the use of a common average reference reduces the rank of the recorded date by one. The output of the ICA algorithm is a set of weights, which determine how all electrodes are weighed in each component. Relevant signal sources can in this way be separated from noise sources (e.g. eye blinks and muscle contractions).

Analysis tools

All data are transformed to the frequency domain, where $X^{[p]}(k)$ represents the Fourier transformed signal of an independent component (obtained with ICA) for each recorded period p.

The signal-to-noise ratio (SNR) for a signal at a component is calculated using the power in the signal (2.2) and the sample variance (2.3).

$$E_X(k) = \left| \frac{1}{P} \sum_{p=1}^{P} X^{[p]}(k) \right|^2 \tag{2.2}$$

$$n_X(k) = \frac{1}{P} \operatorname*{var}_{p}\left(X^{[p]}(k) \right) \tag{2.3}$$

where P is the total number of periods ($P = 1100$). The SNR is subsequently calculated:

$$SNR_X = \frac{\sum_{k=0}^{N-1} E_X(k)}{\sum_{k=0}^{N-1} n_X(k)} \tag{2.4}$$

Only the component with highest SNR is used for further analysis, as this component is assumed to reflect the response most strongly related to the stimulus.

The time domain response at the component with the highest SNR can be obtained by averaging over all periods, thereby reducing the influence of noise. The auto spectral density of the response can be obtained in two ways: (I) by calculating the auto spectral density for each of the 1100 periods and subsequently averaging the auto spectral density over these periods; or (II) by averaging the time domain signal over 1100 periods and subsequently calculating the auto spectral density over the obtained signal. Both methods have been applied before (e.g. Ross et al., 2013) and yield different information on the cortical response. In this paper both methods were applied.

Taking a Fourier transform over one whole 55 s trial allows us to see 'in between' the frequencies which enables detection of slow time-variant behavior (Lataire and Pintelon, 2009). The frequency resolution is now increased from 1 Hz to 1/55 Hz. The frequency points in between the integer frequencies give an indication of the noise level. If there is a higher response at frequency points very close to the integer frequencies, we can conclude that there are slow time variations present. If this behavior occurs, the measured response will not exactly fit the (rectangular) observation window of 1s and leakage will occur.

Additionally we want to investigate the presence of subharmonics. Considering we only stimulated odd integer prime frequencies, these subharmonics are most likely to occur at non-
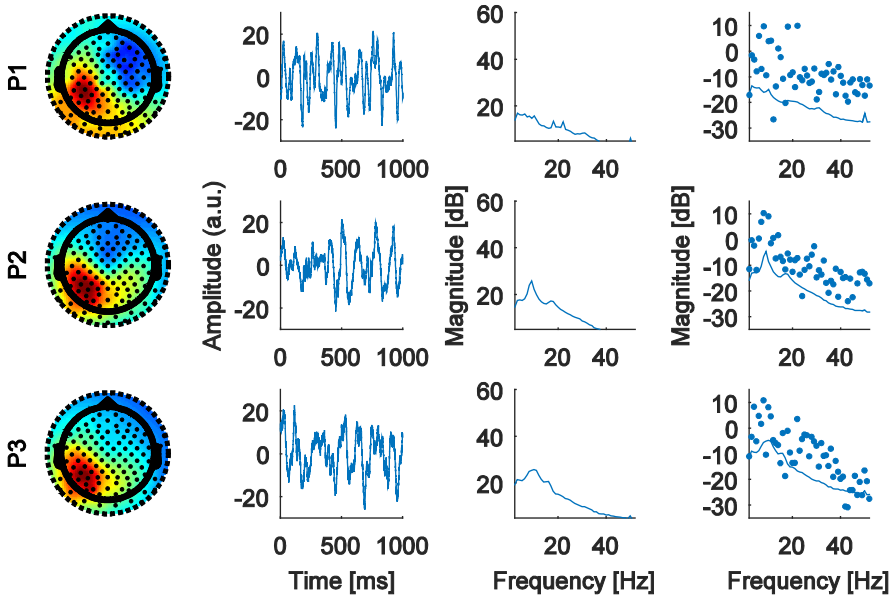
Figure 2.2. Responses at the component with the highest SNR for each participant (P1, P2 and P3). The **first column** shows weight distribution of electrodes in the component (presented on arbitrary symmetric scale: red is positive weighing and blue is negative weighing of the electrodes indicated in black dots). **Second column** shows averaged time response. **Third column** shows the averaged autospectral density for all periods and the **fourth column** shows the auto spectral density for the average of all periods (dots) and additionally the noise level (solid line) as calculated in (2.3).

integer frequencies (e.g. at $1/2$, $1/3$ and $1/4$ of a stimulated frequency). To obtain a frequency resolution that permits the detection of these frequencies we removed some additional periods from the beginning of a trial, leaving 48 periods for each trial. By averaging all twenty trials with 48 consecutively recorded periods, we obtain strong noise reduction as well as a frequency resolution allowing to check for the presence of subharmonics.

A response at unstimulated frequencies indicate nonlinear behavior. Since only odd frequencies were excited, we can distinguish between odd ($y(u) = -y(-u)$) and even ($y(u) = y(-u)$) nonlinear behavior, since they result in a response at even and odd frequencies respectively (Pintelon and Schoukens, 2012). By regarding the unstimulated frequencies that show a response and relating them to the frequencies in the input signal, an estimate of the order of the nonlinearity can be obtained.

2.3 Results

Figure 2.2 shows the response of the component having the highest SNR for each participant. Each of these components has a similar weight distribution, indicating a similar set of electrodes contributes to the signal at this component. Such a distribution is expected to be the result of a cortical source in the contralateral (left) sensorimotor area. The average time domain response for each participant is presented in the second column of **Figure 2.2**. The responses are not identical; however, when directly comparing them in **Figure 2.3** it is apparent that the three response share many features.
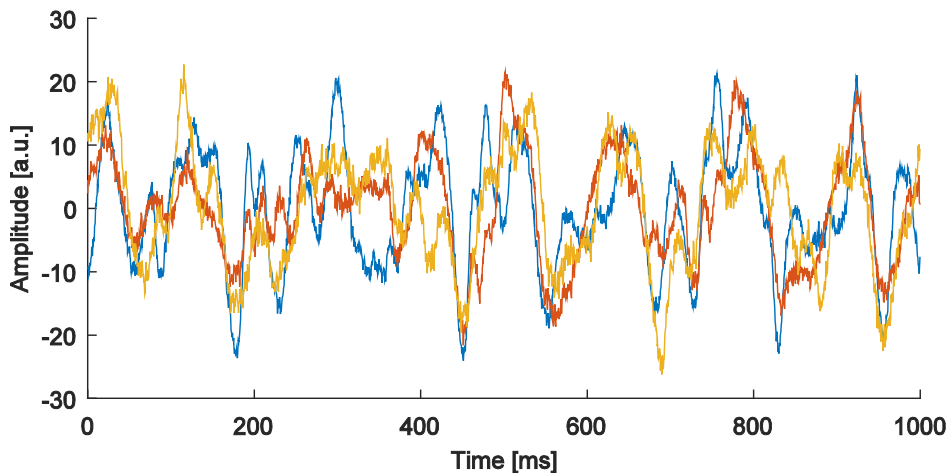
Figure 2.3. Average cortical response for the ICA component with the highest SNR for all three participants. Blue line: participant 1, red line: participant 2, yellow line: participant 3. Correlations between the signals ranged from 0.54 to 0.65, which is relatively high considering these cortical responses come from (low SNR) recordings from different participants.

The auto spectral density (**Figure 2.2**, column 3) shows the presence of the intrinsic alpha (around 10 Hz) and beta (around 20 Hz) rhythms, which are typical for a wakeful relaxed state. The power for these rhythms varies per participant. The typical decrease of power with $1/f$ is often observed in biological systems. When we average all the recorded responses before calculating the power (**Figure 2.2**, column 4), the intrinsic rhythms are less apparent. This occurs because these rhythms are not related to the stimulus and will therefore be removed by averaging. Hence, the intrinsic rhythms will for a large part be regarded as noise, as can be seen in the noise level (**Figure 2.2**, column 4).
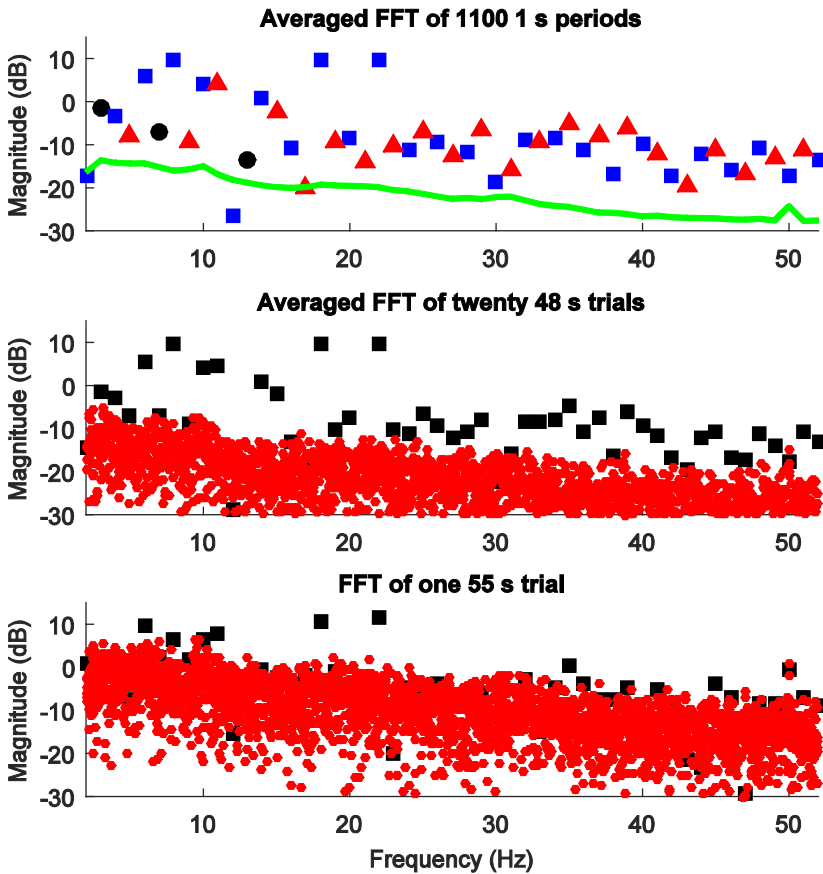
Figure 2.4. Frequency domain results for a representative participant (participant 1). **Top graph** is similar to the top right graph in Figure 2; however, the frequency points have been color/shape coded to provide more details. Black circles: stimulated frequencies (3, 7, 11 Hz), red triangles: odd unstimulated frequencies, blue squares: even unstimulated frequencies, green solid line: noise level $n_X(k)$. **Middle graph** shows the FFT of twenty averaged 48 s trials. Black squares: integer frequencies, red circles: non-integer frequencies. **Bottom graph** shows the FFT of one 55 s trial. Black squares: integer frequencies, red circles: non-integer frequencies.

Our stimulation signal only contained three frequencies. **Figure 2.2** (column 4) illustrates there is a response at many more frequencies than the number of stimulated frequencies. More detailed results are presented for one representative participant in **Figure 2.4**. The top graph of **Figure 2.4** shows the power in the signal after first averaging over 1100 periods. There is little power in the stimulated frequencies compared with the unstimulated frequencies. The relative output power at the stimulated frequencies is limited to 2%, 18% and 5% for the three participants respectively. It is clear that most of the power is in the *even* unstimulated frequencies (e.g. 6, 8, 10, 14, 18 and 22 Hz). **Figure 2.4** (middle graph) shows that there is no response at $1/2$, $1/3$ and $1/4$ of the stimulated frequencies, suggesting there are no subharmonics present. All frequencies with power above noise level are integer frequencies, except around the alpha rhythm and around 50 Hz. **Figure 2.4** (bottom graph) illustrates the magnitude of the Fourier transform of one out of twenty 55 s trials. There are 54 data points in between each integer frequency. The dots around 50 Hz indicate the noise picked up from the mains. Around 8 to 10 Hz the effect of the alpha rhythm is visible. The neighboring non-integer frequencies around 18 and 22 Hz do not show increased power compared with the non-neighboring non-integer frequencies, indicating there is no time variant behavior of the cortical response.

2.4 Discussion

In this study we used novel frequency domain signal analysis techniques to characterize the cortical response to mechanical somatosensory stimuli. Exploring the presence of nonlinearities and time variant behavior is an essential step in system identification, since it determines which analysis techniques can be used to study the system. This initial characterization is often neglected in the neuroscience community, where measures such as linear coherence are often used and where the cortical response is often only analyzed at the stimulated frequency. We provide evidence for a nonlinear yet time-invariant response.

Mechanical sensory stimuli evoke a cortical response

By applying small rotations to the wrist joint we evoked a response in the brain which is correlated to those rotations, as has been correspondingly shown in previous literature on MSSRs. The averaged time domain responses (**Figure 2.3**) reveal similarity between participants, suggesting the signals are generated by a similar system. The applied rotations stimulate the proprioceptive systems, although we cannot exclude contributions from cutaneous receptors. For the proposed method of characterizing the response, the exact origin of the response is not crucial. Dedicated experiments can be designed to separate proprioceptive and cutaneous contributions.

Harmonics and intermodulation

The results show most of the power is in the unstimulated frequencies, more specifically at the even harmonics, indicating the presence of an even nonlinear operator. Therefore, describing the relation between stimulus and response in the EEG using linear techniques should be approached with caution. The response of a nonlinear system depends on the

amplitude and distribution of the stimulus signal, as well as on the operating point in which the system is studied, thereby hindering comparison between recordings. A nonlinear system can be linearized; however, particularly in an even nonlinear system this will have little chance of success. The strongest response appears at twice the stimulated frequencies ($2f_1$) and at combinations between two stimulated frequencies (f_1+f_2 and f_1-f_2), indicating the presence of a second order nonlinear operator. However, the response shows power at other frequencies than the harmonics and intermodulation products for the second order, pointing to a complex static or dynamic nonlinear system.

Subharmonics

Subharmonics are commonly found in VSSRs (e.g. Herrmann, 2001, Angelini et al., 2004). The occurrence of subharmonics in SSSRs was only found by Langdon et al. (2011). In this study we did not encounter the presence of subharmonics. The lack of subharmonics and the presence of a periodic response indicates the system behaves as a "period in, same period out" system which permits the use of a large set of (non)linear system identification techniques (Pintelon and Schoukens, 2012).

Time variant behavior

The observed responses appears to be limited to the integer frequencies; the power at directly neighboring frequencies is not higher than at the non-direct neighbors of integer frequencies, indicating there is no slow time variant behavior within a trial. Because the response of interest occurs at integer frequencies, there will be no leakage when the 1 s segments are analyzed without applying a window.

Recommendations and future work

The apparent nonlinearity in the system can be further investigated using for example cross frequency coupling measures (Yang et al., 2015). Additional research will reveal if the response is governed by a static nonlinear operation with a neural time delay or if there are also dynamics involved. Increased understanding of the cortical response to stimulation during a passive task paves the way for investigating the role of the cortex in active movement control tasks. The presented approach can be similarly applied to different types of mechanical, visual or auditory stimulation.

2.5 Conclusions

The cortical response to mechanical stimulation of the wrist contains substantial nonlinear components. The applied novel system identification techniques allow for the extraction of extra information from the mechanically evoked steady state responses (MSSR) without extra experimental effort. The observed cortical response to a mechanical somatosensory stimulation is time invariant and nonlinear; however, shows no subharmonics, allowing for the application of a broad range of (non)linear system identification tools.

Chapter 3

Quantifying Nonlinear Contributions to Cortical Responses Evoked by Continuous Wrist Manipulation

Martijn P. Vlaar, Teodoro Solis-Escalante, Alistair N. Vardy,
Frans C. T. van der Helm, and Alfred C. Schouten

Cortical responses to continuous stimuli, as recorded using either magneto- or electroencephalography (EEG), have shown power at harmonics of the stimulated frequency, indicating nonlinear behavior. Even though the selection of analysis techniques depends on the linearity of the system under study, the importance of nonlinear contributions to cortical responses has not been formally addressed. The goal of this paper is to quantify the nonlinear contributions to the cortical response obtained from continuous sensory stimulation. Ten unimpaired individuals participated in this study. EEG was used to record the cortical response evoked by continuous robotic manipulation of the wrist joint. Multisine stimulation signals (i.e. the sum of several sinusoids) elicited a periodic cortical response and enabled assessment of nonlinear contributions to the response. Wrist dynamics (relation between joint angle and torque) were successfully linearized, explaining 99% of the response. In contrast, the cortical response revealed a highly nonlinear relation; most power (~80%) occurred at non-stimulated frequencies. Moreover, only 10% of the response could be explained using a nonparametric linear model. These results indicate that the recorded evoked cortical responses are governed by nonlinearities and that linear methods do not suffice when describing the relation between mechanical stimulus and cortical response.

3.1 Introduction

Sensory feedback is crucial for effective movement control and allows compensating for internal and external disturbances. For example, proprioceptors in the human body, such as muscle spindles and Golgi tendon organs, provide sensory feedback on the state of limbs (i.e., position, velocity, and force). Reflexive control action can originate from spinal level (short latency) and from supra-spinal level (long latency) (Pruszynski and Scott, 2012). Disturbed sensory function or sensorimotor integration is often implicated in movement disorders (Patel et al., 2014). The functioning of the somatosensory system can be assessed by applying sensory stimuli and studying muscle or brain response (Mortimer and Webster, 1979, Pisano et al., 2000, Rossini et al., 2001).

Sensory stimuli are commonly presented as transients; such as when investigating the patellar stretch reflex. The response of a muscle to such a stretch can be recorded using electromyography (EMG)(Pruszynski et al., 2011). The dynamic cortical response to a transient sensory stimulus can be noninvasively recorded using magnetoencephalography or electroencephalography (EEG) and is referred to as the event related field or event related potential (ERP). Investigating the sensorimotor system with intermittent short lasting stimuli only reveals the transient response of the system. As an alternative, continuous stimuli, such as sinusoidal, square wave or noise-like signals, are capable of continuously engaging the system in the processing of information; therefore revealing both transient and steady state behavior (Kearney and Hunter, 1990). While transient responses depend on initial conditions, steady state responses present the system behavior accommodated to the stimulation and regardless of the initial state.

Several studies used continuous mechanical stimuli to investigate intrinsic and reflexive limb dynamics by recording the mechanical and muscle response during postural control tasks (Mirbagheri et al., 2001, Perreault et al., 2008, Schouten et al., 2008a). The role of the cortical structures in reflexive feedback control is yet still not fully understood (Pruszynski and Scott, 2012). Cortical sensory processing of continuous mechanical stimulation has been investigated, for example using vibrotactile stimulation to the fingers, hand and foot (Tobimatsu et al., 2000, Müller et al., 2001, Giabbiconi et al., 2004).

Increased insight in normal and pathological sensorimotor function can be obtained by modeling the relation between stimulus and response. To work towards developing these models it is essential to determine which model classes are appropriate. Studies using continuous vibrotactile stimulation report responses at frequencies other than the frequencies present in the stimulus, illustrating a nonlinear relationship between the stimulus and the cortical response measured by EEG (Snyder, 1992, Tobimatsu et al., 1999, Langdon et al., 2011, Jamali and Ross, 2013). Mechanical (i.e. joint angle and torque) and EMG recordings obtained from continuous mechanical stimulation also show a small response at non-stimulated frequencies (Mugge et al., 2010, Campfens et al., 2013, Forbes et al., 2014). Nonlinear responses in the sensorimotor system could result from sensors (e.g. unidirectional sensitivity), muscles (e.g. unidirectional force generation and a nonlinear force-length

relationship) and other parts of the sensorimotor system including the central nervous system.

Although many studies acknowledge the nonlinear properties of the cortical response to sensory stimuli, it remains unclear to which degree the nonlinearities govern the response. Systems with weak nonlinear behavior can be studied in a specific operating range, facilitating linear analysis. Linear system identification techniques are matured, computationally undemanding, require little a priori knowledge and can reveal many characteristics of the system under study, including time delays. Linear techniques are useful if the system under study can be properly linearized, which should be checked during analysis. If the linear approximation only describes a small portion of the behavior of the system, any conclusions based on the linearized system will most likely not be applicable to the actual system under study. The well-established and accessible linear system identification framework should in this case be exchanged for a nonlinear system identification approach. Applying system identification to systems with strong nonlinear behavior requires techniques which are computationally more demanding and often require a priori selection of a model structure or order.

To determine which analysis tools are appropriate to study the cortical response to sensory stimuli, it is imperative to study the contributions in the cortical response to sensory stimuli
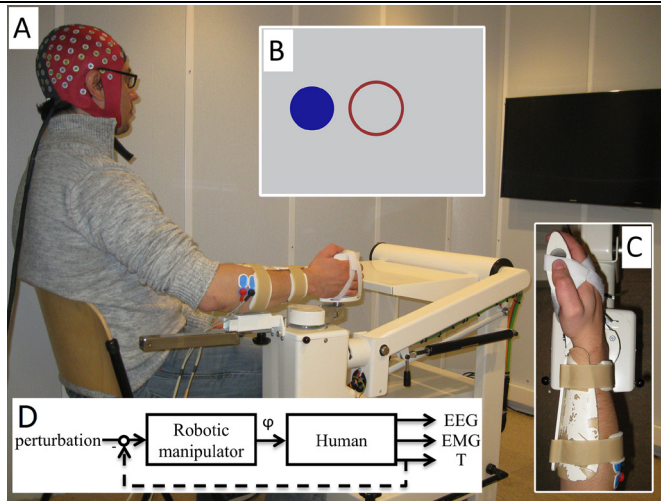
Figure 3.1. Experimental setup. **A)** The right forearm of the participant is strapped into an armrest and the right hand is strapped to the handle, requiring no hand force to hold the handle. **B)** Visual feedback (the target (red circle) is static and always visible during a task, the blue circle is only visible during the active task and indicates the position of the handle and the task is to keep the blue circle in the red circle). **C)** Close up of the hand in the robotic manipulator. **D)** Block scheme depicting the robotic manipulator and the human. The perturbation signal (angle or torque) is applied to the human by the robotic manipulator, which will present the human with a certain angle (φ). In case of the torque perturbation the torque on the handle (T) is fed back to the robotic manipulator (dashed line). The robotic manipulator ensures the angle is set such that the torque on the handle (T) matches the perturbation signal.

due to nonlinearities in the system, which have never been systematically quantified.

Using multisine stimulation signals, which are designed by summing a specific set of sinusoidal signals (Pintelon and Schoukens, 2012), we can detect nonlinearities in the cortical response at frequencies which are not present in the stimulation signal. The goal of this paper is to quantify the nonlinear contributions to the cortical response obtained from continuous sensory stimulation. To the best of our knowledge, the cortical response obtained from continuous joint manipulation has only been investigated in one previous study by Campfens et al. (2013); however, they analyzed the response only at the excited frequencies.

A robotic manipulator was used to apply continuous mechanical manipulation of the wrist joint and the response of the sensorimotor system was analyzed at three levels: mechanical response (joint angle and torque), muscle activity (electromyogram, EMG), and cortical activity (EEG). The nonlinear contributions are quantified in passive and active tasks, where the active tasks are performed to evoke and analyze EMG responses.

3.2 Materials and Methods

Participants

Eleven right-handed unimpaired volunteers (5 men, 6 women; age 22-25 years) with no self-reported history of neurological disorders participated in this study. Participants were all right handed (laterality index greater or equal to 80 according to the Edinburg Handedness Inventory (Oldfield, 1971)). The study was approved by the local research ethics committee. All participants gave written informed consent prior to participation. Participants were well rested and refrained from alcohol and drug intake 12 hours before the experiment.

Experimental setup

A one degree-of-freedom robotic wrist manipulator (Wristalyzer by MOOG Inc, Nieuw-Vennep, The Netherlands) applied the stimulation as angular or torque perturbations to the right wrist of the participants (see **Figure 3.1A**). The handle was adjusted so that the axis of rotation of the wrist was aligned with the axis of rotation of the manipulator (see **Figure 3.1C**). The neutral angle was defined as the angle of the wrist when fully relaxed, resulting in a slight flexion posture. A screen placed at 1.5 m from the participant presented a target and task relevant feedback (see **Figure 3.1A**&**B**). The participants were instructed to gaze at the center of the screen throughout the experiment to minimize head and eye movements. All recordings were performed in a slightly dimmed soundproof cabin.

Figure 3.1D illustrates the closed-loop configuration of the robotic manipulator and the human, and indicates the recorded signals. All signals were sampled at 2048 Hz (136 channel Refa by TMSi, Oldenzaal, The Netherlands), ensuring synchronicity between all signals. Scalp potentials were measured using a cap with 126 Ag/AgCl electrodes (WaveGuard by ANT, Enschede, The Netherlands). The electrodes were arranged according to the 10-5 system (Oostenveld and Praamstra, 2001). The mastoid electrodes on the cap were left unconnected.

The participant ground electrode was connected to the left mastoid (Ag/AgCl electrode, Blue Sensor N by Ambu, Ballerup, Denmark). Muscle activity was measured from the flexor carpi radialis (EMG_F) and extensor carpi radialis (EMG_E) using electrode pairs (Blue Sensor N by Ambu) attached to the skin and placed over the muscle belly with an electrode distance of 10 mm. Handle angle and applied torque were measured from analog output signals of the wrist manipulator and were galvanic isolated from the amplifier using optical isolation amplifiers (TMSi, Oldenzaal, The Netherlands).

Tasks

Each participant performed two tasks: an active task and a passive task. In the passive task the participant was instructed to relax and to ignore the angular perturbations imposed by the manipulator. During the passive task the screen only presented the target and no feedback was given. The intensity of the angular perturbation was set such that the rotation of the handle had a root mean square (RMS) of 0.02 rad (≈1.1 deg). Previous studies on the wrist joint applied perturbations in a similar range (Schouten, 2004, Campfens et al., 2013). In the active task the participant was instructed to put effort in maintaining the wrist in the neutral angle while the manipulator imposed torque perturbations. During the active task the feedback screen presented the angle of the handle (see **Figure 3.1B**), which was low-pass filtered online (0.5 Hz, 2nd order Butterworth) to avoid rapid eye movements and to prevent the frequencies in the perturbation signal from stimulating the visual system. The intensity of the torque perturbations during the active task was iteratively set such that the rotation of the handle had an RMS of around 0.02 rad. By studying the system for both tasks around the
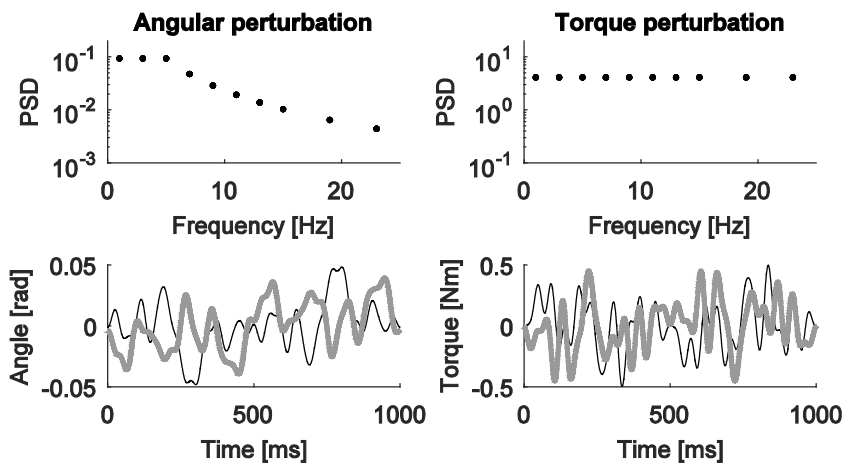
Figure 3.2. Perturbation signals. **Top graphs**: power spectral density (PSD) of the perturbation signals. **Bottom graphs**: a time domain representation of two out of seven realizations (thin black and thick gray) for both types of perturbation signal. The two realizations have identical frequency content and power however the phases are randomly distributed for each of the realizations resulting in different time courses of the signals (maximum correlation for any time shift for the two shown angular perturbation signals was 0.61 and for the torque perturbation signals 0.57).

same operating point and applying small rotations allows for comparison between the tasks and facilitate linearization. Prior to the experiment participants were required to practice the tasks.

Perturbation signal selection

The type of signal used to provide continuous manipulation of the wrist was a random phase multisine signal, which is a periodic signal consisting of several sinusoids summed together (Pintelon and Schoukens, 2012) as in:

$$r(t) = \sum_{k=1}^{N-1} A_k \cos\left(2\pi f_0 kt + \phi_k\right), \tag{3.1}$$

where k is the frequency line (integer number), which corresponds to the Fourier coefficients ($k = 0$ is the DC coefficient and is omitted to obtain a zero-mean signal), A_k is the amplitude at frequency line k which can be zero or nonzero, f_0 is the frequency resolution in hertz, defined by period length T in seconds $\left(f_0 = 1/T\right)$, ϕ_k is the random phase at frequency line k which is taken from a uniform distribution, N is the number of samples in T which is defined by the sampling frequency, and t is the time vector. Frequencies where the amplitude is nonzero compose the set of excited (i.e. stimulated) frequencies $\left\{f_{ex}\right\}$.

Multisine signals allow for broadband excitation and system identification over a desired frequency range, and have several advantages in system identification over random perturbation signals such as (white) noise. Firstly, multisine signals allow concentrating signal power in a limited number of frequencies, which increases the input signal-to-noise ratio (SNR) at those frequencies while maintaining the same stimulation amplitude. Secondly, the noise levels can be quantified and reduced by recording multiple periods. Thirdly, multisine signals allow for leakage-free analysis due to their periodicity. Finally, by proper signal and experiment design a multisine perturbation signal allows for the detection and quantification of nonlinear distortions.

There exists a large class of nonlinear systems which, when excited with a periodic input signal, will generate a periodic response with the same period as the input. This class includes polynomials, saturations and rectifiers amongst many other systems. When repeatedly perturbing such a system with a multisine signal, the system will be excited in the same way and will therefore generate the same output (Pintelon and Schoukens, 2012). The presence of nonlinear distortions generated by these systems can be revealed by using different realizations of a multisine signal, which have different phases but the same excited frequencies and amplitudes per frequency. As for a nonlinear system the superposition principle does not hold, perturbing the system using a different multisine realization (i.e. different time course) will excite the nonlinear system in a different way. This property will be exploited in the analysis by calculating to what extent a nonparametric linear model will be able to describe the input-output relation regarding all different realizations, which should be high for a linear system.

When using a multisine signal where only odd frequency lines are excited (e.g. $k = 1,3,5$) we can, besides quantifying the nonlinear contributions, also further describe the type of nonlinear behavior which will be helpful in a subsequent (non)parametric nonlinear modeling step. A linear system will show a response only at the excited frequencies. Nonlinear systems will show a response at unexcited frequencies, which can be harmonics of the excited frequencies (e.g. $2f_{ex1}$) or intermodulation products (e.g. $f_{ex1} + f_{ex2}$). Nonlinear systems can have an odd or even behavior, or show both behaviors at the same time. When an odd nonlinear system (i.e. $y(u) = -y(-u)$) is excited at an odd frequency line, the response will only contain power at harmonic odd frequency lines. When an even nonlinear function (i.e. $y(u) = y(-u)$) is excited at an odd frequency line, the response will only contain power at harmonic even frequency lines. More generally, when perturbing a system with a signal containing only odd frequency lines, any power that is present in the (noise free) output signal at the even frequency lines must be due to nonlinear distortions generated by an even or even and odd nonlinear function. Additionally, exciting only odd frequency lines ensures there is no disturbing effect of even nonlinear distortions on the excited frequency lines. This characteristic allows for differentiation between even and odd nonlinear distortions, while maintaining the ability to perform system identification over the chosen (odd) frequency range of interest.

Perturbation signal design

Multisine perturbation signals with a period of 1 s were designed, resulting in a frequency resolution of 1 Hz. The excited odd frequency lines are 1, 3, 5, 7, 9, 11, 13, 15, 19, 23 Hz, resulting in a total of 10 excited frequencies. As mentioned above, selecting these frequencies allows for the detection of even and odd nonlinear distortions. Additionally, the dynamics of the wrist are observable within this frequency range (Schouten et al., 2004). Seven different realizations of a random phase multisine were applied, as at least seven realization are needed to preserve the properties of the maximum likelihood estimator (such as consistency) in possible future parametric modeling step (Schoukens et al., 2012).

All perturbation signals were generated offline and the same set of signals was used for all participants (see **Figure 3.2**). The angular perturbation signal was designed to have equal power on the first three excited frequencies and a decreasing power for the higher frequencies (-20dB/decade slope), which is a tradeoff between reduced predictability of the
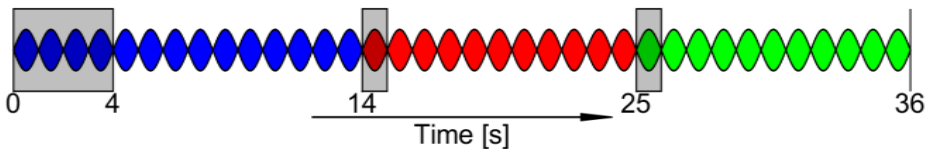

Figure 3.3. Schematic representation of the composition of one 36 s trial. Each lobe represents one 1s period of the perturbation signal and the three different colors represent different multisine realizations. Highlighted periods are excluded from analysis, leaving ten periods per realization in each trial for analysis.

signal (to prevent anticipation) and capabilities of the robotic manipulator. The torque perturbation signal was designed to have equal power on all excited frequencies. For each perturbation signal seven realizations of a random phase multisine were generated. To ensure these realizations are actually different and therefor excite the (non)linear system in a different way, the correlation amongst these seven signals was controlled. This was achieved by generating 25000 random-phase multisine signals and removing 10% of the signals having the highest peak-to-RMS ratio (crest factor) and another 10% having the least normal distribution (chi-square test). Out of the remaining 20000 signals, seven realizations were obtained with a correlation coefficient of less than 0.65 amongst each other for any time shift, which was found to be the lowest achievable number with the signal properties used.

Experimental protocol

To prevent fatigue the experiment was partitioned in trials of 36 s. There was a break between trials of at least 10 s or longer if requested by the participant. The active and passive trials were alternately presented to the participant. To avoid habituation to the signals each trial consisted of three randomly selected multisine realizations, which were repeated several times and smoothly merged. A smooth transition from on multisine realization to another was achieved by shifting all seven multisine realizations to have an amplitude and velocity close to zero at the beginning (and therefore also end) of its period. The transition between two concatenated realizations was further smoothed by interpolating between the last sample of the first realization up to the 50th sample (~25 ms) of the second realization using piecewise cubic spline interpolation. Periods containing the transition between two realizations were removed. Additionally, the first four periods of each trial were removed from the analysis to account for transient effects, resulting in a total of ten useful periods for each of the three multisine realizations in the trial (see **Figure 3.3**). A total of 49 trials (i.e. 1470 useful periods) was recorded per task, consisting of 210 periods ($P = 210$) for each of the seven realizations ($M = 7$). Including mandatory breaks, this protocol resulted in a minimal recording time of 76 minutes for each participant.

Pre-processing

Data processing was performed using FieldTrip (Oostenveld et al., 2011) and MATLAB 8.1 (The Mathworks, Inc., Natick, MA, USA). Line noise (50 Hz and its harmonics) was removed using the discrete Fourier transform as implemented in FieldTrip. The EMG signals were high-pass filtered in two directions (25 Hz, 4th order Butterworth) to remove movement artifacts introduced by the robotic manipulator, and were subsequently rectified. The mean of the rectified EMG signal was removed as we are interested in the response of the muscle to the perturbation (i.e. reflexive contributions) and less in tonic activation and the generated torque (Schouten et al., 2008a). The EEG signals were referenced to the common average and high-pass filtered in two directions (1 Hz, 4th order Butterworth). No artifact rejection was applied.

Data analysis

Since periodic perturbation signals were used, all recorded signals were organized in P periods of M realizations ($x^{[m,p]}(t)$). Consequently any part of the response that is not periodic with the same period as the perturbation signal will be regarded as noise.

Quantifying the relative power of the nonlinear distortions

The frequency domain representation of the recorded signals was obtained by applying the Fourier transform, resulting in $X^{[m,p]}(f)$. An estimate of the total power in each signal was obtained by averaging over periods (*P*) and thereby reducing the noise, calculating the power, averaging over realizations (*M*) and summing over all frequencies (*F*):

$$\hat{E}_{X,total} = \sum_{f=1}^{F} \frac{1}{M} \sum_{m=1}^{M} \left| \frac{1}{P} \sum_{p=1}^{P} X^{[m,p]}(f) \right|^2 . \tag{3.2}$$

The power in the excited $\left(\hat{E}_{X,ex} \right)$, unexcited odd $\left(\hat{E}_{X,unex,odd} \right)$, and unexcited even $\left(\hat{E}_{X,unex,even} \right)$ frequencies can be determined by summing over a specific set of frequencies in (3.2), where:

$$\hat{E}_{X,total} = \hat{E}_{X,ex} + \hat{E}_{X,unex,odd} + \hat{E}_{X,unex,even} . \tag{3.3}$$

The relative power in these frequencies can be estimated by dividing the power in excited, unexcited odd, or unexcited even frequencies by the total power.

Noise-to-signal ratio

An estimate of the noise level in the recorded signals was made by calculating the variance over periods (P), averaging this variance over all realizations (M), and summing over all frequencies (F):

$$\hat{\sigma}_X^2 = \sum_{f=1}^{F} \frac{1}{M} \sum_{m=1}^{M} \frac{1}{P-1} \sum_{p=1}^{P} \left| X^{[m,p]}(f) - \frac{1}{P} \sum_{p=1}^{P} X^{[m,p]}(f) \right|^2 . \tag{3.4}$$

The noise-to-signal ratio (NSR) for each recorded signal was obtained by dividing the estimate of the noise level by the estimate of the power in the signal, and is used to select the electrode showing the strongest response relative to the noise level:

$$NSR = \frac{\hat{\sigma}_X^2}{\hat{E}_{X,total}} . \tag{3.5}$$

The sample noise level on the averaged data (i.e. standard error of the mean) compared to the sample mean is referred to as the NSR$_{scaled}$, and is an estimate of the amount of noise still present in the averaged data:

$$NSR_{scaled} = \frac{NSR}{P}. \qquad (3.6)$$

For each participant the EEG signal at the electrodes with the lowest NSR in the passive and active task were used for subsequent analysis and were named EEG_P and EEG_A respectively.

Determining the best linear approximation

System identification was used to determine how much of the recorded signals can be described by a nonparametric linear model. We obtained such a linear model by non-parametric estimation of the frequency response function (FRF). . In agreement with the system depicted in **Figure 3.1D**, an FRF of the human was estimated with the perturbation signal as external reference signal (R), angle φ as input (U) and the torque, EMG and EEG signals as output signal (Y). The input-output relations are given by the measured FRFs $G_{T\varphi}$, $G_{EMG_F\varphi}$, $G_{EMG_E\varphi}$ and $G_{EEG_A\varphi}$.

Each FRF $G(f)$ consists of three parts (Pintelon and Schoukens, 2012):

$$G(f) = G_{BLA}(f) + G_{SNL}(f) + G_{noise}(f). \qquad (3.7)$$

Here G_{BLA} is the best linear approximation (BLA) of the (non)linear system under study, G_{SNL} represents the stochastic nonlinear distortions, and G_{noise} the errors due to the presence of noise. G_{noise} is assumed to be uncorrelated with the reference signal and to have zero mean. In case of a random reference signal G_{SNL} will appear as uncorrelated zero-mean noise; however, not in case of a periodic deterministic reference signal such as the multisine signals used. This implicates that G_{noise} will be different for each period in each realization whereas G_{SNL} will be the same in each period in a realization, but will differ over realizations. G_{BLA} was estimated for each of the four FRFs using a closed loop estimator:

$$\hat{G}_{BLA}(f_{ex}) = \frac{\hat{S}_{\hat{Y}R}(f_{ex})}{\hat{S}_{\hat{U}R}(f_{ex})}. \qquad (3.8)$$

Here $\hat{S}(f)$ is the estimated cross-spectral density, averaged over periods and realizations, which reduces the contributions of noise and stochastic nonlinear distortions in the final estimate. The cross-spectral density was calculated between the perturbation signal R and input U (φ) and output Y (torque, EMG and EEG) at the excited frequencies. A detailed overview of the equations used to obtain an estimate of G_{BLA} and its noise variance can be found in Appendix 3A.

To quantify how well the nonparametric transfer function G_{BLA} describes the measured data, we used the variance accounted for (VAF). The model output Y_{mod} was determined using:

$$Y_{mod}^{[m]}(f_{ex}) = \frac{1}{P}\sum_{p=1}^{P} U^{[m,p]}(f_{ex})\hat{G}_{BLA}(f_{ex}), \qquad (3.9)$$

and converted to the time domain, using the inverse Fourier transform:

$$y_{mod}^{[m]}(t) = \mathcal{F}^{-1}\left(Y_{mod}^{[m]}(f_{ex})\right) \tag{3.10}$$

The model output $y_{\text{mod},c}^{[m]}$ and the average recorded output $\hat{y}^{[m]}$ of the seven different realizations were concatenated into $y_{\text{mod},c}$ and $\hat{y}_c$ respectively. The VAF for each recorded output signal (torque, EMG$_F$, EMG$_E$ and EEG$_P$ or EEG$_A$) was obtained using:

$$VAF = \left(1 - \frac{\text{var}\left(\hat{y}_c - y_{mod,c}\right)}{\text{var}\left(\hat{y}_c\right)}\right) \cdot 100\% \tag{3.11}$$

3.3 Results

This section presents the averaged NSR, power distribution over frequency groups and VAFs as well as individual results of a representative participant. In both the passive and active task we were able to quantify the nonlinear contributions to the mechanical and EEG data. Additionally, the active task also allowed us to study the nonlinear contributions to the EMG data. One out of the eleven participants was not included in the analysis for not being able to successfully complete the active task. In one other participant one electrode (FT9) was removed from the analysis because it was accidentally disconnected during the experiment due to the improper placement of glasses.

Noise-to-signal ratio

Figure 3.4 illustrates the averaged NSR in the passive and active tasks. The lowest NSR for both tasks appears around the contralateral sensorimotor areas. A decreased NSR indicates there is a periodic response in the brain due to the external perturbation signal, which is reproducible over trials.

For all participants the electrode which had the lowest NSR was found on the contralateral hemisphere, close to the sensorimotor areas in the passive (EEG$_P$: 3x FCC3h, 2x CP3, 2x FCC1h, 1x C3, 1x CCP3h and 1x FC1) and active task (EEG$_A$: 4x CP3, 2x FC1, 2x FCC1h, 1x CCP3h and 1x FCC3h).

The first two columns in **Table 3.1** show the NSR and noise levels in the recorded signals (angle, torque, EMG and EEG) averaged across persons. The NSR of the recorded angle (φ) is lower for the passive task because the robotic manipulator directly controls the angle, while the angle in the active task is the result of the human responding to torque perturbations.

The noise level in the EMG signals for the passive task indicates there is not a consistent EMG response to the perturbations, as expected. The noise levels in the EMG signals for the active task and the EEG$_P$ and EEG$_A$ signals indicate that there is still some noise present after averaging over 210 periods, thereby limiting the maximal attainable VAF. However,

Table 3.1. Average noise-to-signal ratio and relative power distribution over frequency groups

	NSR [dB]	NSR$_{scaled}$ [%]	E$_{ex}$ [%]	E$_{unex-odd}$ [%]	E$_{unex-even}$ [%]
		Passive task mean (sd)			
φ	-30.9	0.0 (0.0)	100 (0.0)	0.0 (0.0)	0.0 (0.0)
T	-18.8	0.0 (0.0)	99.6 (0.2)	0.2 (0.1)	0.2 (0.1)
EMG$_F$	20.0	58.9 (24.4)	-	-	-
EMG$_E$	19.9	55.9 (24.8)	-	-	-
EEG$_P$	14.8	17.1 (7.2)	18.6 (5.7)	6.0 (2.1)	75.4 (5.6)
		Active task mean (sd)			
φ	-8.9	0.1 (0.0)	99.6 (0.2)	0.0 (0.0)	0.4 (0.2)
T	-19.6	0.0 (0.0)	99.4 (0.3)	0.1 (0.0)	0.5 (0.3)
EMG$_F$	10.8	7.4 (3.9)	77.5 (4.9)	5.6 (1.6)	16.8 (4.3)
EMG$_E$	12.0	10.7 (7.8)	76.4 (7.4)	8.8 (3.4)	14.8 (4.8)
EEG$_A$	14.2	13.2 (3.6)	16.8 (3.3)	2.6 (0.9)	80.7 (4.1)

these numbers also indicate that over 80% of the recorded physiological data can be described when a proper model is used.

Power of nonlinear distortions

Figure 3.5 shows the power distribution over frequencies for EEG$_P$ for one realization of a representative participant. We can observe that most power is in the unexcited even frequencies, while the power in the excited and unexcited odd frequencies is much lower. The noise level clearly shows two peaks around 10 and 20 Hz; most likely representing the intrinsic alpha and beta band rhythms. It can also be seen that close to 100 Hz the power becomes small and the NSR increases. The effect of the line noise filter is clearly visible at 50 Hz and 100 Hz. The averaged power distribution, NSR, and noise levels for the signals of interest can be found in **Table 3.1**. The power distribution for the EMG signals in the
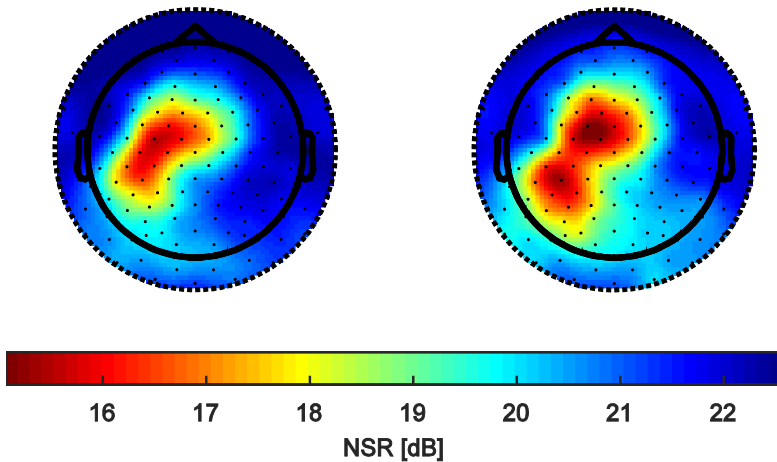
Figure 3.4. NSR per electrode for passive task (left) and active task (right) averaged over all participants. Dots indicate electrode locations. The lowest NSR is found over the contralateral sensorimotor areas.

passive task is not shown, due to the inherently high NSR. **Figure 3.5** as well as **Table 3.1** indicate that most of the power in the EEG signal is in the unexcited even frequencies.

Frequency response functions

The four FRFs for a representative participant are shown in **Figure 3.6**. The mechanical admittance ($G_{\varphi T}$) behaves like a second order system for both tasks, which was previously established (Schouten et al., 2008b). As expected, the mechanical admittance is higher for the passive task compared with the active task, where the instruction was to maintain the angle by resisting the perturbation, i.e., to lower the admittance. This increased stiffness can be generated by co-contracted muscles as well as reflexive activity (primarily from the spinal reflex loop). Due to the increased stiffness in the active task the natural frequency of the wrist also increases from approximately 3 Hz to 5 Hz, which can be observed in the shifted resonance peak in the gain graph. The high frequency response, which is governed by the inertia of the wrist, is similar in both tasks. This result was expected as the inertia does not vary over tasks.

The reflexive impedance ($G_{EMG\varphi}$) for the passive task is much lower than for the active task and is of the same order of magnitude as the noise level, also indicating a high NSR. The reflexive activity was minimal in the passive task as compared with the active task. The reflexive impedance for the active task shows similar behavior between flexor and extensor
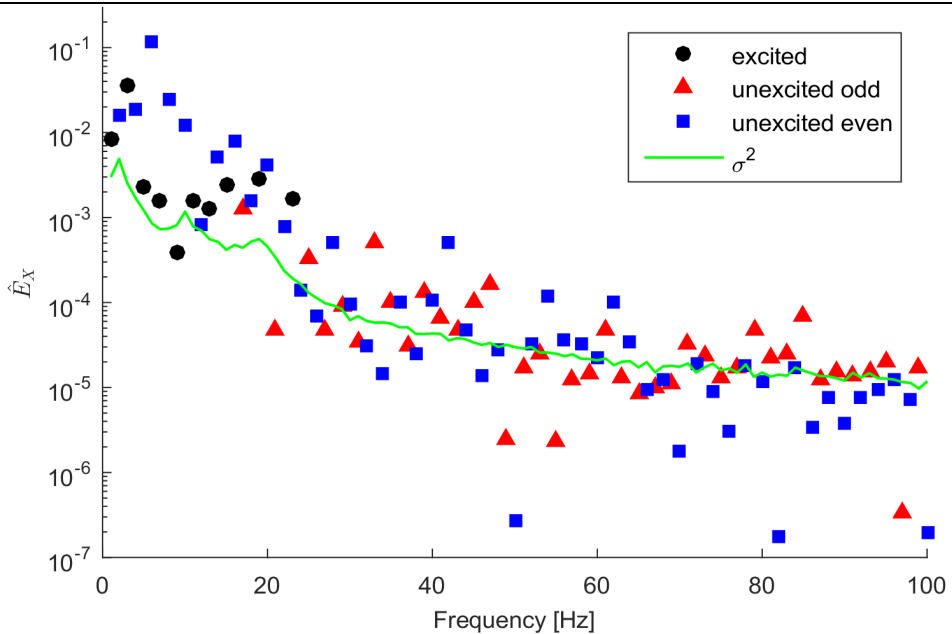
Figure 3.5. Power distribution in EEG$_P$ (CP3) over frequencies for one realization of the passive task for a representative participant. Results are averaged over P = 210 periods. Black dots represent the excited frequencies, red triangles represent the unexcited odd frequencies and the blue squares represent the unexcited even frequencies. The (scaled) noise level is indicated by the green line.

muscles, except for the phase being 180 degrees shifted. This corresponds to the unidirectional nature of the muscles, which are only able to actively contract. The increasing phase lag at the higher frequencies is caused by the neural time delay in the reflex loop.

The FRF for $G_{EEG\varphi}$ indicates that the linear transfer function is of the same order of magnitude as the noise level. Together with the non-smooth and erratic behavior of both gain and phase, this indicates a low quality nonparametric linear model.

Fitting the best nonparametric linear model

We used the best linear approximation as a nonparametric model and obtained the VAF for each of the four input-output relations (see **Table 3.2**). For the passive task the VAF for the relation between the angle φ and the EMG signals is not calculated, since there is no consistent EMG response to the perturbation in this task. An example of the model fit in the time domain for the active task for one representative participant can be found in **Figure 3.7**.

The average VAF for $G_{\varphi T}$ (i.e. mechanical admittance) is around 99% for both the passive task and the active task, indicating the relation between angle and torque is well described by a nonparametric linear model. Due to the high number of recorded periods and subsequent low noise level in this study, the VAF was high compared with other studies were the mechanical admittance was modeled from much less recorded periods. In previous studies on the wrist and other joints (Schouten et al., 2004, Schouten et al., 2008a, Mugge et al., 2010, van Drunen et al., 2013) a VAF between 80% and 95% was obtained when using a parametric linear model to describe the relation between angle and torque. The averaged
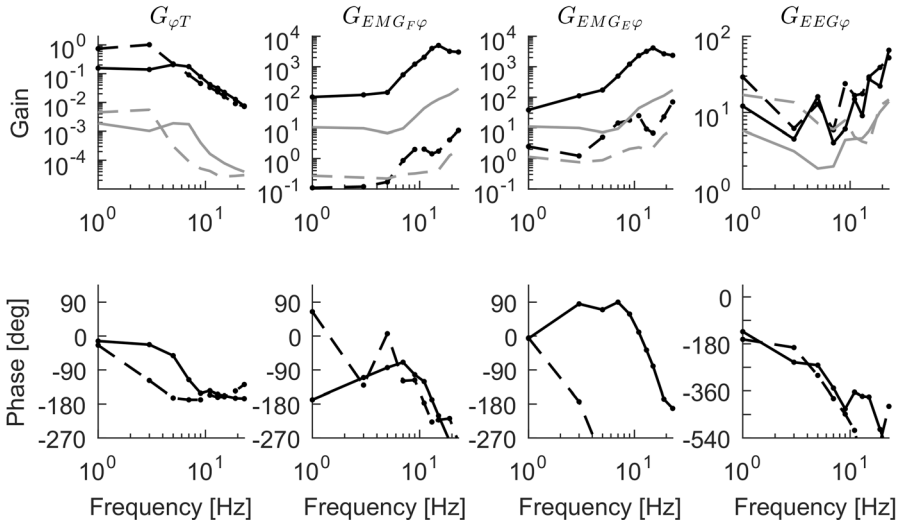
Figure 3.6. Frequency response functions (gain and phase) for a representative participant. The units for $G_{\varphi T}$ are [rad/Nm] and for the other FRF's [μV/rad]. Black lines with markers indicate the FRF at the excited frequencies and gray lines the scaled noise level (see Appendix 3A for equations). Solid and dashed lines represent the active task and passive task respectively. The transfer function $G_{\varphi T}$ is presented as an admittance to correspond to existing literature ($G_{\varphi T} = G_{T\varphi}^{-1}$).

VAF obtained when modeling the EMG signal was around 70% for both muscles, which is slightly higher than the same studies mentioned before where a VAF of 40% to 60% was common when modeling the EMG signals with a parametric linear model. Besides the low noise level, the high flexibility of the nonparametric models used in this study compared with parametric models resulted in a higher VAF. Noteworthy, the relation between the wrist angle and the measured EEG signal is poorly captured by the nonparametric linear model. The averaged VAF is around 10% for both the passive task and active task, thus a linear system description is not appropriate to describe the response in the EEG evoked by mechanical manipulation of the wrist.

3.4 Discussion

Mechanical manipulation of the wrist using multisine signals elicits a periodic response in the EEG, which is shown to be highly nonlinear. Linear system identification techniques were employed and indicate that the wrist torque and EMG response to small changes in wrist angle can be explained for 99% and 70% respectively using a nonparametric linear model. Following the same approach, the response in the EEG could only be explained for 10% with linear methods. Moreover, the power in the cortical response at the unexcited frequencies (i.e. due to nonlinear behavior) is over 80%. Similar results were obtained for all
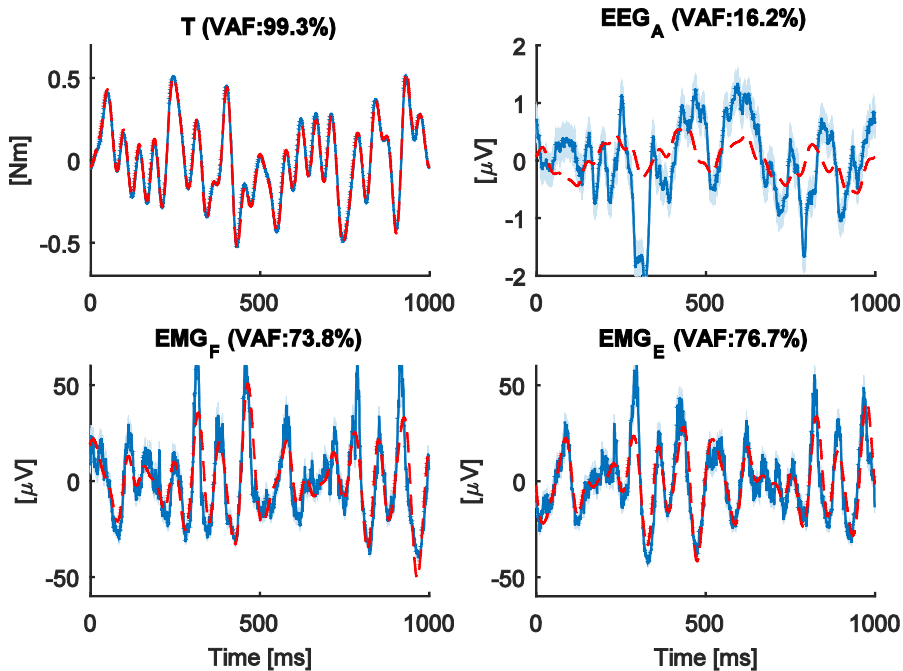
Figure 3.7. Time domain fit of nonparametric linear model (dashed red line) on top of the averaged recorded output (blue line, light blue area represents the averaged response ± the noise level) for one realization of the active task for a representative participant.

Table 3.2. Average VAF for the four nonparametric linear models

	Passive task [%]	Active task [%]
$G_{T\varphi}$	99.5 (0.2)	99.0 (0.3)
$G_{EMG_F\varphi}$	-	70.0 (6.4)
$G_{EMG_E\varphi}$	-	68.0 (8.1)
$G_{EEG\varphi}$	10.0 (4.0)	10.3 (2.3)

participants. Thus, we conclude that a linear description of the relation between stimulus and response in the EEG is inappropriate and a nonlinear description is required.

Quantification of the nonlinear contributions

The use of multisine perturbation signals with power concentrated in a limited number of odd frequency lines, allowed assessment of any power transferred from excited to unexcited frequency lines, which is caused by nonlinear behavior. The method used can detect nonlinear distortions which are periodic with the same period as the perturbation signal. Nonlinear distortions generated by nonlinearities such as chaos and bifurcations, as well as distortions due to time-variant behavior, can therefore not be detected and will increase the noise level. In a previous study using a similar setup, we demonstrated there was no substantial time-variant behavior in the EEG signals evoked by wrist manipulation (Vlaar et al., 2015).

The power in the excited frequencies should not be regarded as 'the linear part of the response' (Snyder, 1992) because odd nonlinear functions can very well affect the signal at the odd excited frequencies. Therefore analyzing the response only at the fundamental (excited) frequencies must be differentiated from studying the linear part of the response. By estimating a (linear) FRF at the excited frequencies and by calculating the VAF, we can assess how well such a linear nonparametric model can describe the input-output relations.

Our results show that for small excursions around an operating point as used in this study the wrist dynamics are mainly linear, as almost 100% of the power in the recorded angle and torque signals is present in the excited frequencies and the VAF when using a nonparametric linear model is over 99%.

For the EMG recordings in the active task the power in the excited frequencies is around 76%. There is clear evidence of nonlinear distortions in the EMG signals, which are possibly introduced by the unidirectional nature of a muscle and stretch reflex. Previous studies on reflex dynamics indeed showed the muscle spindle and reflex loop behaving as a half-wave rectifier (Mirbagheri et al., 2000). A linear model can still describe the EMG response for approximately 70%. Even though the reflexive impedance is nonlinear, paradoxically the mechanical admittance behaves linear. The relation between joint angle and muscle EMG is

nonlinear; however, the flexor and extensor muscles act as two opposing half-wave rectifiers, therewith linearizing the net reflexive behavior.

In contrast to the mechanical and EMG signals, the excited frequencies for the EEG signal account for only 17% of the total signal power, indicating the EEG signal is dominated by nonlinear contributions. The relation between input and output therefore cannot be described by an FRF at the excited frequencies, since it only takes a small portion of the output into account and therefore results in a low VAF (~10%). Most power in the EEG signal, over 75% for both the passive and active task, is in the even frequency lines, indicating the presence of a dominant even nonlinear function. Examples of an even nonlinear function are $y(u)=u^2$, $y(u)=u^4$ and $y(u)=abs(u)$. Seiss et al. (2002) and Campfens et al. (2015a) showed that a stretch of respectively the finger and wrist resulted in a similar ERP for both flexion and extension direction, which also indicates an even nonlinear relation.

Origin of nonlinear contributions

The nonlinear behavior of the muscle spindles (Houk et al., 1981, Hasan, 1983, Mileusnic et al., 2006) is likely to add to the nonlinear contributions in the EMG response. Their unidirectional sensitivity to velocity changes, together with their position in antagonistic muscles, could result in a similar neural signal for both flexion and extension. When using EEG to record these neural signals from the cortex, the distance between processing sites might be too small to be distinguishable, resulting in a lumped response of flexor and extensor muscle spindles. This response would, due to the similar signal for flexion and extension, result in an even nonlinear relation between stimulus and recorded EEG.

Passive and active task

Similar results for the EEG response are obtained for the passive and active task: the NSR as well as the distribution of power over frequency groups are of the same order of magnitude in both tasks. The NSR is slightly lower in the active task and low NSR is found in a larger region compared with the passive task. There are several possible explanations for these small changes. In the active task the muscles are generating force due to both co-contraction and reflexive activity, resulting in increased wrist torque. Compared with the passive task, this will result in changed muscle spindle sensitivity (Dimitriou, 2014) and an increase in output of the Golgi tendon organ (Crago et al., 1982). Changes in EEG could also be due to the involvement of additional brain regions in voluntary co-contraction during the active task (e.g., supplementary motor area, pre-motor cortex, posterior parietal cortex) (Scott, 2012).

Implications

When applying a mechanical (multi)sine stimulus signal to a linear system, the response will occur only at the exited frequencies. In a nonlinear system, the frequency domain analysis of the response must consider excited frequencies and their harmonics and intermodulation products. Taking all these components into account will elucidate which nonlinear model could appropriately describe the relationship. In this study we have shown that the larger part

of the EEG response to small mechanical perturbations, and therefore most information, is found in the unexcited frequencies, indicating nonlinear behavior.

When applying transient sensory stimuli, the resulting average response is called the event-related potential (ERP). Information about the sensory system is derived from the timing of certain components in the ERP, for example the negative deflection 20 ms after electrical stimulation (N20) (see (Cruccu et al., 2008) for more details on somatosensory evoked potentials). Although the ERP technique is widely used, it often overlooks that neurophysiological systems exhibit nonlinear behavior. In a linear system the response scales proportionally with the stimulus amplitude and the shape of the response remains the same (e.g. doubling the input amplitude results in a doubled output amplitude), whereas in a nonlinear system both the shape and amplitude of the response will vary with applied stimulus amplitude. Several studies on mechanically somatosensory responses show that the shape of the ERP changes with the amplitude of the mechanical stimulus (Franzén and Offenloch, 1969, Johnson et al., 1980, Hashimoto et al., 1992, Lin and Kajola, 2003). Due to this nonlinear behavior of the system (also shown in our results) the shape of the response and subsequently the timing of characteristic peaks will change with a change in amplitude of the sensory stimulus. Due to the nonlinear behavior of the system its characteristics cannot be fully captured by responses to a transient stimulus (ERP) or by responses to a continuous stimulus at only the excited frequency (e.g. Goto et al., 2003, Nangini et al., 2006, Voisin et al., 2011a).

Our results have shown that the relation between mechanical manipulation of the wrist joint and the response in the EEG cannot be described by a nonparametric linear model (VAF: ~10%), demonstrating nonlinear behavior. Consequently, a linear model or method will not be able to capture the relation between stimulus and response. An example is found in directed corticomuscular (linear) coherence, where poor linearization might contribute to inconsistently estimated time delays between cortex and muscle (e.g. Witham et al., 2011).

The observed nonlinear behavior is periodic with the same period as the perturbation signal. Even though there is still substantial noise left in the EEG signals after averaging, a perfect model should be able to describe over 80% of the relation between wrist movement and recorded EEG. By using nonlinear modeling techniques we should be able to provide a better description of the input-output relationship. There exists an infinite amount of nonlinear operators and nonlinear model structures and this study provides essential information on the nature of the nonlinearity in the system. The next step in this research will be to obtain a nonlinear model relating the imposed wrist movement to the recorded EEG signals, therewith improving the understanding of the human sensory system and ultimately providing insight in movement disorders.

Both ERP's and cortical responses to continuous stimulation have been obtained using other types of stimuli such as visual, auditory and electrical nerve stimulation. The cortical responses to these types of stimuli also shows higher harmonics of the stimulation frequency

(Narici et al., 1998). The nonlinear contributions to the response, when these stimuli are applied, can be quantified using the techniques described in this study.

3.5 Conclusions

- Multisine perturbation signals applied to the wrist elicit a periodic cortical response and allow assessment of nonlinear contributions to the response.
- When studied in a small range, wrist dynamics can be successfully linearized.
- The relationship between mechanical stimulus and cortical response is highly nonlinear. Over 80% of the cortical response is caused by nonlinear behavior of the system. We showed that a nonparametric linear model only explains 10% of the cortical response to mechanical joint manipulation.
- Event related potentials are insufficient to fully characterize the highly nonlinear relationship between mechanical stimulus and EEG response.

3.6 Acknowledgments

3.7 Appendix 3A

The following equations allow for estimation of the sample mean and sample (co)variance for each recorded signal or signal combination (Pintelon and Schoukens, 2012). $X(f)$ and $Z(f)$ refer to Fourier transformed recorded signals, which can be the same or different signals.

First the phase in the recorded signal is turned back by the phase in the perturbation signal (R) (3.12), which allows for averaging over the different realizations (3.14):

$$X_R^{[m,p]}(f) = \frac{X^{[m,p]}(f)}{e^{j\angle R^{[m]}(f)}}, \tag{3.12}$$

$$\hat{X}_R^{[m]}(f) = \frac{1}{P}\sum_{p=1}^{P} X_R^{[m,p]}(f), \tag{3.13}$$

$$\hat{X}_R(f) = \frac{1}{M}\sum_{m=1}^{M} \hat{X}_R^{[m]}(f). \tag{3.14}$$

The sample (co)variance for each recorded signal or signal combination is estimated in (3.15) and averaged over realizations in (3.16):

$$\hat{\sigma}_{X_R Z_R,n}^{2[m]}(f) = \frac{1}{P(P-1)}\sum_{p=1}^{P}\begin{pmatrix}\left(X_R^{[m,p]}(f) - \hat{X}_R^{[m]}(f)\right)\\ \cdot\left(Z_R^{[m,p]}(f) - \hat{Z}_R^{[m]}(f)\right)\end{pmatrix}, \tag{3.15}$$

$$\hat{\sigma}_{X_R Z_R,n}^{2}(f) = \frac{1}{M^2}\sum_{m=1}^{M}\hat{\sigma}_{X_R Z_R,n}^{2[m]}(f) \tag{3.16}$$

The FRF and its noise variance at the excited frequencies are obtained by inserting the recorded input and output signals of interest into equation A1-A5 and subsequently inserting the result in (3.17) and (3.18):

$$\hat{G}_{BLA}(f_{ex}) = \frac{\hat{S}_{\hat{Y}R}(f_{ex})}{\hat{S}_{\hat{U}R}(f_{ex})} = \frac{\hat{Y}_R(f_{ex})}{\hat{U}_R(f_{ex})}, \tag{3.17}$$

$$\hat{\sigma}_{N_G}^{2}(f_{ex}) = \left|\hat{G}_{BLA}(f_{ex})\right|^2\begin{pmatrix}\dfrac{\hat{\sigma}_{Y_R,n}^{2}(f_{ex})}{\left|\hat{Y}_R(f_{ex})\right|^2} + \dfrac{\hat{\sigma}_{U_R,n}^{2}(f_{ex})}{\left|\hat{U}_R(f_{ex})\right|^2}\\ -2\,\mathrm{Re}\left(\dfrac{\hat{\sigma}_{Y_R U_R,n}^{2}(f_{ex})}{\hat{Y}_R(f_{ex})\overline{\hat{U}_R(f_{ex})}}\right)\end{pmatrix}. \tag{3.18}$$

Chapter 4

Modeling the Nonlinear Cortical Response in EEG Evoked by Wrist Joint Manipulation

Martijn P. Vlaar, Georgios Birpoutsoukis, John Lataire, Maarten Schoukens,
Alfred C. Schouten, Johan Schoukens, and Frans C.T. van der Helm

Joint manipulation elicits a response from the sensors in the periphery which, via the spinal cord, arrives in the cortex. The evoked cortical response recorded using electroencephalography was shown to be highly nonlinear; a linear model can only explain 10% of the response, and over 80% of the response is generated by nonlinear behavior. The goal of this study is to obtain a nonparametric nonlinear dynamic model, which can consistently explain the recorded cortical response requiring little a priori assumptions about model structure. Wrist joint manipulation was applied in ten unimpaired participants during which their cortical activity was recorded and modeled using a truncated Volterra series. The obtained models could explain 46% of the cortical response, thereby demonstrating the relevance of nonlinear modeling. The high similarity of the obtained models across participants indicates that the models reveal common characteristics of the underlying system. The models show predominantly high-pass behavior, which suggests that velocity-related information originating from the muscle spindles governs the cortical response. In conclusion, the nonlinear modeling approach using a truncated Volterra series with regularization, provides a quantitative way of investigating the sensorimotor system, offering insight into the underlying physiology.

4.1 Introduction

Healthy movement control requires proprioceptive information from the periphery to reach the cortex; this sensory information is required for generating internal models enabling accurate planned movements (feedforward control) and for generating appropriate responses to disturbances (feedback control). Understanding the relationship between a movement and the cortical response improves the understanding of the sensorimotor system and can aid in unravelling sensorimotor dysfunction in movement disorders. Studying the dynamic relations within the sensorimotor system requires applying a proprioceptive stimulus, a clear task instruction and a cortical measurement technique with high temporal resolution such as electroencephalography (EEG) or magnetencephalography. EEG is a noninvasive technique with mild experimental restrictions with respect to movement and is widely available. Applying a continuous proprioceptive stimulus by manipulation a joint (e.g. wrist or finger) allows for studying the system in steady state, i.e. when it is continuously and consistently engaged in processing sensory signals.

Cortical responses to continuous proprioceptive stimulation in unimpaired individuals have been investigated during both active (Campfens et al., 2013, Yang et al., 2016b, Vlaar et al., 2017b) and passive (Vlaar et al., 2017b) conditions using EEG. These studies revealed that the system under study is highly nonlinear. A linear approach to model the relation between proprioceptive stimulus and cortical response can only capture 10% of the relationship (Vlaar et al., 2017b; Chapter 3); nonlinear modeling of this relation has not been done before.

This study sets out to obtain a nonparametric nonlinear dynamic model which consistently (i.e. consistently over different input signals) describes the relation between wrist movement and the average evoked cortical response recorded using EEG. The evoked cortical response showed no strong presence of subharmonics (Vlaar et al., 2015; Chapter 2), therefore a Volterra series should be able to describe the underlying physiological process. Here, the system is modeled using a truncated Volterra series with regularization (Birpoutsoukis et al., 2017a). Such a model requires limited a priori knowledge about the system, while allowing for a quantitative description of the dynamics of the sensorimotor system.

The experimental setup, perturbation signals used, and the modeling approach are presented in the Methods section. The Results section provides the characteristics of the recorded cortical signals, the performance of the models and their dynamic behavior. The Discussion section interprets the models based on physiology and provides a reflection on the approach, including suggestions for future work.

4.2 Methods

Participants and experimental protocol

Ten unimpaired right-handed participants (age range 22-25 years; 5 men) participated in the study (Vlaar et al., 2017b). The study was approved by the local ethics committee and all participants gave written informed consent prior to participation. Data of these participants

were collected in a previous study; a summary of the relevant aspects of the experimental protocol will be presented here, for a full description the reader is referred to (Vlaar et al., 2017b; Chapter 3). Participants were seated with their right forearm fixated to an arm support and their hand strapped to the handle of a robotic manipulator (Wristalyzer by MOOG Inc, Nieuw-Vennep, The Netherlands). Participants were instructed to relax their wrist and not react to the continuous angular perturbation applied by the robotic manipulator.

The perturbation signals were random phase multisine signals (i.e. the sum of several sinusoids, each with a random phase). In multisine perturbation signals, there is full control over the frequency content, leading to several advantages over random signals when performing system identification (Pintelon and Schoukens, 2012). These advantages include the ability to detect even and odd nonlinear behavior, which is facilitated by the use of multisine signals with only odd frequency lines excited (Pintelon and Schoukens, 2012). The perturbations were multisine signals with a period of 1 s, resulting in a fundamental frequency of 1 Hz. Only selected odd harmonics of the fundamental frequency were excited, namely 1, 3, 5, 7, 9, 11, 13, 15, 19, and 23 Hz. Exciting the nonlinear system using different phase realizations of a multisine signal (i.e. same amplitude per frequency, yet other random phases) allows for using different data sets for estimation and validation when modeling. Seven different multisine realizations were generated which were alternatingly applied during 49 trials of 36 seconds. Six seconds were removed from each trial to reduce transient effects, resulting in a total of 1470 recorded periods, i.e. 210 periods available for each of the seven realizations.

The angular perturbations had a root-mean-square (RMS) of 0.02 rad (see left insert in **Figure 4.1**) and were applied with the wrist in a relaxed angle (i.e. slight flexion). The signals were designed to have equal power on the first three excited frequencies and a decreasing power for the higher frequencies (-20dB/decade slope), which is a tradeoff between reduced predictability of the signal (to prevent anticipation) and capabilities of the robotic manipulator.

Cortical activity was sampled at 2048 Hz from 126 electrodes using an EEG amplifier (Refa by TMSi, Oldenzaal, The Netherlands). The handle angle of the robotic manipulator was, via a galvanic isolation transformer (TMSi, Oldenzaal, The Netherlands), recorded by the same amplifier.

Preprocessing

EEG data were high-pass filtered using a fourth order Butterworth filter with a cut-off frequency of 1Hz to attenuate noise at frequencies lower than the fundamental frequency of the perturbation signal. This filter was applied in two directions to achieve zero-phase filtering. Independent component analysis (ICA)(Makeig et al., 1996a) was performed using the Infomax algorithm (Bell and Sejnowski, 1995) as implemented in CUDAICA (Raimondo et al., 2012). Subsequently, the data at component level were segmented into periods, resulting in $x^{(c,m,p)}(n)$, where x is the response, $c = 1,…,C$ is the component (C=125), $m =$

$1,\dots,M$ is the multisine realization ($M=7$), $p = 1,\dots,P$ is the period ($P = 210$) and $n = 1,\dots,N$ is the time index. An ideal filter was used to remove line noise (50 Hz) and to remove all frequencies from 100 Hz onward; i.e. signals were transformed to the frequency domain using the discrete Fourier transform (DFT)(Briggs and Henson), all mentioned frequency lines were set to zero, and the signals were converted back to the time domain using the inverse DFT. The use of periodic perturbation signals allows for the application of such a frequency domain filter without causing transient effects in the time domain representation of the data. Subsequently, all signals were resampled to 256 Hz ($N = 256$ samples) to reduce the amount of data; as there are no high frequencies present in the data anymore, this can be done without loss of information.

To characterize the response of each component both the power in the average response (4.1) as well as the sample variance (4.2) were calculated at each frequency

$$\hat{E}_X^{[c,m]}(f) = \left| \frac{1}{P} \sum_{p=1}^{P} X^{[c,m,p]}(f) \right|^2 \tag{4.1}$$

$$\hat{\sigma}_X^{2[c,m]}(f) = \frac{1}{P(P-1)} \sum_{p=1}^{P} \left| X^{[c,m,p]}(f) - \frac{1}{P} \sum_{p=1}^{P} X^{[c,m,p]}(f) \right|^2 \tag{4.2}$$

where X(f) is the DFT of x(n). To find the component which is most associated with the perturbation signals, the noise-to-signal ratio (NSR) was calculated; the component with the lowest NSR demonstrates the most consistent response. The NSR is defined as
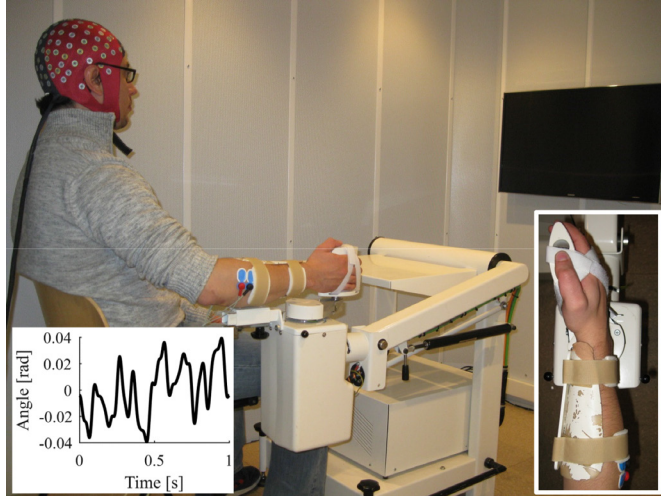
Figure 4.1. Experimental setup. The right forearm of the participant is strapped into an armrest and the right hand is strapped to the handle, requiring no hand force to hold the handle. Participants were instructed to gaze at the screen, which showed a static target. The insert on the left shows one of the realizations of the perturbation signal. The insert on the right shows a close up of the hand in the robotic manipulator. The wrist joint was aligned to the axis of rotation of the manipulator.

$$NSR^{[c,m]} = \frac{\sum_{f \in F} \hat{\sigma}_X^{2[c,m]}(f)}{\sum_{f \in F} \hat{E}_X^{[c,m]}(f)}, \tag{4.3}$$

where F is the set of considered frequencies. For each participant, the NSR of each component c was determined by calculating the NSR over all frequencies and by subsequently averaging across realizations m. The signal of the component with the lowest NSR is defined as $y^{[m,p]}(n)$ and this signal was used for subsequent modeling. This signal was averaged over the recorded periods to reduce noise, and was subsequently defined as $y^{[m]}(n)$ and transformed to the frequency domain using the DFT, resulting in $Y^{[m]}(f)$. Similarly, the recorded input signal (i.e. wrist joint angle) was averaged over the recorded periods, giving $u^{[m]}(n)$ and transformed to the frequency domain, resulting in $U^{[m]}(f)$.

Distinguishing the spectral contributions

The frequency content of the response of a static nonlinear system is governed by the order of the system as well as by the frequency content of the input signal. A quadratic static nonlinear system ($y=u^2$, which is an even nonlinearity) generates an output spectrum containing all possible combinations of two (positive or negative) input frequencies. In the case where only one input frequency is excited (e.g. f_0), the output will contain $f_0 + f_0 = 2f_0$, and also $f_0 - f_0 = 0$. This concept extends for higher order systems and is described in more detail in (Schoukens et al., 2016, pp. 43, Fig. 9).

By the virtue of exciting only the odd frequency lines in the perturbation signals, the frequencies in the averaged output signal can be split into four groups. The first frequency group ($f_{\{1\}}$) consists of the excited frequencies in the input signal. The response at these frequencies will represent the linear contributions as well as part of the higher order odd (e.g. 3rd, 5th and 7th order) nonlinear contributions. The second group ($f_{\{2\}}$) consists of all the frequencies that can come from 2nd order nonlinear contributions ($f_{\{1\},1} \pm f_{\{1\},2}$), as well as part of the higher order even (e.g. 4th and 6th order) nonlinear contributions. The third group ($f_{\{3\}}$)
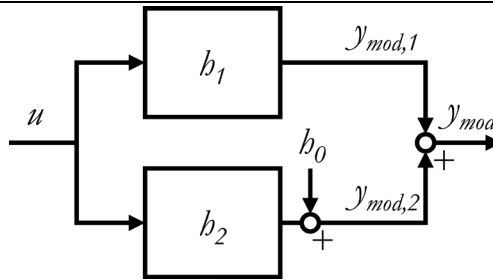
Figure 4.2. Block schematic of the model structure. The top branch is a linear model which governs the output at the excited frequencies (i.e. $f_{\{1\}}$). This model is estimated by calculating the linear frequency response function. The bottom branch is a nonlinear model which is estimated using two terms of the Volterra series, namely the 2nd order kernel h_2 and the 0th order kernel h_0. The 2nd order kernel governs the output at $f_{\{2\}}$. The 0th order kernel is included to account for the potentially nonzero-mean signals generated by the 2nd order kernel.

consists of all odd frequencies not in $f_{\{1\}}$, which are the result of higher order odd (3rd order or higher) nonlinear contributions. The fourth and final group ($f_{\{4\}}$) consists of all even frequencies not in $f_{\{2\}}$, which are the result of higher order even (4th order or higher) nonlinear contributions. The total power in the signal can be split amongst these frequency groups to determine their individual contributions. Additionally, in all frequency groups there are still noise contributions present, given that the NSR is not reduced to zero. The NSR per frequency group is calculated using (4.3). The noise level in the averaged output signals puts a theoretical limit on the modeling accuracy, as that portion of the output data cannot be explained by a model.

Model structure

The block scheme in **Figure 4.2** illustrates the modeling approach. The relation between joint angle (input) and cortical response as represented by the selected component (output) is modeled. The model consists of two parallel branches, specifically one 1st order and one 2nd order model. The latter also includes a 0th order model; due to filtering, the recorded output signal is zero-mean, yet the 2nd order model should not be restricted to produce a zero-mean output. The models in the two branches can be obtained in two separate modeling steps, as the 1st order model can only affect the output at $f_{\{1\}}$, and the 2nd order model can only affect the output at $f_{\{2\}}$ (i.e. using an odd perturbation signal, the two models are orthogonal). As a final step the two models are combined.

The 1st order (linear) model h_1 will be estimated in the frequency domain at the excited frequencies ($f_{\{1\}}$) in the input and at the same frequencies in the output, resulting in the best linear approximation (BLA) (Pintelon and Schoukens, 2012). The frequency domain representation of this model is defined as $H_1(f)$.

The 2nd order (nonlinear) model is estimated using a truncated Volterra series expansion (Schetzen, 1980), which is similar to a Taylor series expansion, yet it includes dynamics. Regularization is used to incorporate prior information during the modeling procedure. Namely, by assuming that the model parameters are correlated and that the models decay to zero after a certain time, appropriate penalties can be imposed on the model estimation, which results in estimated models of substantially lower uncertainty. Regularization has previously been applied to linear (Chen et al., 2012, Lataire and Chen, 2016) and nonlinear (Pillonetto et al., 2011, Risuleo et al., 2015) model estimation, such that prior information about the estimated models is used during the identification step. Regularization imposing correlation and model decay for estimation of Volterra kernels has only recently been introduced (Birpoutsoukis et al., 2017a).

Volterra kernel estimation using regularization

The true underlying even nonlinear contributions in the output y at $f_{\{2\}}$ (defined as y2) are modeled with two terms of a discrete-time Volterra series (Schetzen, 1980), namely the 2nd order kernel h_2 and the 0th order kernel (i.e. constant term) h_0:

$$y_{mod,2}(n) = \sum_{\tau_1=0}^{d_2-1}\sum_{\tau_2=0}^{d_2-1} h_2(\tau_1, \tau_2) u(n-\tau_1) u(n-\tau_2) + h_0 \tag{4.4}$$

where $u(n)$ denotes the recorded joint angle, $y_{mod,2}(n)$ represents the modeled cortical response at $f_{\{2\}}$ (including 0 Hz), $h_2(\tau_1, \tau_2)$ is the 2nd order Volterra kernel, τ_1 and τ_2 denote lag variables, and d_2 corresponds to the memory of h_2. Without loss of generality, the estimated Volterra kernels are considered to be symmetric. An example of a function $h_2(\tau_1, \tau_2)$ is given in **Figure 4.3**. Given the measured signals u and y, the goal is to efficiently estimate the Volterra kernel coefficients h_0 and $h_2(\tau_1, \tau_2)$. Equation (4.4) can be rewritten into a vectorial form as:

$$\overline{y}_{mod,2} = K \begin{bmatrix} h_0 \\ \theta_2 \end{bmatrix} \tag{4.5}$$

where $\theta_2 \in \mathbb{R}^{n\theta_2}$ is a vectorized version of h_2, $n\theta_2$ denotes the number of coefficients in h_2, $K \in \mathbb{R}^{(N\cdot M)\times(n\theta_2+1)}$ is the regressor matrix, and $\overline{y}_{mod,2} \in \mathbb{R}^{(N\cdot M)}$ contains the modeled output.

The regressor matrix K contains the input signal, which includes samples from time instants before the beginning of the input signal ($u(n)$, $n<0$); however, due to the periodicity of the data the signal at those time instants is known.

The model parameters h_0 and θ_2 are estimated by minimizing the regularized least squares cost function:

$$\begin{bmatrix} \hat{h}_0 \\ \hat{\theta}_2 \end{bmatrix} = \arg\min_{\theta} \left\| \overline{y}_2 - K \begin{bmatrix} h_0 \\ \theta_2 \end{bmatrix} \right\|_2^2 + \sigma^2 \begin{bmatrix} h_0 \\ \theta_2 \end{bmatrix}^{\mathrm{T}} \mathcal{P}^{-1} \begin{bmatrix} h_0 \\ \theta_2 \end{bmatrix}$$
$$= \left(K^T K + \sigma^2 \mathcal{P}^{-1} \right)^{-1} K^T \overline{y}_2 \tag{4.6}$$

where $\overline{y}_2$ is the vectorized recorded output data, which is assumed to be contaminated by zero mean i.i.d. white noise with finite variance σ^2. The first term of the summation in the cost function minimizes the difference between the recorded output and the modeled output in a least-squares sense. Matrix $\mathcal{P}$ penalizes the parameters such that prior information about the underlying dynamics of the true system is taken into account. The regularization matrix $\mathcal{P} \in \mathbb{R}^{(n\theta_2+1)\cdot(n\theta_2+1)}$ is constructed using a Bayesian perspective as explained in (Pillonetto et al., 2011, Chen et al., 2012). The matrix $\mathcal{P}$ is a block-diagonal covariance matrix:

$$\mathcal{P} = \begin{bmatrix} \mathcal{P}_0 & 0 \\ 0 & \mathcal{P}_2 \end{bmatrix}, \tag{4.7}$$

where $\mathcal{P}_0 = \mathrm{E}\left[h_0 h_0^{\mathrm{T}} \right]$, $\mathcal{P}_2 = \mathrm{E}\left[\theta_2 \theta_2^{\mathrm{T}} \right]$ and $\mathrm{E}[\cdot]$ denotes the mathematical expectation operator.

The prior information encoded in the matrix $\mathcal{P}$ assumes that the Volterra kernels used to describe the true system are decaying and smooth. The property of decaying refers to the fact that $h_2(\tau_1,\tau_2){\to}0$ for $\tau_1,\tau_2{\to}\infty$. For the discrete-time Volterra series used in the current study, a smooth estimated kernel means that there exists a certain level of correlation between neighboring coefficients, which decreases the larger the distance between two Volterra coefficients. The properties of decaying and smoothness for the 2nd order Volterra kernel are encoded into the matrix $\mathcal{P}_2$. The (i,j)-element, which corresponds to $\mathrm{E}\left[\theta_{2,i}\,\theta_{2,j}\right]\forall i,j$ where $\theta_{2,i}\,\theta_{2,j}$ denote two Volterra coefficients in θ_2, is given by (Birpoutsoukis et al., 2017a):

$$\mathcal{P}_2\left(i,j\right) = c\,e^{-a_\mu\left\|\mu_i\right|-\left|\mu_j\right\|}e^{-\beta_\mu\frac{\left\|\mu_i\right|+\left|\mu_j\right\|}{2}}e^{-a_\nu\left\|\nu_i\right|-\left|\nu_j\right\|}e^{-\beta_\nu\frac{\left\|\nu_i\right|+\left|\nu_j\right\|}{2}} \qquad (4.8)$$

where the coordinate system μ,ν is rotated 45 degrees counter-clockwise with respect to coordinate system τ_1,τ_2 (see **Figure 4.3**):

$$\begin{bmatrix} \mu_i \\ \nu_i \end{bmatrix} = \begin{bmatrix} cos(45^o) & -sin(45^o) \\ sin(45^o) & cos(45^o) \end{bmatrix}\begin{bmatrix} \tau_{1,i} \\ \tau_{2,i} \end{bmatrix} \qquad (4.9)$$

The so-called hyper-parameters a_μ and a_ν are used to control the smoothness property of the coefficients along the μ and ν direction, respectively. The hyper-parameters β_μ and β_ν determine the decay rate along the μ and ν direction, respectively. Hyper-parameter c is a scaling factor used to determine the optimal trade-off between the measured data and the prior information encoded in $\mathcal{P}_2$.

Efficient tuning of the prior knowledge

All the hyper-parameters, namely c, a_μ, β_μ, a_ν, β_ν, σ^2 and $\mathcal{P}_0$ are tuned with the use of the input and output data by maximizing the marginal likelihood of the measured output (Rasmussen and Williams, 2006). Once the optimal values for the hyper-parameters are obtained, the model can be estimated from (4.6). Tuning the hyper-parameters is a non-convex
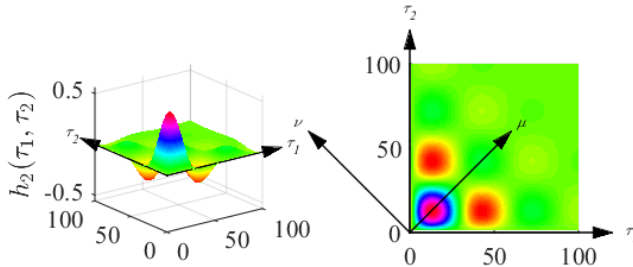
Figure 4.3. Example of a function $h_2(\tau_1,\tau_2)$. The model corresponds to a Wiener-structure with a linear system followed by a square-operator. The **left graph** shows a 3D view of the model h_2. The **right graph** shows the same model from a top view, with additionally an indication of the directions μ and ν, along which the smoothness and decay rate of the model were quantified during regularization. The colors of the surface indicate amplitude.

optimization problem. To facilitate the algorithm and increase the probability of reaching the global maximum, the hyper-parameter space is restricted. Specifically: (i) $c, \sigma^2, \mathcal{P}_0 > 0$ because they are all directly linked to a measure of variance; (ii) The upper bound for a_μ and a_ν is 2 samples^{-1} which results in no correlation between the coefficients in the corresponding direction. The lower bound is set equal to $1/(5d_2)$ samples^{-1}, which would result in a strong correlation between all the coefficients of $h_2(\tau_1, \tau_2)$ and therefore an almost flat surface; and (iii) the upper bound for β_μ and β_ν is 2 samples^{-1}, which means that the estimated surface will decay in general almost immediately after one or two lags. The lower bound is set equal to $3/d_2$ samples^{-1}, which means that the estimated model will have virtually decayed to zero at the truncation lag of the model imposed by the memory d_2 [see (4.4)]. To further minimize the risk of resulting in a local maximum of the non-convex marginal likelihood function, the models presented in this paper have been obtained after multi-start optimization of the hyper-parameters.

Preparing the data for modeling

The perturbation signals were designed to have power at particular frequencies: the excited frequencies. Any power in the recorded wrist joint angle signal (i.e. the input to the human) at the unexcited frequencies was assumed to be due to nonlinear behavior of the robotic manipulator or noise; namely it is assumed that the human does not influence the angle of the robotic manipulator. The power at these frequencies was checked to be minimal and was subsequently removed from the recorded input signal to prevent the estimated model from using the power at the unexcited frequencies to explain the recorded output signals.

The recorded signals for the seven realizations were scaled to set their RMS to approximately one. The same scaling was applied to each realization to maintain their interrelations. The scaling was performed for both the input and output signals to prevent numerical problems in the nonlinear optimization of the hyper-parameters.

There is a time delay between the applied joint manipulation at the wrist and the evoked response in the cortex, which is a consequence of the limited conduction velocity in the afferent nerve fibers as well as of synapses in the pathway. For all participants the recorded output signals were shifted in time to impose a time delay of 20 ms.

Model estimation procedure

There are $M = 7$ multisine realizations available in the input and output data. Out of those seven, six realizations are used for estimation and the remaining realization is used for validation to assess the quality of the model. This procedure is repeated seven times to achieve seven-fold cross-validation, resulting in seven models for each branch in **Figure 4.2**.

The linear and odd nonlinear contributions are modeled at the excited frequencies ($f_{\{1\}}$) in the input and output by calculating the average linear frequency response function for the different sets of estimation realizations:

$$\hat{H}_1^{[v]}\left(f_{\{1\}}\right) = \frac{1}{M-1}\sum_{w\in W_v}\frac{Y^{[w]}\left(f_{\{1\}}\right)}{U^{[w]}\left(f_{\{1\}}\right)} \ . \tag{4.10}$$

$$W_v = \{w \in \mathbb{R} \mid 1 \le w \le M, w \ne v\}$$

Here, $\hat{H}_1^{[v]}$ is the model obtained when using realization v for validation, and U and Y are the frequency domain representation of the input (angle) and the output (selected independent component) respectively.

The even nonlinear contributions are also modeled using alternatingly six realizations for estimation and one for validation. The 0th and 2nd order kernels are estimated using (4.6), from $f_{\{1\}}$ in the input signal to $f_{\{2\}}$ in the output signal. As the required memory for the 2nd order kernel is unknown, different memory lengths in the range 10 to 75 samples (approximately 40 to 300 ms) are tried. This results in a set of models $\hat{b}_0^{[v,d_2]}$ and $\hat{b}_2^{[v,d_2]}(\tau_1,\tau_2)$, where v is the realization used for validation and d_2 is the number of samples included as memory of the model [see Eq. (4.4)].

Selecting the memory length of the 2nd order kernel

Modeling the 1st order contributions (the BLA) generates one model for each validation realization and does not require further model selection.

For the 0th and 2nd order Volterra kernel, the modeling error on the validation datasets was calculated for all lags

$$\varepsilon^{[v,d_2]} = \sum_{n=1}^{N}\left(y_{mod,2}^{[v,d_2]}(n) - y^{[v]}(n)\right)^2 , \tag{4.11}$$

where ε is the sum-squared error and $y_{mod,2}^{[v,d_2]}(n)$ is the modeled output using the corresponding 0th and 2nd order models (i.e. $\hat{b}_0^{[v,d_2]}$ and $\hat{b}_2^{[v,d_2]}(\tau_1,\tau_2)$), with validation dataset v as input. The set of 0th and 2nd order models which demonstrated the lowest error were selected and were defined per validation realization v as $\hat{b}_0^{[v]}$ and $\hat{b}_2^{[v]}(\tau_1,\tau_2)$. The obtained set of 2nd order models was transformed to the frequency domain using the two-dimensional DFT at a frequency resolution of 1 Hz, resulting in $\hat{H}_2^{[v]}(f_1,f_2)$.

Model evaluation

The performance of the set of seven models for both the 1st and the 2nd order was evaluated by calculating the variance accounted for (VAF) on the validation data. As there are seven models available, the VAF is reported as its mean across the seven models including the standard deviation. The modeled output was calculated by summing the output of the 0th, 1st and 2nd order models

$$y_{mod,val}^{[v]}\left(n\right) = \hat{b}_0^{[v]} + y_{mod,val,1}^{[v]}\left(n\right) + y_{mod,val,2}^{[v]}\left(n\right) , \tag{4.12}$$

from which the mean was removed. The VAF can be calculated on the 1st and 2nd order contributions separately, or on the total modeled output using

$$VAF_{val}^{[v]} = \left(1 - \frac{\mathrm{var}\left(y_{val}^{[v]}\left(n\right) - y_{mod,val}^{[v]}\left(n\right)\right)}{\mathrm{var}\left(y_{val}^{[v]}\left(n\right)\right)}\right) \cdot 100\% . \tag{4.13}$$

For completeness, the VAF was also calculated on the data used for estimation. This was achieved by calculating the modeled output using the estimation data and concatenating the result into $y_{mod,est,c}^{[v]}$. The six estimation realizations of the recorded averaged output signals $y^{[m]}$ were concatenated into $y_{est,c}^{[v]}$, enabling calculation of the VAF on the estimation data.

4.3 Results

Component selection

Figure 4.4A shows for each participant the topographic representation of the independent component (IC) with the lowest noise-to-signal ratio (NSR). These components for all participants suggest a similarly located cortical source in the contralateral sensorimotor cortices. For each participant, the signal of the shown component was used for modeling.

Signal characteristics and model fit

Table 4.1 reveals that the noise level in the averaged recorded output signal is around 8% for all participants, indicating that the maximum achievable total VAF is around 92%. Additionally, **Table 4.1** shows the ability of the models to fit both the validation and estimation.

Figure 4.5 illustrates for one representative participant how each set of frequencies contributes to the averaged recorded output signal, and further splits the power into modeled (validation) data, unmodeled data and noise. **Figure 4.4B** reveals that the bulk of the power in the averaged recorded output signal is concentrated in $f_{\{2\}}$ and that the contribution of $f_{\{3\}}$ and $f_{\{4\}}$ is small. This finding supports this paper's modeling approach, which focuses on the 1st (linear) and 2nd order (nonlinear) contributions in the recorded output signal.

Between the two models included, the main contribution in terms of VAF comes from the 2nd order model (around 39%). The model performance strongly depends on which realizations were used for estimation and which for validation. The VAF obtained from 1st order model (around 8%) is comparable to that obtained from modeling the electrode level response (Vlaar et al., 2017b; Chapter 3). Besides the modeled data (46%) and the remaining noise in the averaged cortical signals (8%), there is still approximately 46% of unmodeled data.
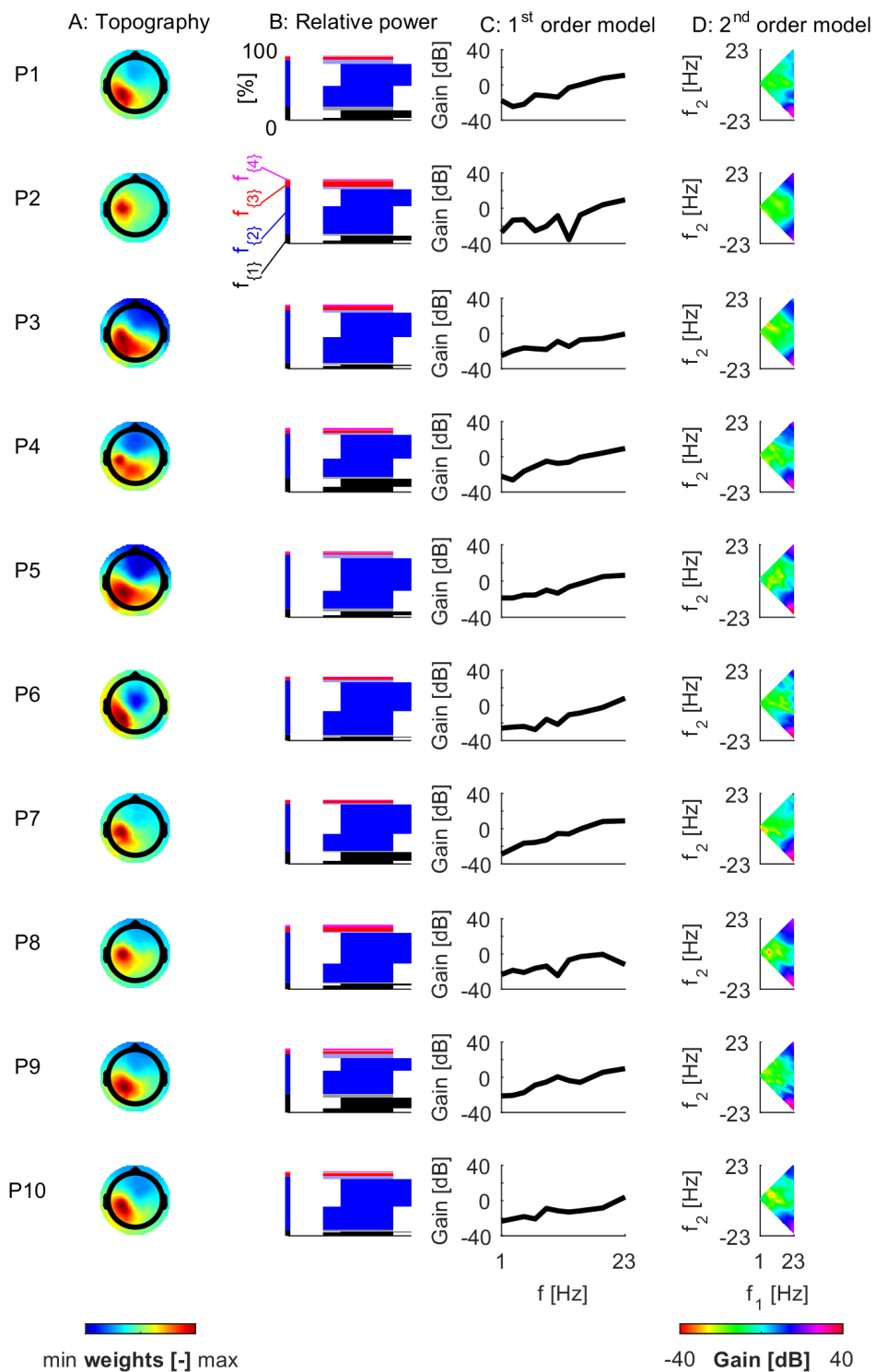
A: Topography   B: Relative power   C: 1st order model   D: 2nd order model

min **weights [-]** max

-40 **Gain [dB]** 40

Table 4.1. Noise levels and model fits. The first ten rows represent the data for the ten participants. NSR presents the noise-to-signal ratio in the cortical response. VAF_{val} total presents the total variance-accounted-for on the validation data. The VAF is also reported separately for the 2nd and 1st order models (H_2 and H_1 respectively) on both the validation and estimation data (VAF_{val} and VAF_{est} respectively). Mean (and standard deviation in parenthesis) across different realizations are presented. The last row represents the mean (and standard deviation in parenthesis) of the results across all participants.

| | NSR | VAF_{val} total | VAF_{val} H_2 | VAF_{est} H_2 | VAF_{val} H_1 | VAF_{est} H_1 |
	[%]	[%]	[%]	[%]	[%]	[%]
P1	15 (2)	45	34 (8)	42 (2)	11 (4)	14 (1)
P2	9 (4)	34	26 (12)	40 (12)	8 (3)	10 (1)
P3	7 (3)	40	38 (13)	48 (14)	2 (2)	4 (0)
P4	6 (1)	50	37 (8)	48 (9)	13 (5)	16 (1)
P5	11 (4)	56	50 (11)	58 (7)	6 (3)	8 (1)
P6	8 (2)	46	45 (25)	64 (3)	1 (2)	3 (0)
P7	4 (1)	60	46 (9)	52 (4)	14 (4)	15 (1)
P8	4 (1)	51	48 (7)	55 (7)	3 (4)	5 (1)
P9	15 (3)	36	19 (7)	34 (10)	17 (4)	20 (1)
P10	11 (3)	44	43 (21)	60 (6)	1 (1)	3 (0)
mean	*8 (5)*	*46 (8)*	*39 (10)*	*50 (9)*	*8 (6)*	*10 (6)*

Representative models

Figure 4.4C and **Figure 4.4D** show for each participant one representative model for the 1st and 2nd order respectively (a detailed example of a 2nd order model is given in **Figure 4.6**). Models obtained for the different validation realizations were very similar. The obtained 1st and 2nd order models for all validation realizations can be found in Appendix 4A and 4B, respectively.

The 1st order models shown in **Figure 4.4C** on average only describe 8% of the output data, yet there exists a similarity for models obtained for the different participants; all 1st order models attenuate the low frequencies and amplify the high frequencies.

Figure 4.6 shows the two-dimensional frequency response functions (gain and phase) of the obtained 2nd order model for one representative participant. **Figure 4.6** clearly illustrates which input frequencies contribute to the output. The model has the highest gain in the bottom-right corner, where high frequency input combinations generate low frequency output through intermodulation (e.g. $f_1 = 23$ Hz and $f_2 = -19$ Hz in the input signal contribute to $f_1+f_2 = 4$ Hz in the output signal). The other region with high gains is found in the top right corner, which is again where the high frequencies interact. The lowest gains are found in

---

Figure 4.4 on left page. Signal characteristics and models for each participant (represented by columns). **Column A**: Topographic representation of the weighing of electrodes in the independent component with the lowest NSR. **Column B**: Power distribution over frequency groups in the output signal. The black and blue indented segment represent the VAF_{val} for the 1st and 2nd order models respectively. Shaded segments represent the noise level in that frequency group. See **Figure 4.5** for a detailed explanation for one representative participant. **Column C**: 1st order model for validation realization 5 (linear frequency axis). **Column D**: 2nd order model for validation realization 5 (linear frequency axis). See **Figure 4.6** for a detailed explanation for one representative participant.

the region where the low frequencies in the input interact. This same behavior can be observed in the models for all participants, as shown in **Figure 4.4D**. Similarly to the 1st order model, the 2nd order models seem to exhibit high-pass behavior.

The memory of the selected 2nd order kernels [d_2 in (4.4)] strongly depended on which realization was used for validation and therefore varied within each participant (combined standard deviation of 15 samples). However, the average memory across realizations was similar across participants, with an average memory of 33 samples (standard deviation of 4 samples), corresponding to approximately 130 ms at a sampling rate of 256 Hz.

For each participant, the seven different models obtained from cross-validation were very similar. This holds for both the 1st order and the 2nd order models. Interestingly, the models obtained from the different participants are also similar; all obtained models strongly attenuate the low-frequent input signal and amplify the high-frequent input, resulting in high-pass behavior. The difference between the 1st order and 2nd order model is that although the 2nd order model acts as a high-pass filter, most power in the output is generated at the low frequencies.
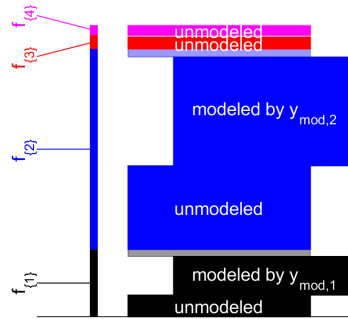
Figure 4.5. Power distribution over frequency groups in the output signal for one representative participant (participant 4). Narrow bar on the left indicates the relative power in the four frequency groups. Wide bar segments on the right further split the power per frequency group into noise (shaded segments without text) and modeled data; the black and blue indented segment represent the VAF_{val} for the 1st and 2nd order model respectively. In this example, the total noise contributions are 6% and the total VAF on the validation data is 50%, where the 1st and 2nd order models explain 13% and 37% respectively (numbers from **Table 4.1**). The power in $f_{\{3\}}$ and $f_{\{4\}}$ cannot be explained using the current model structure.
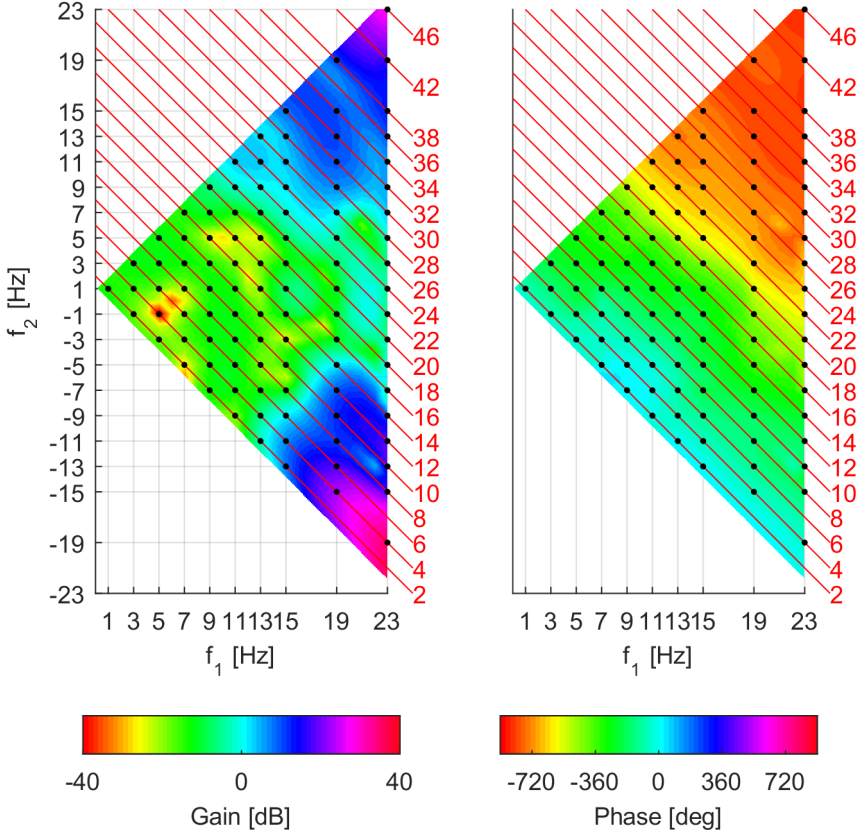
Figure 4.6. Frequency domain representation of a 2nd order model (gain and phase) for one representative participant (participant 4) for validation realization 5. The obtained surface is symmetrical with respect to the line $f_1 = f_2$, as f_1 and f_2 are exchangeable in $\hat{H}_2(f_1, f_2)$. Additionally, as the model at the negative frequencies is the complex conjugate of the model at the same positive frequencies, the full behavior of the model can be represented using one quarter of the entire surface. Red lines and numbers at the right vertical axes indicate the frequencies (in Hz) in $f_{\{2\}}$ in the output signal that result from the excited input frequency combinations $f_{\{1\},1}$ (on the x-axes) and $f_{\{1\},2}$ (on the y-axis) that are indicated by the black dots. The gain graph on the left reveals that combinations of low input frequencies are strongly attenuated (i.e. gains are very low). The highest gains are found in the bottom right corner; in this region the model generates low-frequent output (as indicated by the red numbers) through the intermodulation of the high-frequencies in the input signal. Relatively high gains are also found in the top right corner; in this region the model generates high-frequent output through the intermodulation of again the high-frequencies in the input signal. This behavior can be classified as high-pass behavior.

4.4 Discussion

The goal of this study was to obtain a dynamic nonparametric nonlinear model that could explain the observed cortical response recorded using EEG and evoked by continuous wrist joint manipulation. The high similarity in the cortical response across participants, in terms of location, distribution of power over frequencies, and observed dynamics in both the 1st order (linear) and 2nd order (nonlinear) parts of the model, allow for confident interpretation of the results. On average, 46% of the cortical response could be modeled by the proposed approach; additionally, a clear distinction was made between parts of the cortical signal which could and could not be modeled. Around 8% of the averaged cortical signals could be attributed to noise. The obtained models reveal attenuation of low frequencies and amplification of high frequencies; this behavior can be interpreted as high-pass filtering, probably linked to dominant contributions from velocity-related information via Ia afferents originating from the muscle spindles. This study provides first evidence that the nonlinear cortical response to a proprioceptive stimulus can be quantitatively modeled, as was demonstrated using a truncated Volterra series expansion.

Selection of cortical response

This study focuses on the response most associated with the perturbation signal (i.e. with the lowest NSR). The independent component with the lowest NSR reveals a source at a similar location for each participant, namely the contralateral sensorimotor cortices. This finding is in line with previous literature on somatosensory evoked responses evoked by tactile stimulation of the hand (Snyder, 1992) and by wrist joint manipulation (Campfens et al., 2013), and is also expected based on where afferent fibers carrying proprioceptive and tactile information reach the cortex (Kandel et al., 2000). Besides the similarity in location, these selected cortical responses shared more characteristics across participants. The power distribution over frequencies is very much alike, where most power is concentrated in $f_{\{2\}}$ (see **Figure 4.4B**). Additionally, the dynamics for both the 1st and 2nd order model revealed a comparable high-pass behavior for all participants. These similarities point towards a generalizable cortical response to the applied joint manipulation.

Although the participants also have other components which show a response related to the perturbation signal, none of those were as strong as the one selected for modeling. Other brain regions which are known to be active during somatosensory stimulation under passive conditions include the posterior parietal cortex (Forss et al., 1994a) and the secondary somatosensory cortices (Onishi et al., 2010). The anatomical pathway for both tactile and proprioceptive information is the dorsal column-medial lemniscus pathway. This pathway connects the sensors in the periphery to the contralateral primary somatosensory cortex with only two intermediate synapses, namely in the spinal cord and the thalamus. Responses in other cortical areas are likely to be relayed by the primary somatosensory cortex to the secondary somatosensory cortex and the posterior parietal cortex (Kandel et al., 2000). In those cortical regions the somatosensory signals are further processed and integrated with

motor control. The proposed modeling approach could also be applied to other parts of the cortex that respond to an external somatosensory stimulus.

Physiological origin of the evoked cortical response

The imposed joint rotation is registered by the sensory organs in the periphery and is transported to the cortical regions, where the response is recorded using EEG. This study cannot differentiate to what extent the obtained models are governed by the dynamics of the sensors or by the dynamics in the pathways between sensors, spinal cord and brain regions.

The applied joint manipulation stimulated at least the muscle spindles, Golgi tendon organs (GTO), joint capsules, and tactile sensors (e.g. Meissner's corpuscles, Pacinian corpuscles and Merkel's discs). Applying anesthesia which blocks afferents from tactile sensors and joint capsules did not substantially alter the cortical evoked response to passive finger flexion (Mima et al., 1996), to passive wrist extension (Abbruzzese et al., 1985), or to passive plantar flexions of the ankle (Starr et al., 1981). Additionally, GTO do not generate strong signals under passive conditions, as a slack muscle has lower stiffness than the fibrils of the tendon that activate the GTO. Therefore, it is argued that in this particular study under passive conditions the cortical evoked response is mainly generated by muscle spindles. Muscle spindles sense both length and changes in length (i.e. velocity information). There are two types of fibers originating from the muscle spindles Information is transmitted via Ia and II afferent fibers, which have a high and medium conduction velocity respectively. The II afferent fibers provide position information, while Ia afferent fibers provide either velocity or position information, where the former is dominant during movement. The observed high-pass behavior could originate from the velocity sensitivity of the Ia afferents.

The contribution of the afferent pathways in the observed dynamic behavior is less clear. Insight can be obtained by including a measurement point within those pathways, for example by measuring the output of the muscle spindles using microneurography (Prochazka and Gorassini, 1998).

A possible explanation for the even nonlinear relation between joint manipulation and cortical response is found in the signals generated by muscle spindles in antagonistic muscles (i.e. wrist flexor and extensor); muscle spindles register velocity mainly when the muscle is lengthened and less when shortened (Matthews, 1964), which might be altered by fusimotor activity (Appenteng et al., 1982, Mileusnic et al., 2006). This unidirectional sensitivity makes the muscle spindle behave like a half-wave rectifier for velocity input. In contrast to the stretch reflex, which will activate different muscles depending on stretch direction, the cortical response to either direction generates similar responses in the cortex (Seiss et al., 2002, Campfens et al., 2015a) of which the locations are probably too near to be distinguishable when using EEG; possibly, the half-wave rectifiers in antagonistic muscle pairs together behave as a full-wave rectifier. The resulting insensitivity to direction is a typical characteristic of even nonlinear behavior.

Relation to previous continuous joint manipulation studies

Cortical responses evoked by continuous mechanical stimulation have been studied before (see Vlaar et al. (2015) for an overview); however, most of those studies stimulate the tactile system using high frequent vibrations. The number of studies that apply continuous joint manipulation is limited. The studies that do so, investigate the relation between joint movement and cortical evoked response by perturbing with one specific periodic joint perturbation signal and quantify the relation between stimulus and cortical response using either linear coherence (Campfens et al., 2013, Piitulainen et al., 2013) or higher order cross-spectral coherence (Yang et al., 2016a). Linear coherence in combination with periodic perturbation signals impedes the detection of nonlinear behavior (Maki, 1986) and the obtained coherence is a mix of linear and nonlinear contributions. In contrast, higher order cross-spectral coherence (e.g. bi-coherence) does allow for the detection of nonlinear interactions. Although coherence can detect the strength of the coupling between input and output signal at certain frequencies, it fails to inform on how much of the output signal reflects that specific coupling. For example, in the case of significant coherence it can be concluded there exists a consistent relation between a frequency (or combination of frequencies) in the input and a frequency in the output signal; however, it is unclear to what extent the output signal at that frequency is governed by the input signal at the investigated frequency. In contrast, the current study provides an approach for quantifying the nonlinear interactions in the sensorimotor system through a nonlinear dynamic model, which creates insight into which frequencies in the perturbation signal govern the observed cortical response.

The use of multiple different perturbation signals is essential when modeling a nonlinear system; as the superposition principle does not hold, the model obtained from one perturbation signal is not generalizable to other perturbation signals, even if they have similar characteristics (e.g. RMS and excited frequencies). In the current study, this can be illustrated by estimating the linear relation between the input and output signals for just one realization of the perturbation signal; the resulting frequency response function does not reveal the high-pass behavior observed when using multiple realizations for estimation, and the VAF on any other realization is very poor.

Regardless of which approach is used to investigate the nonlinear relation between joint movement and cortical response, when exciting the system with one specific perturbation signal it is difficult to investigate the characteristics of the underlying system; the cortical response could drastically change when a different perturbation signal is used. Evidently, the use of a repeatedly applied transient stimulus, which is the most common EEG recording paradigm when the investigating somatosensory system, suffers from the same weakness.

Reflection on the experiment

To further improve the perturbation signals for use in nonlinear modeling there are several options. Firstly, by using a longer period more frequencies can be accommodated. This would allow for including lower frequencies and more intermediate frequencies, thus creating

a richer perturbation signal. Secondly, more phase realizations could be used, as apparently the seventh (i.e. validation) realization is in many cases still very different from the six used for modeling. By exciting the system with more phase realizations, the nonlinearity of the system is explored in more detail, which allows for more accurate modeling. Lastly, recording more periods per realizations would further reduce the noise level, although the noise is currently not the main issue as the noise level is much lower than the level of unexplained data (8% and 46% respectively, see **Table 4.1**). As one might expect, any of these three improvements would be accompanied by increased recording time.

The current study investigates the relation between joint manipulation and cortical response under passive conditions, i.e. without voluntary muscle activation. Under both passive and active conditions, any cortical efferent motor drive is not likely to be periodic to the perturbation; feedforward control synchronized to the perturbation would require a predictable perturbation signal, and feedback control via the cortex would be ineffective due to the relative large time delay of a cortical reflex loop. Thus, the evoked cortical response recorded during the execution of a task as described in the current study would reflect mainly sensory information processing.

In this study the joint was studied in a specific 'operating point'. This point constitutes, amongst other aspects, the angle in which the wrist is studied, the frequency content and amplitudes of the perturbation signal, task instruction, and the efferent motor drive. With a change in any of these parameters the operating point could change, possibly requiring a different model. The current study illustrates that by controlling the 'operating point', it is possible to obtain similar models across participants.

Reflection on modeling approach

In the current study, the system under study is described by a 1st and 2nd order model. The power in $f_{\{3\}}$ and $f_{\{4\}}$ is small (around 10%, see **Figure 4.4B**), indicating that the cortical response has little power at frequencies that can only be generated by 3rd and higher order nonlinearities. However, from this observation it cannot be concluded that there are no nonlinearities in the system higher than the 2nd order; high frequencies generated by higher order nonlinearities could be attenuated by low-pass dynamics. Any attempt to model higher order odd nonlinear behavior would result in a maximal VAF increase of around 9%, which corresponds to the unmodeled signal in $f_{\{1\}}$ and $f_{\{3\}}$. It would be beneficial to include higher order even Volterra kernels (e.g. a 4th order model); if the system under study indeed includes a rectifier as proposed before, higher order even kernels would be needed to better approximate that behavior. However, the estimation of higher order Volterra kernels would increase the number of parameters to be estimated, and therefore might require an experiment with a richer perturbation signal (i.e. more excited frequencies and increased period length). For the estimation of the model parameters in Equation 4.6 it was assumed that the recorded data is contaminated with white noise. As the contaminating noise in this type of data is colored (see for example **Figure 2.4** and **Figure 3.5**), the proposed approach is suboptimal for the data at hand.

For all participants a time delay of 20 ms was imposed in the model, which is based on findings in literature for transient wrist joint manipulation (Abbruzzese et al., 1985, Campfens et al., 2015a) as well as for electrical stimulation at the median nerve (Abbruzzese et al., 1985). Although the actual time delay is participant specific (e.g. depending on arm length), due to the small differences observed in literature, here the time delay was set to 20 ms for all participants in the study.

The best performing 2nd order models had an average memory of about 130 ms; hence, the impulse response of such a model will, including the imposed time delay of 20 ms, have an approximate duration of 150 ms. Such a response duration is close to those obtained in the contralateral sensorimotor cortex by applying a brief transient stimulus (Onishi et al., 2013, Campfens et al., 2015a).

Nonparametric modeling of a nonlinear system using a Volterra series has the major advantage of requiring limited a priori information about the exact nature of the nonlinearity, making it a powerful tool for exploring the characteristics of the nonlinear system under study. Hammerstein or Wiener cascades (e.g. the combination of a static nonlinearity with linear dynamics) are also often used to model nonlinear (neuro-)physiological systems (Westwick and Kearney, 2000), for example to study the relation between electrical nerve stimulation and muscle force output (Bai et al., 2009) or to study muscle reflexes due to joint movement (Mirbagheri et al., 2000). The number of parameters required to estimate Hammerstein or Wiener cascades is substantially lower than for Volterra series estimation; however, the former methods require prior assumptions about the nonlinearity. The drawback of a high number of parameters required for Volterra series estimation is mitigated by the use of regularization. Especially in the case of noisy data, regularization can reduce the uncertainty of the obtained models substantially. Nonparametric modeling is a necessary step before obtaining a quantitative dynamic nonlinear parametric model, which would provide crucial insights in the cortical involvement in processing of sensory information and cortical involvement in for example reflex modulation.

4.5 Conclusions

- A nonparametric nonlinear modeling approach requiring little assumptions captures 46% of the relation between joint manipulation and evoked cortical response.
- For each participant, the similarity among the models obtained when using different parts of the data for estimation provides confidence in the estimated models.
- The observed consistency of the obtained models across participants indicates that these models are able to capture the behavior of the sensorimotor system.
- Multisine perturbation signals with only odd frequency lines excited reveal dominant even nonlinear behavior in the cortical response evoked by joint manipulation. Additionally, the odd and even contributions can be modeled separately due to orthogonality of odd and even models when using such a perturbation signal.

4.6 Appendix 4A
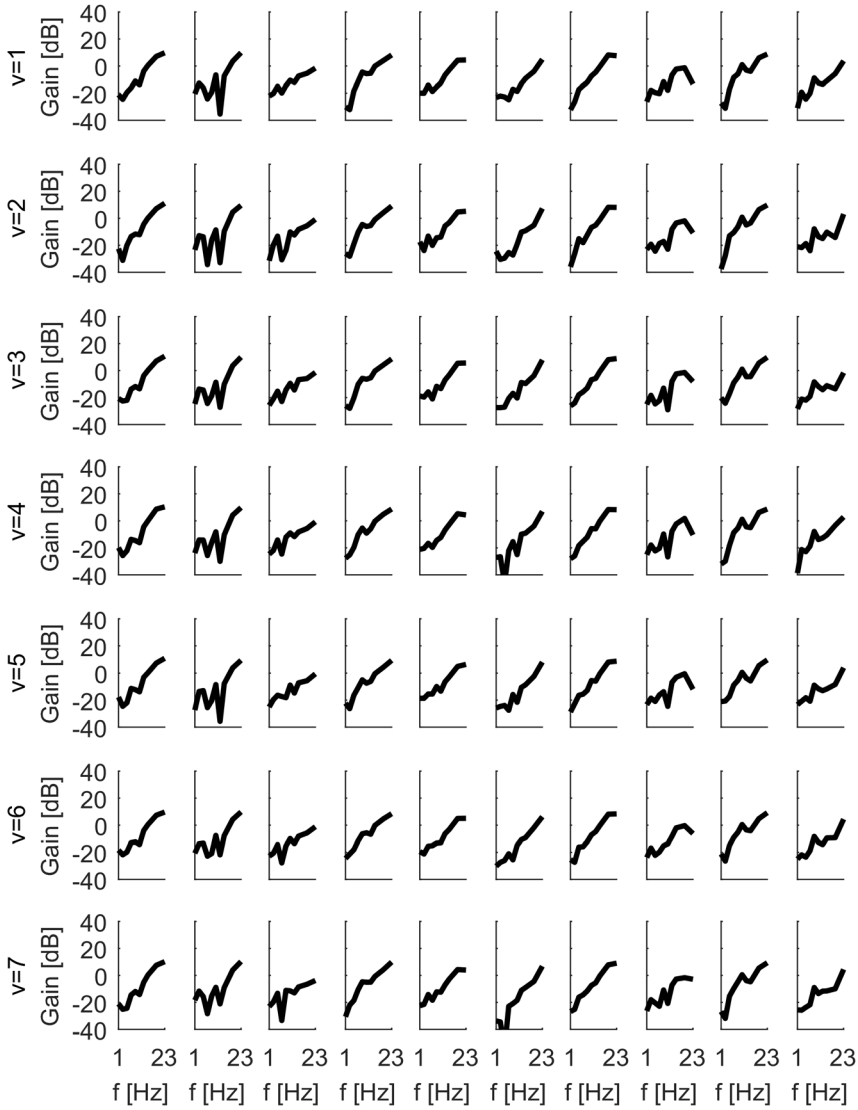
Supplementary figure. Frequency domain representation (gain) of the estimated models $\hat{H}_1(f)$ for each participant (P1,P2,…,P10) and each validation realization ($v = 1$, $v = 2$,…,$v = 7$).

4.7 Appendix 4B
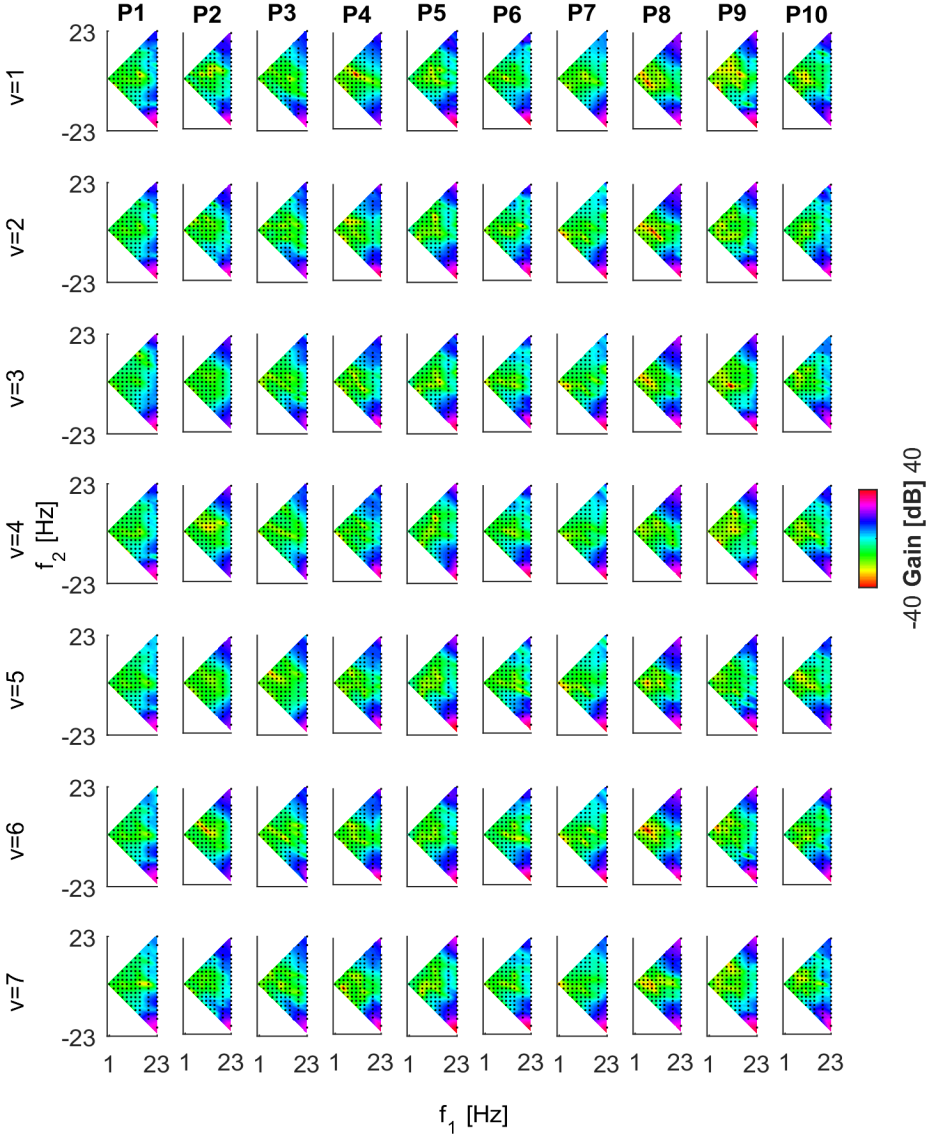
Supplementary figure. Frequency domain representation (gain) of the estimated models $\hat{H}_2\left(f_1, f_2\right)$ for each participant (P1,P2,…,P10) and each validation realization ($v = 1$, $v = 2$,…,$v = 7$). Black dots indicate the excited frequencies in the input signal.

Chapter 5

Quantification of Task-Dependent Cortical Activation Evoked by Robotic Continuous Wrist Joint Manipulation in Chronic Hemiparetic Stroke

Martijn P. Vlaar*, Teodoro Solis-Escalante*, Julius P.A. Dewald, Erwin E.H. van Wegen, Alfred C. Schouten, Gert Kwakkel, and Frans C.T van der Helm, on behalf of the 4D-EEG consortium

Cortical damage after stroke can drastically impair sensory and motor function of the upper limb, affecting the execution of activities of daily living and quality of life. Motor impairment after stroke has been thoroughly studied; however, sensory impairment and its relation to movement control has received less attention. Integrity of the somatosensory system is essential for feedback control of human movement, and compromised integrity due to stroke has been linked to sensory impairment. The goal of this study is to assess the integrity of the somatosensory system in individuals with chronic hemiparetic stroke with different levels of sensory impairment, through a combination of robotic joint manipulation and high-density electroencephalogram (EEG). A robotic wrist manipulator applied continuous periodic disturbances to the affected limb, providing somatosensory (proprioceptive and tactile) stimulation while challenging task execution. The integrity of the somatosensory system was evaluated during passive and active tasks, defined as 'relaxed wrist' and 'maintaining 20% maximum wrist flexion', respectively. The evoked cortical responses in the EEG were quantified using the power in the averaged responses and their signal-to-noise ratio. Thirty individuals with chronic hemiparetic stroke and ten unimpaired individuals without stroke participated in this study. Participants with stroke were classified as having severe, mild, or no sensory impairment, based on the Erasmus modification of the Nottingham Sensory Assessment. Under passive conditions, wrist manipulation resulted in contralateral cortical responses in unimpaired and chronic stroke participants with mild and no sensory impairment. In participants with severe sensory impairment the cortical responses were strongly reduced in amplitude, which related to anatomical damage. Under active conditions, participants with mild sensory impairment showed reduced responses compared with the passive condition, whereas unimpaired and chronic stroke participants without sensory impairment did not show this reduction. Robotic continuous joint manipulation enables studying somatosensory cortical evoked responses during the execution of meaningful upper limb control tasks. Using such an approach it is possible to quantitatively assess the integrity of sensory pathways; in the context of movement control this provides additional information required to develop more effective neurorehabilitation therapies.

Chapter 5

5.1 Introduction

The cerebral cortex plays an important role in feedforward (i.e. voluntary motor drive) and feedback control (i.e. reflexes and modulation of spinal reflexes) of human movement (Scott, 2012). Cortical damage after stroke impairs both feedforward and feedback control. Altered feedforward control after stroke has been thoroughly studied and may lead to motor impairments such as weakness and abnormal synergy-dependent motor control (Krakauer, 2005, Miller and Dewald, 2012).

Cortical involvement in feedback control (including sensorimotor integration and spinal reflex modulation) requires connectivity between somatosensory receptors in the periphery and the sensorimotor cortex, yet compromised integrity of this somatosensory system after stroke has received little attention in the literature. Understanding the impact of sensory impairment, as well as motor impairment, is highly relevant for the development and selection of neurorehabilitation therapies aimed to enhance and normalize motor control (Winward et al., 1999, Stolk-Hornsveld et al., 2006, Buma et al., 2013, Bolognini et al., 2016) and for evaluating their effectiveness.

Proprioceptive and tactile information are required for feedback control of a joint, and can be studied in an experimental setting by disturbing the joint via a robotic manipulator during motor control tasks. This robotic joint manipulation results in activation of spinal reflex loops (Mirbagheri et al., 2000, Ludvig et al., 2007, Schouten et al., 2008a) as well as in activation of the somatosensory cortex via high-resolution sensory pathways (Matthews, 1991). However, the cortical activity evoked by joint manipulation and consequently the cortical involvement in feedback control have received less attention.

In able-bodied individuals, evoked cortical responses to robotic joint manipulation have been studied with transient (Mima et al., 1996, Seiss et al., 2002) and continuous disturbances (Campfens et al., 2013, Yang et al., 2016b, Vlaar et al., 2017b). Continuous disturbances uninterruptedly provide input to the sensory system, allowing for studying movement control and somatosensory cortical activity during meaningful motor tasks. This study determines the cortical representation of afferent (proprioceptive and tactile) information in individuals with chronic hemiparetic stroke under different upper limb control conditions, relying on objective metrics derived from the electroencephalogram (EEG). Here, the goal is to quantify evoked cortical activation in individuals with chronic hemiparetic stroke, through a combination of robotic continuous joint manipulation of the paretic limb and high-density EEG. The evoked cortical activation reveals the integrity of the connections between sensory receptors in the periphery and the sensorimotor cortices.

It is hypothesized that, due to stroke-induced damage to the somatosensory system, individuals with clinically assessed proprioceptive and tactile impairment will show decreased cortical evoked responses to continuous joint manipulation in the absence of voluntary motor activity of the affected upper limb, as compared with unimpaired persons. In general, when voluntary motor activity of the affected upper limb is required, individuals with

hemiparesis have been shown to recruit their contralesional brain hemisphere, i.e. ipsilateral to the movement (Serrien et al., 2004, Buma et al., 2010, Ward, 2011, Grefkes and Fink, 2014). It is unclear, however, what this recruitment means with regard to somatosensory (i.e. afferent) evoked cortical activity, as the anatomical pathways conducting proprioceptive and tactile information mainly connect to the contralateral hemisphere (Kandel et al., 2000); thus, increased evoked cortical activation of the ipsilateral hemisphere is not expected.

5.2 Methods

Participants

Thirty participants with chronic hemiparetic stroke (i.e. at least six months post stroke, with initial hemiparesis) participated in this study (12 female, average age 64 years, SD = 11, see **Table 5.1**). The inclusion criteria were (i) first-ever ischemic stroke in an area supplied by the anterior, medial, and/or posterior cerebral arteries, (ii) age ≥ 18 years, (iii) no severe cognitive deficits (mini-mental state examination score of ≥19) (Folstein et al., 1983), and (iv) able to sit in a wheelchair for at least two hours. Exclusion criteria were previously existing pathological neurological conditions, pacemaker or other metallic implants, previously existing orthopedic limitations of the upper limb that would affect the results, and botulinum-toxin injections or medication that may influence upper limb function in past 3 months. Additionally, ten unimpaired age-matched volunteers without stroke were recruited as control group (3 female, average age 59 years, SD = 9). The inclusion (ii-iv) and exclusion criteria for the unimpaired volunteers were the same as for the participants with stroke. All participants gave written informed consent prior the experiments. The study has been approved by the Medical Ethics Reviewing Committee of the VU Medical Center, Amsterdam (protocol number 2014.140, Dutch Central Committee on Research Involving Human Subjects, CCMO, protocol number NL47079.029.14). This study was conducted in accordance with The Declaration of Helsinki.

The levels of sensory and motor impairment of each participant with chronic stroke were assessed using the Erasmus modification of the Nottingham Sensory Assessment for the upper extremity (EmNSA-UE) (Stolk-Hornsveld et al., 2006) and the Fugl-Meyer Assessment for the upper extremity (FMA-UE) (Fugl-Meyer et al., 1974), respectively. Participants with stroke were classified in three groups according to their level of sensory impairment in a similar way as in Stolk-Hornsveld et al. (2006). Participants who achieved a full score on each subtest of the EmNSA-UE were classified as having no sensory impairment. Participants with a reduced score in one or two subtests were classified as having mild sensory impairment, whereas participants with a reduced score on more than two subtests of the EmNSA-UE were classified as having severe sensory impairment.

Table 5.1. Participants with stroke grouped by level of sensory impairment (sub-sorted by FMA-UE score). Number of participants in sensory impairment groups: severe (6), mild (13), none (11). Subscores for EmNSA-UE (2: no impairment, 1: some impairment 0: fully impaired) LT:light touch, P:pressure, PP:pinprick, D:discrimination, PR:proprioception. N/A means this test was not performed due to tactile impairment as established in LT, P and PP.

ID	Sensory group	EmNSA					FMA-UE (max 66)	Months Post stroke	Age (yr)	Gender M:male F:female	Affected side	Handed-ness
		LT	P	PP	D	PR						
1	severe	0	1	1	N/A	1	6	6	71	F	L	R
2	severe	0	1	1	N/A	1	8	21	54	M	L	L
3	severe	1	1	1	N/A	0	9	212	66	F	R	R
4	severe	1	1	1	0	1	10	6	64	M	R	R
5	severe	1	1	1	N/A	1	20	142	68	M	L	L
6	severe	1	1	1	N/A	1	26	15	72	M	L	L
7	severe	1	2	2	1	1	62	7	77	M	L	L
8	mild	1	2	2	1	2	9	71	59	M	L	L
9	mild	1	2	2	1	2	10	81	48	M	L	L
10	mild	2	2	2	1	2	10	6	93	F	R	R
11	mild	2	2	2	1	2	54	26	67	M	R	R
12	mild	2	2	2	1	2	56	11	56	M	L	L
13	mild	1	2	2	1	2	59	53	50	F	R	R
14	mild	2	2	2	1	2	60	11	61	F	R	R
15	mild	2	2	2	1	2	63	35	76	F	L	L
16	mild	2	2	2	1	2	63	10	78	F	R	R
17	mild	2	2	2	1	2	64	23	65	M	L	L
18	mild	2	2	2	1	2	64	6	70	F	R	R
19	mild	2	2	2	1	2	64	6	75	F	L	R
20	none	2	2	2	2	2	11	6	52	F	R	R
21	none	2	2	2	2	2	13	82	64	M	L	L
22	none	2	2	2	2	2	20	6	77	M	L	R
23	none	2	2	2	2	2	39	50	62	M	R	R
24	none	2	2	2	2	2	48	35	50	M	R	R
25	none	2	2	2	2	2	58	75	55	M	L	L
26	none	2	2	2	2	2	59	41	49	F	L	L
27	none	2	2	2	2	2	60	6	73	M	L	R
28	none	2	2	2	2	2	66	67	68	F	R	R
29	none	2	2	2	2	2	66	10	57	M	L	L
30	none	2	2	2	2	2	66	88	48	M	R	R
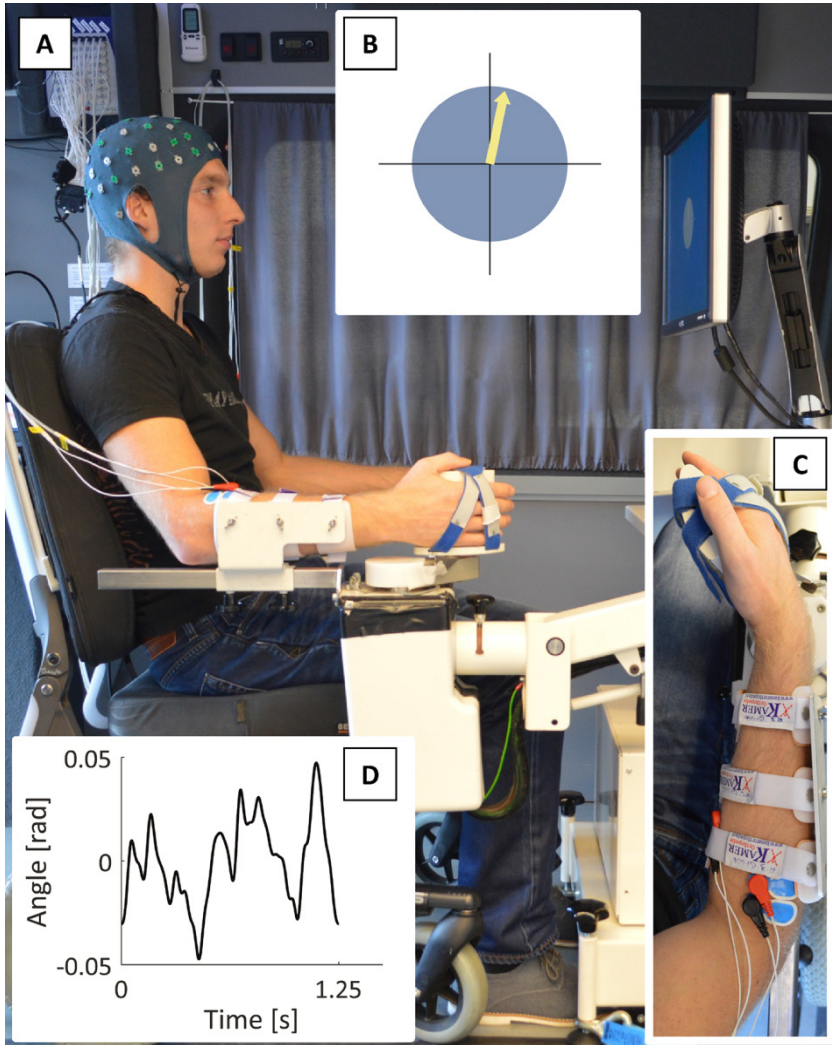
Figure 5.1. Experimental setup. **A)** The forearm of the participant is strapped into an armrest and the hand is strapped to the handle of the robotic manipulator, requiring no hand force to hold the handle. **B)** Visual feedback as presented to the participant. The circle and crosshairs are always visible. The yellow arrow is only visible during the active task and points up if the target torque is applied. **C)** Close-up of the arm in the robotic manipulator. The wrist joint is aligned with the axis of the motor and is placed in the neutral angle, defined as 20° wrist flexion. **D)** One period of the disturbance signal applied to the wrist (root-mean-square of 0.02 rad). Zero radians corresponds to the neutral angle of the wrist.

Experimental protocol

Processing and integration of sensory information was evaluated with a passive and an active upper limb control task. In this protocol a robotic manipulator applied continuous periodic disturbances to the wrist to provide sensory stimulation and to challenge task execution. This protocol focuses on the paretic forearm acknowledging that the upper limb is often more severely affected and return of some dexterity is essential for activities of daily living (Langhorne et al., 2011, Nijland et al., 2011, Raghavan, 2015).

Experimental setup

All EEG recordings were performed in a customized measurement van (Volkswagen Crafter, Wolfsburg, Germany) equipped with stabilizing feet, shaded windows, curtains, a wheelchair (Ibis, Sunrise Medical Incorporated, Fresno, CA, USA), and all experimental equipment (see **Figure 5.1A**). The participant's stimulated forearm (i.e. paretic arm for participants with stroke or dominant arm for unimpaired participants) was attached to the robotic manipulator (Wristalyzer, MOOG, Nieuw-Vennep, The Netherlands). The wrist joint was aligned to the motor axis and the hand was strapped to the handle of the robotic manipulator using Velcro straps, requiring no active grip from the participant. The shape of the handle ensured forces were applied to the palmar surface of the hand and prevented fingertips from holding the edge. Both tasks were performed with the wrist positioned in a neutral angle, defined as 20° wrist flexion (see **Figure 5.1C**), which allowed for comparison between tasks and participants. A computer screen showed a circle during all tasks, with an arrow that presented task relevant feedback during the active task, as explained below. All visual feedback signals were low-pass filtered (cut-off frequency of 0.6 Hz) to prevent correlation between eye movement and the disturbance signal.

Structural magnetic resonance images of each participant were obtained at the VU Medical Center, Amsterdam, using a Discovery MR750 3T scanner (GE, Waukesha, WI, USA). T1-weighted volumes were acquired with a 3D fast spoiled gradient-recalled-echo sequence, consisting of 172 sagittal slices (256 x 256), using the following acquisition parameters: TR = 8.208 ms, TE = 3.22 ms, inversion time = 450 ms, flip angle = 12°, voxel size 1 x 0.94 x 0.94 mm.

Recording system

All signals were recorded using a Refa amplifier (TMSi, Oldenzaal, The Netherlands) sampling at 2048 Hz and without hardware filters (only anti-aliasing). Scalp potentials were recorded using an electrode cap with 64 Ag/AgCl electrodes (TMSi), arranged according to a subset of the extended 10/20 system. A separate electrode (Blue Sensor N, Ambu, Ballerup, Denmark) was connected to the left mastoid process and served as the participant ground. Muscle activity was recorded from two muscles in each forearm (m. flexor carpi radialis and m. extensor carpi radialis brevis) using pairs of unipolar electrodes (Blue Sensor N, Ambu). Signals from the robotic manipulator (recorded and commanded angle and torque) were recorded via optical isolation amplifiers (TMSi) to ensure participant safety.

Upper limb control tasks

Passive tasks require no active involvement of the participant, allow for assessment of connectivity between the periphery and the sensorimotor cortex, and are feasible for individuals with severe motor impairment (FMA-UE score lower than 40). Active tasks engage the sensorimotor system in movement control, therewith requiring motor activity and sensorimotor integration. Hence, contrary to passive tasks, active tasks require sensory information for adequate task execution. The active task was included to investigate if voluntary motor drive would be accompanied by an abnormal lateralization of sensory-related cortical activity. This task was chosen such that individuals who suffered a stroke and are capable of some wrist flexion can perform it.

Passive task – relaxed wrist. In this task, participants were instructed to relax their wrist and ignore the applied disturbances. A screen in front of the participants showed a static image without any task-related feedback. The periodic angular disturbances applied by the robotic manipulator elicit sustained oscillatory responses in the EEG commonly referred to as steady state responses (SSR) (Snyder, 1992, Tobimatsu et al., 1999). In unimpaired persons, the SSR obtained under the passive condition appear in the contralateral sensorimotor cortices.

Active task – isotonic wrist torque. In this task participants were instructed to maintain a wrist flexion torque of 20% of the maximum voluntary contraction (MVC), for which they received visual feedback (see **Figure 5.1B**). During this task the participants received the same angular disturbances as in the passive task. The active task was not performed if the participant was not capable of voluntary wrist flexion. Due to limitations of the robotic manipulator, the maximum torque level for the active task was set to 4 Nm. There were three unimpaired participants for whom 20% MVC was higher than 4 Nm (i.e. 5.7 Nm, 5.6 Nm and 4.5 Nm). Additionally, two participants with chronic stroke executed the active task at a higher level than 20% MVC, as the task was not challenging for them at 20% MVC (ID 10, MVC was 1.8 Nm, active task performed at 40% MVC or 0.7 Nm; and ID 20, MVC was 2.8 Nm, active task performed at 50% MVC or 1.4 Nm).

The passive task was performed before the active task. To prevent fatigue in the active tasks, a trial lasted only 12.5 s. For each task 20 trials were recorded. There was a short break between trials which was at least five seconds, or longer if the participant or experimenter deemed necessary. Recording of the active task was stopped in case of severe fatigue or discomfort.

MVC during wrist flexion was determined for the stimulated arm. Participants were verbally encouraged to perform wrist flexion with maximal effort. For participants with wrist flexion torque lower than 5 Nm (experimentally established), the MVC was measured using the robotic manipulator, which maintained a fixed angle (neutral angle). Stronger participants performed this MVC test by exerting flexion torque on a handheld force transducer (MicroFet, Draper, UT, USA). The hand was attached to the robotic manipulator and the neutral angle was approximately maintained.

Disturbance signal design

During both the passive and active task the robotic manipulator applied the same continuous periodic angular disturbance signal to the wrist. The disturbance signal was a random-phase multisine signal (e.g. the sum of several sinusoids, each with a random phase) (Pintelon and Schoukens, 2012), which was designed to stimulate the sensory system in a frequency range relevant to movement control. Control of the wrist at high frequencies is limited by inertia of the limb and by the ability of the muscle to contract at high rates. To accommodate low frequencies the period of the disturbance signal was set to 1.25 s (i.e. frequency resolution of 0.8 Hz). This selection is a tradeoff between frequency resolution and number of periods that can be recorded in a given measurement time, where recording more periods allows for better estimation of an average response. The included sinusoids in the multisine signal were: 0.8, 1.6, 2.4, 3.2, 4.0, 4.8, 5.6, 6.4, 8.0, 9.6, 11.2, 13.6, 16.0, and 19.2 Hz. The frequencies below the natural frequency of the wrist (approximately 3 to 5 Hz for a relaxed wrist) had the highest amplitudes, since in the low frequency region reflexes are most effective due to the inherent time delay associated with them. Frequencies above 4 Hz had decreasing amplitudes (-20 dB/dec). The reason for this is twofold. Firstly, due to inertial properties of the wrist, the forces required to manipulate the wrist increase quadratically with increasing frequency for frequencies above the natural frequency, surpassing the capabilities of the robotic manipulator. Secondly, the muscle spindles serving the Ia afferents are particularly sensitive to velocity information (Kandel et al., 2000, Mileusnic et al., 2006).

The angular disturbances were identical for all participants, were always applied in the neutral angle, and had an excursion of 0.02 radians root mean square (see **Figure 5.1D**). The disturbance signal was flipped for recordings on the left hand to have similar flexor/extensor stimulation as in right handed participants. Each trial consisted of ten consecutive periods of the disturbance signal.

Data processing

All data was processed using MATLAB 8.1 (The Mathworks, Inc., Natick, MA, USA). Topographic representations were generated using EEGLAB (Delorme and Makeig, 2004).

Pre-processing

Recorded EEG trials were band-pass filtered between 0.8 Hz and 120 Hz and band-stop filtered in narrow bands around 50 and 100 Hz (line noise and its harmonic). Data were filtered using 4th order Butterworth filters applied bi-directionally to achieve zero-phase filtering. EEG electrodes with high impedance (automatically detected by the recording equipment) were excluded from further analysis. The remaining EEG channels were re-referenced to the common average.

Period rejection

After filtering, the trials (12.5 s) were split up into ten periods (1.25 s), according to the period of the disturbance signal. The first two periods were discarded to reduce the influence of transient effects, resulting in a total of 160 periods for each task. Periods were rejected

from the active task if the mean wrist torque in the period was not within ±50% of the target torque. If there were less than 80 successfully recorded periods in the active task, the task was excluded from analysis.

EEG analysis

Independent component analysis

To separate brain signal from artifacts, an independent component analysis (ICA) was performed using the Infomax algorithm (Bell and Sejnowski, 1995, Makeig et al., 1996a) as implemented in CUDAICA (Raimondo et al., 2012). ICA was performed on the EEG data of both upper limb control tasks combined, with subsequent rejection of independent components (ICs) corresponding to non-brain signals. ICs representing muscle activity were detected based on an increase of power in the power spectrum for increasing frequency. Components related to blinking and eye movement were detected based on their topographical representation, as well as time course of each component. ICs representing contributions mainly from one electrode were removed. Remaining components were projected back to the electrode level.

Outcome metrics

Processing of afferent information was analyzed using the steady state response (SSR), obtained for each electrode by averaging the responses to all periods:

$$\hat{x}(k) = \frac{1}{P} \sum_{p=1}^{P} x^{[p]}(k), \tag{5.1}$$

where, $\hat{x}$ is the SSR, x is the recorded signal from one electrode, k is a sample in a period p, and P is the total number of recorded periods. As the recorded EEG signals are electrical potentials measured on the scalp, the magnitude of the signal can easily vary across participants, for example due to differences in skull and scalp conductivity. Therefore, to enable comparison across participants the signal-to-noise ratio (SNR) was used. The SNR was calculated for each electrode by dividing the power in the SSR by the variance across recorded periods:

$$SNR = \frac{\hat{E}_x}{\hat{\sigma}_x^2} = \frac{\sum_{k=1}^{N} \hat{x}(k)^2}{\sum_{k=1}^{N} \frac{1}{P-1} \sum_{p=1}^{P} \left(x^{[p]}(k) - \hat{x}(k) \right)^2}. \tag{5.2}$$

Due to the applied filtering and rejection of components representing artifacts, the major cause of variance across periods is expected to be background cortical activity, which is uncorrelated to the periodic disturbance signal. Note that the SNR is not scaled with the number of periods as in Chapter 3 and 4; the number of periods might vary between participants and between tasks, which would hinder any comparisons.

The difference in power in the SSR between the passive and the active task is calculated to see the intra-participant effect of the active task on the SSR power:

$$\Delta E = \frac{\hat{E}_{x,active} - \hat{E}_{x,passive}}{\hat{E}_{x,passive}} \cdot 100\% . \tag{5.3}$$

Calculation of changes in power in the SSR is facilitated by the use of ICA for artifact rejection, as EMG signals coming from facial and shoulder muscles would otherwise contaminate the EEG signals, biasing the power in the SSR. Alterations in evoked cortical activation during the active tasks are expressed relative to the passive task by comparing the power in the SSR. The obtained metric is dimensionless, thereby allowing comparison between participants. This metric is also less sensitive to changes in noise (e.g. changes in background cortical activity and EMG activity) due to the voluntary force production.

Laterality indices were calculated for the evoked responses at the electrode level using two sets of electrodes located over the sensorimotor cortices. On the left side of the cortex the following (odd) electrodes were included: F1, F3, F5, FC1, FC3, FC5, C1, C3, C5, CP1, CP3, CP5, P1, P3 and P5. On the right side of the cortex their even counterparts were included: F2, F4, F6, FC2, FC4, FC6, C2, C4, C6, CP2, CP4, CP6, P2, P4 and P6. The electrode sets are referred to as ipsilateral (same side) or contralateral (opposite side) relative to the manipulated wrist. The SNR was averaged for the electrodes on the side contralateral to the disturbance (SNR_{contra}) and for the ipsilateral side (SNR_{ipsi}), and the sum of both was expressed as ΣSNR. The laterality index for SNR was obtained using:

$$LI = \frac{SNR_{contra} - SNR_{ipsi}}{SNR_{contra} + SNR_{ipsi}} , \tag{5.4}$$

which is similar to lateralization indices previously obtained in for example fMRI (Pujol et al., 1999) and EEG (Jung et al., 2003). The laterality index is bounded between -1 and 1, where 1 indicates only contralateral activity and -1 indicates only ipsilateral activity.

Statistical analysis
Statistical analysis on the outcome metrics SNR and LI was performed using a one-way analysis of variance (ANOVA) over the different sensory impairment groups (severe, mild, none, and control). Post hoc analysis using Tukey's honest significant difference criterion was performed if a significant difference between groups was observed. Statistical analysis on the outcome metric ΔE was performed within each group using a Wilcoxon signed rank test. All tests were performed using a two-tailed significance level of 95% (α = 0.05).

Relation between EEG-derived outcome metrics and estimation of anatomical damage

Anatomical damage

The structural magnetic resonance images were analyzed to estimate the volume of the sensory and motor tracts (SMT) affected by the stroke lesion. A participant-specific lesion mask was created from the T1-weighted volumes using the LINDA toolbox for automatic segmentation of chronic stroke lesions (Pustina et al., 2016). The volume of the SMT affected by the stroke lesion was estimated by comparing the person-specific lesion mask against the mask *corticospinal tract* obtained from the John Hopkins University white-matter tractography atlas (Hua et al., 2008) included in the FMRIB Software Library (Jenkinson et al., 2012). Noteworthy, this mask incorporates both descending and ascending fibers. To validate the SMT lesion volume as a metric of sensory impairment, the rank correlation between EmNSA-UE and SMT lesion volume was computed.

Regression analysis

Linear regression was used as a means to evaluate the relationship between the EEG-derived outcome metrics and sensory impairment. LASSO regression (Tibshirani, 1996) was used to fit a linear model from the outcome metrics to the SMT lesion volume, using ten-fold cross-validation. The LASSO regression improves the generalization of the linear model (via shrinkage) and can help determining the importance of the predictor variables. The evaluation was conducted for the passive and active tasks separately, with an additional model combining the outcome metrics of both tasks. The performance of the linear model was evaluated using the variance-accounted-for (VAF). Statistical significance was determined by comparing the model performance against data generated using 1000 permutations of the SMT lesion volume.

5.3 Results

The average torque in the passive task was expected to be close to 0 Nm, which could be altered due to passive wrist stiffness when the wrist was placed in the neutral position. Only one participant (ID 8, individual with mild sensory impairment) demonstrated a substantial (>0.3 Nm) passive wrist torque of 2.9 Nm. Due to this large torque under passive conditions, this participant (who only performed the passive task) was excluded from further analysis, as such alteration results in a different task execution. All other participants performed the passive task without substantial wrist torque and without significant increases in EMG activity on wrist flexor and extensor (paired t-test between wrist EMG during passive task and rest: relaxed wrist without robotic manipulation). Participants who successfully performed the active task had a high percentage of periods which fulfilled the task criteria: 93% (SD = 8) for the severe group, 95% (SD = 12) for the mild group, 98% (SD = 3) for the no impairment group and 93% (SD = 11) for the control group.

Signal-to-noise ratio and laterality index

Figure 5.2 shows the SNR for each electrode averaged across the participants in each group and **Figure 5.3** shows the individual results. As expected, in the passive task (**Figure 5.2**, top row) the control group demonstrates the highest SNR over the contralateral sensorimotor cortex (left side in **Figure 5.2**). The groups of participants with mild and no sensory impairment also show the highest SNR over the contralateral sensorimotor cortex. The lateralization of the SNR is not observed in the group of participants with severe sensory impairment. Moreover, the SNR is low in the severe sensory impairment group compared with the other groups, indicating that sensory input does not reach the scalp electrodes. The laterality index for the passive task (**Figure 5.3**, top row, most left graph) quantifies the differences seen in the scalp maps and shows a significantly altered laterality index for the severe sensory impairment group. The laterality index of close to zero indicates equal contributions from the contra- and ipsilateral cortices. The other graphs in **Figure 5.3** illustrate that this group has a significant reduction in SNR on both sides of the cortex. One participant in the severe sensory impairment group (ID 7) demonstrated a markedly higher SNR and FMA-UE score in comparison to other participants in this group. This participant had problems with concentration during EmNSA-UE, which could have interfered with the clinical assessment resulting in a low EmNSA-UE score as opposed to actual sensory impairment.

In the active task (**Figure 5.2**, middle row), the scalp distribution of the average SNR for the different sensory impairment groups show higher SNR for the control and no impairment groups than the mild and severe impairment groups. Once again, these differences are quantified by the laterality index (see **Figure 5.3**, middle row, most left graph). The laterality index is positive for the control and no sensory impairment groups. The laterality index for the severe and mild sensory impairment groups still presents positive values, but it also includes participants with a laterality index close to zero. The low SNR for participants with severe and mild sensory impairment is evident in the components of the laterality index (contralateral, ipsilateral, and total SNR).

Power change

The bottom row of **Figure 5.3** shows the percentage power change (ΔE) in the SSR in the active compared with the passive task. The active task results for the mild sensory impairment group not only demonstrate a lower SNR than the unimpaired participants and participants with stroke without sensory impairment as concluded from **Figure 5.3** (middle row), these participants also have a negative ΔE. The negative ΔE indicates that the reduced SNR is not (solely) due to an increase in "noise" in the active task, but that the "signal" (e.g. SSR) is reduced. The ΔE for the severe sensory impairment group has a high variance across participants. This can be explained by the total absence of an SSR in the passive task and a minor SSR in the active task, causing the percentage change to be very large. The active task was only performed if allowed by time and stamina. Other reasons for not performing the

active task included complications with the experimental setup in setting the correct force level.

Evaluation of sensory and motor tract integrity

The rank correlation between EmNSA-UE and SMT lesion volume indicates that lower EmNSA-UE scores are associated with larger SMT lesion volumes (Spearman's ρ = -0.5, p = 0.005), thus enabling the use of SMT lesion volume as supporting anatomical evidence for sensory impairment.
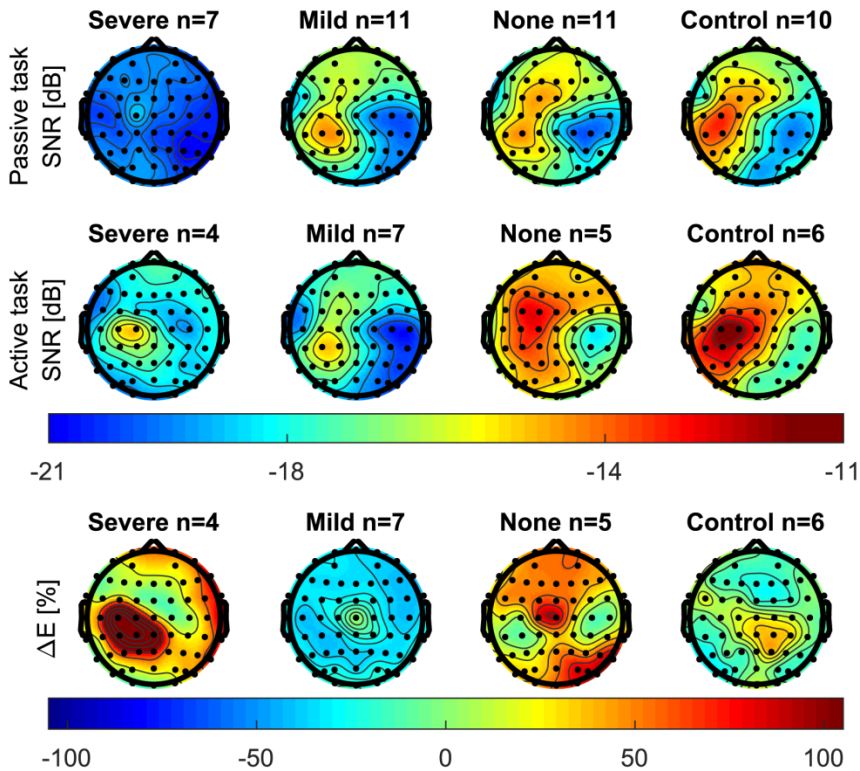
Figure 5.2. Average SNR and change in power in the SSR for the different sensory impairment groups. The number of participants in a group is indicated by *n*. The results for all recordings performed on the left hand were flipped with respect to the sagittal plane, such that left in these topographic representations is always contralateral to the perturbation. Topographic representations of SNR reveal that: (i) in the passive task the group with severe sensory impairment has a reduced evoked response as compared with all other groups, (ii) in the active task both the severe and mild sensory impairment groups demonstrate a reduced evoked response as compared with the no sensory impairment group and the control participants, and (iii) all the observed response occur around the contralateral sensorimotor cortices. Topographic representation of ΔE reveals an overall decrease of power in the evoked response for the group with mild sensory impairment.

The linear model for estimation of SMT lesion volume based on EEG-derived outcome metrics obtained from the passive task (SNR_{contra}, SNR_{ipsi}, and LI_{SNR}) explained 75% of the variance in the actual SMT lesion volume (p < 0.01, n = 29), where the algorithm indicated that all outcome metrics contributed to this model. This finding indicates a relation between the proposed EEG outcome metrics and the anatomical damage to the SMT. To further investigate the relevance of these outcome metrics in the active task, several steps were performed. The model was again estimated using the outcome metrics from the passive task, yet only for the participants who performed the active task. This resulted in a similar model performance of 77% (p < 0.01, n = 16). Interestingly, when using the outcome metrics (SNR_{contra}, SNR_{ipsi}, and LI_{SNR}) obtained from the active task, the model performance decreased to 45% (p < 0.05, n = 16). Additionally, a model including outcome metrics from both tasks explained 75% of the variance (p < 0.01, n = 16), which does not represent an improvement over using the outcome metrics from only the passive task exclusively.

5.4 Discussion

The goal of this study was to quantitatively assess the integrity of the somatosensory system in individuals with chronic hemiparetic stroke using a combination of robotic continuous joint manipulation and high-density EEG. Continuous wrist manipulation under *passive* conditions results in contralateral cortical evoked responses in unimpaired participants and participants with chronic stroke with mild and no sensory impairment. In contrast, in participants with chronic stroke and severe sensory impairment the evoked responses are strongly reduced or absent in both ipsi- and contralesional sides of the brain and thus not lateralized to either hemisphere. Under *active* conditions, participants with mild sensory impairment show a reduction in power of the cortical evoked responses in both hemispheres, as compared with the passive condition, whereas unimpaired age-matched participants and participants with no sensory impairment do not show this reduction.

Cortical activation in the passive task

The distribution of SNR over the scalp of unimpaired participants covered electrode sites overlaying the contralateral primary somatosensory cortex. Continuous joint manipulation provokes the flow of proprioceptive and tactile sensory information to the cerebral cortex. This information is mainly mediated by the dorsal column-medial lemniscal pathway, which connects the mechanoreceptors in the periphery to the contralateral primary somatosensory cortex via the ventral posterolateral nucleus of the thalamus. From the primary somatosensory cortex, the somatosensory information is distributed mainly to the secondary somatosensory and posterior parietal cortices (Kandel et al., 2000, Chang et al., 2009, Vakorin et al., 2010). The results of this study are consistent with the distribution of cortical areas listed above, and are similar to cortical activation patterns previously reported for mechanically evoked SSR (Langdon et al., 2011, Severens et al., 2013, Vlaar et al., 2017b).
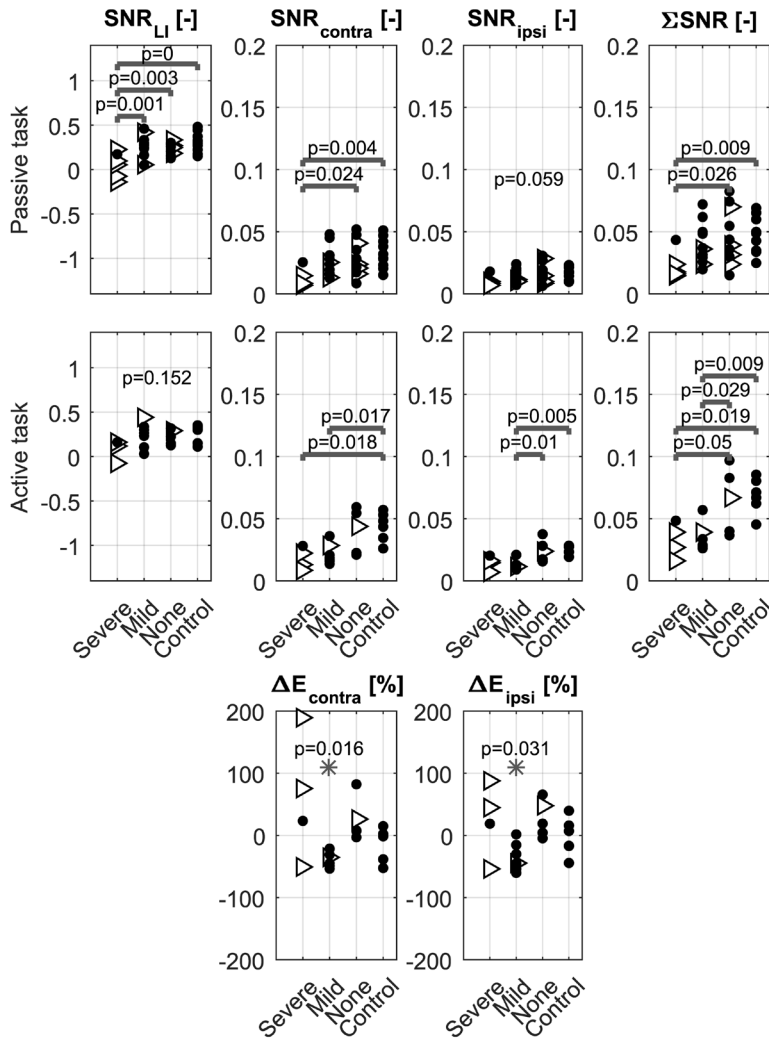
Figure 5.3. Outcome metrics and statistical analyses. **Top and middle row:** laterality index for SNR, SNR over contralateral (SNR_{contra}) and ipsilateral (SNR_{ipsi}) sensorimotor cortices and the total SNR (ΣSNR) for the passive and active task respectively. Horizontal bars (in gray) indicate significant differences between groups; in case there was no significant difference between groups, the p-value of the ANOVA is reported. **Bottom row:** change in power in the SSR in the active task as compared with the passive task (ΔE). The left graph is the ΔE for the contralateral hemisphere and the right graph is the ΔE for the ipsilateral hemisphere. Asterisks indicate a median power change significantly different from zero. Triangles indicate participants with FMA-UE score lower than 40 (i.e. with severe motor impairment), and dots indicate participants with higher FMA-UE scores (i.e. with mild or no motor impairment). The statistical analysis shows that most outcome metrics obtained from the passive task significantly differ for the group with severe sensory impairment. For the active task, the laterality index does not differ over groups; the other parameters indicate reduced responses for the severe and mild sensory impairment groups.

In the current study, participants with chronic stroke and mild and no sensory impairment do not demonstrate a significantly altered SNR (both contra- or ipsilateral) as compared with unimpaired participants. In contrast, participants with severe sensory impairment show a lower contralateral SNR in comparison with the other groups. This finding is in line with previous research in individuals with stroke and sensory impairment, in which the cortical responses to median nerve stimulation were reported to be severely decreased or absent (see Coupar et al., 2012). A recent study showed that the cortical responses to joint manipulation are reduced in individuals with subacute stroke and motor impairment (Campfens et al., 2015b). The lower SNR suggests altered connectivity between the periphery and the contralateral sensorimotor cortices, as a result of stroke-induced damage along the sensory and motor tracts. As demonstrated in the participants with stroke included in the current study, the diminished cortical responses to a sensory stimulus seem to be related to the level of sensory impairment, which does not necessarily correspond to the level of motor impairment (see **Table 5.1**). In general, sensory function can be unimpaired while there might be severe motor impairment, depending on which neural tracts are affected (Park et al., 2016). As human movement control requires sensorimotor integration, it requires functioning of both the afferent and efferent pathways. Damage to either pathway will affect motor control.

Besides lower contralateral responses, participants with severe sensory impairment also exhibit lower ipsilateral responses, in comparison to unimpaired participants. The combination of reduced contralateral and ipsilateral responses causes the laterality index to shift towards zero, i.e. no lateralization of the response. Previous neuroimaging studies using a laterality index to assess cortical activity during hand movement reported a shift in the laterality index (i.e. closer to zero or negative) associated with an increased recruitment of ipsilateral (i.e. contralesional) cortical brain areas (Serrien et al., 2004, Buma et al., 2010, Ward, 2011, Grefkes and Fink, 2014), possibly via corticobulbospinal pathways (Schwerin et al., 2008). Such lateralization is likely related to changes in voluntary motor drive instead of sensory afferents. Campfens et al. (2015b) reported, in individuals with subacute stroke, lateralization of cortical evoked responses towards the ipsilateral hemisphere (relative to the stimulated arm). This shift was interpreted as increased responses of the ipsilateral cortex (i.e. contralesional), without reporting the actual metrics for the responses of the ipsilateral cortex. Ipsilateral evoked responses to continuous joint manipulation could be mediated by transcallosal or thalamic pathways (Kandel et al., 2000, Reis et al., 2008, Welniarz et al., 2015). Although transcallosal pathways can transfer information from the contralateral (i.e. ipsilesional) to the ipsilateral (i.e. contralesional) hemisphere this requires information arrives first at the contralateral sensorimotor cortex. Moreover, there is no evidence of thalamic pathways connecting mechanoreceptors in the periphery to the ipsilateral sensorimotor cortices. In general, increased ipsilateral activation could be the result of reduced interhemispheric inhibition, potentially allowing information from the periphery to reach the ipsilateral somatosensory cortices. Interhemispheric inhibition is drastically altered in individuals who underwent a hemispherectomy; in these individuals ipsilateral activation of somatosensory cortices is sometimes observed in response to sensory stimulation (Holloway

et al., 2000, Yao et al., 2013). However, the hemispherectomy was often performed at a young age and these individuals were studied many years after surgery, resulting in a long time span during which brain plasticity can occur. In the current study there is no evidence for an increase of ipsilateral evoked responses to joint manipulation.

The group with severe sensory impairment consisted of participants with both proprioceptive and tactile impairment, as established from the EmNSA-UE. The mild sensory impairment group consisted of participants with only tactile impairment. Interestingly, in this study there were no participants with chronic stroke who only had proprioceptive impairment but no tactile impairment. The recorded cortical evoked responses are generated by mechanoreceptors; however, in the current approach it is not possible to distinguish between contributions from proprioceptive and tactile sensors. Inclusion of participants with stroke and only proprioceptive impairment would allow for further investigation of the corresponding sources of the cortical evoked response. Previous research by Mima et al. (1996) established that under passive conditions the cortical evoked responses due to finger joint manipulation are mainly due to proprioceptive and not tactile sensors. This is in line with the current finding that the lowest SNR under passive conditions was obtained for participants with proprioceptive impairment. The nature of the responses under active conditions might be altered as information about pressure on the hand (i.e. obtained by tactile sensors) would aid task execution when the objective is to maintain a certain force level.

Alterations to cortical activation during the active task

In the current study, participants with mild sensory impairment show a significant decrease of SSR power in both the contra- and ipsilateral hemispheres during the active task, as compared with the passive task. For participants with severe sensory impairment, the change in power in the SSR could not be accurately determined due to the absence of responses in the passive task. However, during the active task, participants with severe sensory impairment show an equally low SNR as compared with the participants with mild sensory impairment. Thus, the groups of participants with mild and severe sensory impairment demonstrate lower cortical evoked responses during the active task, as compared with unimpaired participants and participants with stroke without sensory impairment. In unimpaired participants and participants with no sensory impairment no significant differences were observed between passive and active conditions. The latter finding is in agreement with previous studies. Cortical activity during a wrist flexion task with joint manipulation was performed in individuals with stroke in two other studies with transient (Campfens et al., 2015a) and continuous (Campfens et al., 2015b) joint disturbances. Both studies reported metrics based on evoked responses for passive and active conditions, with small differences between conditions. Interestingly, in these studies the active condition was only performed by individuals with stroke and FMA-UE scores above 40 points without any sensory impairment.

The decreased evoked responses in participants with mild sensory impairment suggest a reduction in sensory information relayed to the brain, either due to reduced sensory signals from the periphery, changes in the mechanisms of sensorimotor integration related to sensory impairment, or both. Importantly, the disturbance signal applied by the robotic manipulator was the same under passive and active conditions. In the peripheral nervous system, the active wrist flexion causes the proprioceptive and tactile sensors to operate in a different range in comparison to the passive task, as the proprioceptors are shortened due to the muscle contraction (and lengthened for the antagonist muscle) and the tactile sensors on the hand register the increase pressure applied to the handle. In response, the central nervous system might modulate the sensitivity of the muscle spindles using alpha-gamma motor neuron co-activation, to compensate for the changing afferent signals (Prochazka et al., 1985). Impaired sensory function may lead to impaired feedback control, which could affect the modulation of muscle spindle and gamma motor neuron co-activation. Additionally, active movement induces changes in the activity of the sensorimotor cortices observed as suppression of the mu and beta rhythms during preparation and execution of movement (Pfurtscheller and Da Silva, 1999). A similar phenomena occurs during passive movements (Müller et al., 2003, Parkkonen et al., 2015, Tacchino et al., 2016), suggesting that suppression of cortical rhythms is partly related to neural processing of sensory input. In individuals with motor impairments after stroke, suppression of the beta rhythm is significantly reduced during active movement (Rossiter et al., 2014) and following somatosensory stimulation (passive movement and tactile stimulation) (Laaksonen et al., 2012, Parkkonen et al., 2015). These alterations are related to changes in excitation and inhibition through varying levels of γ-aminobutyric acid (GABA) (Rossiter et al., 2014), which are considered detrimental for motor control and could be linked to the observed decrease of the evoked responses. Extra insight into the source of the reduced responses could be obtained by directly measuring the output of the sensors in the periphery, for example using microneurography (Prochazka and Gorassini, 1998), and by measuring the induced changes to cortical mu and beta rhythms as metrics of impaired sensorimotor integration (Laaksonen et al., 2012).

Ipsilateral cortical activity during voluntary motor drive has been shown before in individuals with chronic stroke and severe motor impairments (Serrien et al., 2004, Buma et al., 2010, Ward, 2011, Grefkes and Fink, 2014). Here, the focus is on quantifying the cortical responses evoked by continuous joint manipulation (sensory information) and determining if there is lateralization of sensory information to the ipsilateral hemisphere. The results in this study do not show a consistent shift of cortical evoked responses towards the ipsilateral hemisphere for any group. This result suggests that proprioceptive and tactile information is transmitted to the contralateral hemisphere only, in accordance with known anatomic constraints (i.e. dorsal columns). This lack of sensory information reaching the contralateral and the ipsilateral cortex is likely to hamper any role of the ipsilateral cortex in feedback control (e.g. reflex modulation).

Robotic joint manipulation to assist the assessment of sensory impairment

Continuous joint manipulation allows studying somatosensory cortical evoked responses during the execution of meaningful control tasks. With this approach it is possible to measure the SNR and SSR to quantitatively assess the integrity of the sensory pathways under passive and active conditions, while being certain of stimulating the sensory systems involved in movement control (i.e. proprioceptive and tactile). Determining the integrity of sensory pathways in the context of movement control provides additional information for the accurate description of sensory impairment of a stroke patient. This information can assist the development and selection of patient-specific rehabilitation programs (and interventions) that promote plastic reorganization of the remaining cerebral networks (Dimyan and Cohen, 2011, Langhorne et al., 2011), with the ultimate goal to improve functional outcome.

Current clinical practice determines sensory and motor impairment based on subjective expert evaluation using established clinical assessments, which are vulnerable to issues related to validity and reliability (Connell and Tyson, 2012). The majority of the existing clinical assessments focus on describing motor-related impairments such as weakness, spasticity, and pathological synergies (e.g. Ashworth, 1964, Fugl-Meyer et al., 1974, Lyle, 1981), even though the assessment of sensory impairment is necessary for proper selection and evaluation of stroke rehabilitation interventions (Winward et al., 1999, Stolk-Hornsveld et al., 2006, Veerbeek et al., 2014, Bolognini et al., 2016). Alternatively, methods for objective quantification of brain function rely on neuroimaging techniques (Ward, 2015). When using indirect, blood oxygenation level dependent neuroimaging techniques, the poor temporal resolution hampers studying the cortical evoked response, which in turn hinders any distinction between cortical activation due to sensory information processing or voluntary motor drive. A known way of quantitatively assessing *sensory* function of the upper limb using neuroimaging techniques is the characterization of somatosensory evoked responses to electrical stimulation of the median nerve. Sensory function is then described based on the latency of the peaks in the cortical evoked response as measured using MEG or EEG (Huang et al., 2004). However, by applying an electrical stimulus one cannot be sure which sensory system is actually being stimulated, as there are many types of afferent fibers (e.g. for conveying pain, temperature, tactile, or proprioceptive information). Furthermore, electrical stimulation is generally applied under passive conditions and provides a non-physiological type of activation of sensory nerves. Because control of human movement demands ongoing sensorimotor integration, it is desirable to evaluate the status of the sensory system while engaged in a meaningful sensorimotor task.

In this study, the relation between the EEG-derived outcome metrics and the integrity of sensory and motor tracts is demonstrated by the successful estimation of SMT lesion volume by a linear regression model obtained from the outcome metrics measured from the passive task. Adding the outcome metrics measured from the active task did not improve the model performance. This finding emphasizes the importance of the passive task for revealing the

integrity of the connections between the periphery and sensorimotor cortices. The information obtained from the active task likely reflects other aspects of the sensorimotor system, for example altered sensorimotor integration.

This study demonstrates the quantitative assessment of the integrity of the somatosensory system through continuous joint manipulation. Although the passive and active task require some capabilities of the participants in terms of cognition and ability to sit upright independently, the protocol is feasible for individuals with chronic stroke, even in the presence of severe motor impairment. The passive task could be executed by all participants in this study. The active task could be executed by most participants, except for participants lacking voluntary wrist flexion ($n = 3$), which is related to severe motor impairment. In the current study, participants with FMA-UE scores of nine and lower were incapable of voluntarily flexing their wrist.

Limitations and future directions

Previous work by Vlaar et al. (2015, 2017b) revealed that the relation between continuous wrist manipulation and cortical evoked responses is highly nonlinear, yet the responses are periodic with the disturbance signal. The implication is that a linear metric will not be able to capture the relationship between disturbance at the wrist and cortical responses. Although the metrics in the current study do not attempt to describe this relationship, they can successfully quantify the full periodic response (i.e. both linear and nonlinear contributions). The repeatability of these metrics has yet to be verified; however, test-retest reliability of mechanically evoked steady state responses has previously been established. Pang and Mueller (2014) demonstrated that the amplitude of the evoked cortical response does not vary over recording sessions in unimpaired young participants using continuous tactile stimulation.

Due to the specific focus on the wrist in this study, some elements of the EmNSA could have been omitted (e.g. tactile sensation of the upper arm and proprioception of the shoulder and elbow). However, omitting these scores would not alter the way participants are classified. Two participants (ID 2 and 5) would receive a 0 instead of a 1 for proprioception, but both would still remain in the severe sensory impairment group. Indeed, sensory impairment is highly correlated between segments of a limb for the same sensory modality (Connell et al., 2008).

To further develop relevant outcome metrics for sensory impairment, it would be important to relate these outcome metrics to the current golden standard in sensory assessment, i.e. EmNSA. However, this raises several issues, as clinical assessments typically use ordinal scales and no normative data are available. The EmNSA only assesses passive movement and investigates all sensory modalities separately. During (natural) movement control, there is always interplay between sensory modalities. Although the applied wrist joint manipulation stimulates multiple sensory systems at the same time and therewith reduces the ability to distinguish them, the system is assessed in a way reflecting everyday control, making

comparison to EmNSA not straightforward. In the current study, sensory impairment was related to SMT integrity as estimated from the location of the stroke lesion. An attractive alternative is the quantification of SMT integrity by means of diffusion tensor imaging (Kim and Winstein, 2017), which can directly measure the integrity of the sensory and motor tracts.

The metrics demonstrated in this study (SNR, SSR, and the laterality index) may allow for tracking sensory impairment over time, which is of specific interest in the acute and subacute phases of stroke recovery. Most recovery of neurological impairment is spontaneous and takes place in the first six months after stroke (Cramer, 2008, Langhorne et al., 2011). At the end of this period, a significant number of individuals show poor recovery of upper limb function and thus do not follow the proportional recovery rule (Prabhakaran et al., 2008, Krakauer and Marshall, 2015), which predicts that individuals with stroke will recover approximately 70% of the difference between the maximum FMA-UE score and their initial score. Although the underlying cause of poor recovery is not understood, recent studies indicate that early assessment of corticospinal tract integrity has the potential to identify individuals with poor recovery (Byblow et al., 2015, Buch et al., 2016). Importantly, individuals with poor recovery of upper limb function also present impairments such as aphasia (Lazar et al., 2008) and visuospatial neglect (when affected in the same brain hemisphere) (Winters et al., 2016c). Thus, poor recovery after stroke may be linked to a multimodal suppression of brain function, which possibly also includes sensory function. Quantitative outcome metrics obtained from longitudinally monitoring sensory impairment, starting very early after stroke onset, allows investigating the effects of therapy on the recovery after stroke and the potential use of these metrics as neurophysiological biomarkers of recovery that may predict final outcome post stroke (Kwakkel and Kollen, 2013). This latter aim is in line with previous worldwide initiatives to achieve consensus in stroke recovery research (Bernhardt et al., 2016) and prognostic modeling (Reinkensmeyer et al., 2016).

Added value

This study demonstrates an approach to quantitatively assess the integrity of the somatosensory system using EEG and a robotic manipulator that applies periodic disturbances to the wrist joint. This setup allows for analysis of the evoked cortical responses to robotic joint manipulation in individuals with stroke during upper limb control. The advantage of this approach is that it specifically stimulates sensory systems involved in movement control, in contrast to electrical stimulation. The evoked responses can be studied during a passive condition, revealing connectivity between the periphery and the cortex. Additionally, studying the evoked responses under active conditions allows insight in alterations due to engagement of the sensorimotor system in a meaningful movement control task.

5.5 Conclusions

- Using the electroencephalogram and a robotic manipulator allows for quantitative assessment of evoked cortical activity reflecting proprioceptive and tactile information during meaningful upper limb control tasks executed under both passive and active conditions.

- In individuals with mild and no sensory impairment in the chronic phase of stroke, the cortical representation of somatosensory stimuli of the affected upper limb is lateralized to the contralateral hemisphere, as seen in age-matched unimpaired individuals.

- The cortical representation of somatosensory stimuli is not lateralized to the contralateral hemisphere in individuals with severe sensory impairment in the chronic phase after stroke. The absence in lateralization results from a reduction in responses in the contralateral hemisphere and not by an increase in responses in the ipsilateral hemisphere.

- Individuals with mild sensory impairment after stroke have reduced cortical representation of somatosensory stimuli under active conditions as compared with passive conditions. This reduction does not occur in unimpaired individuals and individuals without sensory impairment after stroke.

5.6 4D-EEG consortium

In addition to the authors of the present study, the consortium consists of Jan de Munck, Carel Meskers, Mique Saes*, Luuk Haring*, Caroline Winters*, Aukje Andringa*, Dirk Hoevenaars*, Ines de Castro Fernandes, and Sarah Zandvliet from VU University Medical Centre; Andreas Daffertshofer from MOVE Research Institute Amsterdam; Jun Yao from Northwestern University; Yuan Yang, Mark van de Ruit, Konstantina Kalogianni, and Lena Filatova from Delft University of Technology.

*These consortium members performed the measurements.

Chapter 6

Tracking Neuroplasticity during Recovery after Hemiparetic Stroke by Measuring Cortical Activation Patterns Evoked by Robotic Upper Limb Manipulation

Martijn P. Vlaar, Teodoro Solis-Escalante, Julius P.A. Dewald, Erwin E.H. van Wegen, Alfred C. Schouten, Gert Kwakkel, and Frans C.T van der Helm, on behalf of the 4D-EEG consortium

Stroke is a leading cause of long-term disability in the developed world. Prediction of recovery of upper limb function in stroke survivors is important for stroke management, yet is challenging in individuals with severe initial impairments. Understanding of stroke recovery and accuracy of prediction may be enhanced by using functional neuroimaging to measure cortical mechanisms of neurological recovery (i.e. neuroplasticity). The goal of the study is to present preliminary results of a protocol that tracks time-dependent neuroplasticity from the subacute to the chronic phase after stroke, focusing on the sensorimotor system. Cortical activity of hemiparetic stroke survivors was recorded at four fixed time points during recovery after stroke using electroencephalography. Participants performed passive and active wrist control tasks with the affected wrist, during which a robotic manipulator applied continuous periodic wrist manipulation. The intensity and location of the response evoked by the manipulation were studied. Preliminary results are presented for the fifteen participants who completed the four recording sessions. Eleven unimpaired participants performed the same protocol. Cortical responses evoked by joint manipulation were less strong in participants with severe sensory impairment and increased over time in participants who regained sensory function. The cortical sources generating the evoked responses were in all participants with intact contralateral primary sensorimotor cortices located within this region (all participants except one). No altered balance between contralateral and ipsilateral cortical evoked responses was observed under passive and active conditions. Cortical responses evoked by joint manipulation contain information about the status of the sensorimotor system. Recovery of sensory function is associated with return of responses to the contralateral hemisphere; we did not observe a compensatory mechanism for processing sensory information involving the ipsilateral hemisphere. Sensory information is essential to movement control. This study suggests that severe sensory impairment hinders recovery of motor function after stroke.

6.1 Introduction

Stroke is a leading cause of long-term disability in the developed world (Feigin et al., 2014). Upper limb paresis affects about 80% of stroke survivors (Langhorne et al., 2009) and less than half of these individuals regain some dexterity at the chronic phase (>6 months) after stroke; the majority is left with disabilities in activities of daily living (ADL)) (Kwakkel et al., 2003, Dobkin, 2005, Langhorne et al., 2011). Most neurological recovery occurs in the first three months after stroke (Cramer, 2008, Langhorne et al., 2011, Winters et al., 2016b) and largely occurs by spontaneous, time dependent recovery processes (Kwakkel et al., 2016). Early prediction of final functional outcome of the paretic upper limb is important for stroke management, and specifically rehabilitation therapy selection (Kwakkel and Kollen, 2013, Kwakkel et al., 2015).

The proportional recovery model (Prabhakaran et al., 2008) is based on initial upper limb impairment as measured using the Fugl-Meyer assessment for the upper extremity (FMA-UE, maximum score of 66) (Fugl-Meyer et al., 1974). The model predicts that the final upper limb improvement is approximately 70% of what was initially lost (ΔFMA-UE$_{predicted}$ = 0.7 · (66 - FMA-UE$_{initial}$) + 0.4). Individuals with a moderate to mild initial upper limb impairment generally fit the model and thus have good chance to regain almost full function (Winters et al., 2015b). However, prediction in the case of severe initial impairment is less accurate: some patients recover the predicted 70% of their maximum possible improvement, while others barely show improvement and are left with severe disabilities (Byblow et al., 2015, Ward, 2015, Winters et al., 2015b). The recovery of individuals with severe initial upper limb impairment is of specific interest: why do some recover and others do not? Absence of recovery has been associated with clinical observations such as lack of finger extension, facial palsy, and more severe lower extremity motor impairments (Winters et al., 2015b). Accurate prediction of functional outcome of stroke survivors with severe initial impairments may be enhanced by using functional neuroimaging to study cortical mechanisms of neurological recovery (i.e. neuroplasticity) and extracting metrics which possess predictive value regarding functional outcome (i.e. biomarkers).

Functional neuroimaging studies on recovery after stroke are predominantly performed using functional magnetic resonance imaging (fMRI). These studies typically investigate voluntary motor drive and have revealed an abnormal balance between ipsilesional and contralesional cortical activity (i.e. abnormal lateralization) (see Kim and Winstein, 2017 for a review). Although somatosensory impairments are very common after stroke (Connell et al., 2008, Meyer et al., 2016a) and somatosensory information reaching the cortex is important for motor recovery after stroke (Murphy and Corbett, 2009), altered cortical processing of somatosensory information after stroke has received little attention (Ward, 2015). It is currently unclear if lateralization of sensory-related cortical activity is altered during stroke recovery.

Existing neuroimaging studies on sensory information processing are mostly performed by applying an electrical somatosensory stimulus to the median nerve and recording the cortical

evoked response using electroencephalography (EEG) or magnetoencephalography (MEG). For example, Feys et al. (2000) conducted a longitudinal study with 64 stroke survivors and concluded that the electrically evoked responses have limited prognostic value for motor recovery by themselves; prediction accuracy was increased when clinical variables were combined with the absence of a somatosensory evoked response. A recent study by Rollnik (2015) confirmed an association between absence of evoked responses and poor motor outcome in 449 stroke patients; however, there was no association between motor outcome and characteristics (e.g. timing and amplitude of peaks) in the evoked response. Electrical stimulation is known to stimulate a variety of fibers (Forss et al., 1994b). As an alternative, tactile stimulation is more specific to certain sensors and thus fibers, and can be considered a more natural type of stimulation (Forss et al., 1994b); however, the tactile system is not as relevant for movement control as the proprioceptive system. Importantly, the type of mechanoreceptors being stimulated determines which part of the somatosensory cortex receives the somatosensory information; tactile and proprioceptive information arrives in Brodmann area 3b and 3a, respectively (Kandel et al., 2000).

The goal of the current study is to present preliminary results of a protocol that tracks time-dependent neuroplasticity from the subacute to the chronic phase after stroke, focusing on the sensorimotor system. The approach proposed in the current study increases the specificity of the stimulation by targeting sensors specifically involved in motor control (i.e. proprioceptors); this approach enables the study of relevant sensory information processing and its role in motor control after stroke. Cortical activity related to control of the paretic upper limb is recorded using electroencephalography (EEG), which allows for the noninvasive recording of cortical signals during experiments involving movement. Passive and active upper limb control tasks are performed using a robotic manipulator, enabling the controlled study of cortical activity during motor control in the absence of compensation strategies (i.e. the use of different limbs or muscles to achieve the same task) (Buma et al., 2010). Specifically, sensorimotor control of the wrist is studied, as the wrist is an important joint with respect to ADL and it is often affected after stroke. To stimulate the sensory system involved in sensorimotor control, the robotic manipulator applies small proprioceptive stimuli to the wrist joint; these stimuli generated a cortical response which is periodic with the periodic manipulation signal (Vlaar et al., 2015; Chapter 2) and is defined as the evoked response. The joint manipulation is applied during both the passive task (i.e. relaxed wrist) and the active task (voluntary muscle contraction of the wrist flexor). The protocol addresses the following questions at four measurements during recovery after stroke:

i.   Does the sensory information from the periphery reach the cortex?
ii.   Where in the cortex is the somatosensory evoked response generated?
iii.   Which hemisphere is involved in generating voluntary muscle contraction?
iv.   Does the voluntary muscle contraction affect the cortical representation of sensory signals?

Based on our previous work in the chronic phase after stroke (Vlaar et al., 2017a; Chapter 5) and existing literature, it is expected that after recovery, (i) the absence of sensory related signals in the cortex is associated with poor recovery; (ii) that evoked responses are localized around the contralateral sensory motor cortex; (iii) that stroke patients show altered cortical lateralization of voluntary motor drive; and (iv) that lateralization of sensory information is not altered under active conditions. Changes in cortical representation of somatosensory evoked responses during recovery after stroke have been investigated in few studies in small cohorts. To the best of our knowledge, source locations of the cortical response evoked by continuous robotic joint manipulation have not been obtained before, not in unimpaired individuals nor in individuals who suffered a stroke. The current study presents the description of the experimental protocol and the analysis techniques for a longitudinal study. A preliminary exploration is presented of the relationship between the EEG-parameters extracted from upper limb control tasks and clinically assessed recovery of upper limb capacity during the first six months post stroke in the first fifteen stroke survivors who have completed the four recording sessions.

6.2 Methods

Part of the methods have been discussed before in (Vlaar et al., 2017a; Chapter 5) and this section focuses on the differences with that study.

Patient sample

The current study presents the preliminary results for the first fifteen participants who finished the longitudinal recordings. The inclusion criteria were: (i) first-ever ischemic stroke in an area supplied by the anterior, medial, and/or posterior cerebral arteries, which took place within the last three weeks, (ii) upper limb paresis (NIHSS item 5a/b > 0), (iii) age ≥ 18 years, (iv) no severe cognitive deficits (mini-mental state examination score of ≥ 19) (Folstein et al., 1983), and (v) able to sit without support. Exclusion criteria were: previously existing pathological neurological conditions, pacemaker or other metallic implants, previous existing orthopedic limitations of upper limb that would affect the results, and botulinum-toxin injections or medication that may influence upper limb function in past three months. All participants received regular physical therapy. Additionally, eleven control participants (age 60 ± 9 years, 8 men) were included using inclusion criteria iii-v and the same exclusion criteria. These control participants were recorded in one session and their results are included as a reference. The data for ten of these control participants and the data for the final session of nine participants who suffered a stroke were previously analyzed in another (chronic stroke) study (Vlaar et al., 2017a; Chapter 5); the latter participants are indicated in **Table 6.1**.

All participants gave written informed consent prior the experiments. The study was approved by the Medical Ethics Reviewing Committee of the VU Medical Center, Amsterdam (protocol number 2014.140, Dutch Central Committee on Research Involving Human Subjects, CCMO, protocol number NL47079.029.14). This study was conducted in accordance with The Declaration of Helsinki.

Experimental setup

All recordings were performed in a mobile recording setup using a robotic wrist manipulator (see Section 5.2 and **Figure 5.1**). In short, experiments were conducted on the affected arm of participants who suffered a stroke and on the dominant arm of control participants. Cortical activity was recorded using a 62 channel EEG amplifier and a cap arranged according to a subset of the extended 10/20 system. Electromyography (EMG) was recorded from m. flexor carpi radialis and m. extensor carpi radialis brevis on both arms. All signals were sampled at 2048 Hz. Maximum voluntary contraction (MVC) for wrist flexion was obtained using a handheld force transducer. All recordings were performed with the wrist in its neutral angle, defined as 20 deg flexion.

EEG electrode positions were determined using a 3D optical system (Polaris Vicra, Northern Digital Incorporated, Ontario, Canada). Structural magnetic resonance images of each participant were obtained at the VU Medical Center, Amsterdam, using a Discovery MR750 3T scanner (GE, Waukesha, WI, USA). T1-weighted volumes were acquired with a 3D fast spoiled gradient-recalled-echo sequence, consisting of 172 sagital slices (256 x 256), using the following acquisition parameters: TR = 8.208 ms, TE = 3.22 ms, inversion time = 450 ms, flip angle = 12°, voxel size 1 x 0.94 x 0.94 mm. The anatomical MR-image of participants who suffered a stroke was obtained at least six months after stroke.

Experimental protocol

Four EEG recordings were performed during the first six months post stroke. The aim was to record early after stroke (expected to be in week 2), and subsequently at fixed time points during recovery: week 5, 12, and 26. The actual recording moments were scheduled in consultation with the patient. EEG was recorded during a set of upper limb control tasks, namely the **passive task** and the **active task**. In the passive task the participant was instructed to relax the wrist and to ignore the angular joint manipulation applied to the wrist joint by the robotic manipulator. This passive task was performed first. In the active task the participant was instructed to apply a constant wrist flexion torque at 20% of maximum voluntary contraction (MVC); this task was only performed if the participant was capable of voluntary wrist flexion and if allowed by time and stamina. Each task was performed in 20 trials of 12.5 s each, with breaks of at least 5 s between trials. In both tasks the robotic wrist manipulator applied the same periodic wrist manipulation (1.25 s period, root-mean-square wrist excursion of 0.02 rad ≈ 1.1 deg). The manipulation signal was a multisine signal (Pintelon and Schoukens, 2012), with 14 excited frequencies in a range between 0.8 and 19.2 Hz.

Around the same time as each robotic manipulator experiment, a set of clinical assessments was performed. The current study reports the Erasmus modification of the Nottingham Sensory Assessment for the upper extremity (EmNSA-UE) (Stolk-Hornsveld et al., 2006) and the Fugl-Meyer Motor Assessment for the upper extremity (FMA-UE). The EmNSA-UE tests five aspects of sensory function (light touch, pressure, pinprick, discrimination and

proprioception) which are evaluated at four location in the upper limb. Each aspect can receive 0, 1 or 2 point, where 0 indicates no stimuli were perceived, 1 indicates some stimuli were perceived and 2 indicated all stimuli were perceived. Hence, the maximum score for EmNSA-UE is 10 (i.e. no sensory impairment), scores between 5 and 10 are considered as mild sensory impairment and scores of 5 and lower are considered severe sensory impairment. The maximum score of FMA-UE is 66, where scores lower than or equal to 31 were considered as severe motor impairment (Hayward et al., 2017) and higher scores as moderate to mild impairment. Participants were grouped based on their upper limb recovery as assessed using the FMA-UE; participants for whom the predicted outcome and observed outcome differed by less than 10 points were considered **fitters** and participants with less accurately predicted outcome were considered **non-fitters** to the proportional recovery model. Participants were further grouped based on presence of severe initial motor impairments and severe initial sensory impairments.

Data analysis

All data were processed with MATLAB 8.1 (The Mathworks, Inc., Natick, MA, USA), using both FieldTrip (Oostenveld et al., 2011) and custom scripts.

Data pre-processing

Section 5.2 describes the preprocessing steps. In short, EEG data were band-pass filtered between 0.8 and 120 Hz. Segments of the active task which did not meet the task criteria were removed. Independent component analysis (ICA) was used to remove sources of artefacts (e.g. ocular and muscle activity). The recorded cortical activity is segmented in $x^{(e,p)}(k)$, where $e = 1…E$ is the electrode index ($E = 62$), $p = 1…P$ is the period index (ideally $P = 160$), and $k = 1…N$ is the sample index ($N = 2560$).

Electrode level analysis

Afferent connectivity is studied by quantifying the cortical activity which is periodic with the applied stimulation signal (i.e. the evoked cortical response). As the recorded EEG signals are electrical potentials measured on the scalp, the magnitude of the signal can easily vary across participants, for example due to differences in skull and scalp conductivity. Therefore, to enable comparison across participants the signal-to-noise ratio (SNR) was used. To obtain an estimate of the cortical response and to quantify the noise level the average and variance across periods is calculated, resulting in $\hat{x}^{[e]}(k)$ and $\sigma_x^{2[e]}(k)$ respectively. The signal-to-noise ratio is subsequently calculated using

$$SNR^{[e]} = \frac{\sum_{k=1}^{N}\left(\hat{x}^{[e]}(k)\right)^2}{\sum_{k=1}^{N}\hat{\sigma}^{2[e]}(k)} \tag{6.1}$$

To avoid inclusion of any remaining ocular or muscular activity in these metrics, a regions-of-interest (ROI) analysis is used. Two ROI over the sensorimotor cortices were defined (one

for each hemisphere), which included F1, F3, F5, FC1, FC3, FC5, C1, C3, C5, CP1, CP3, CP5, P1, P3 and P5 on the left side, and their even counterparts of the right side. The electrode sets are referred to as ipsilateral (same side) or contralateral (opposite side) relative to the manipulated wrist. The highest observed SNR value within both ROI is used to quantify the intensity of the cortical response and is defined as SNR_{max}. A laterality index is used to calculated in which hemisphere the afferent information is processed

$$LI_{SNR} = \frac{SNR_{contra} - SNR_{ipsi}}{SNR_{contra} + SNR_{ipsi}}, \qquad (6.2)$$

where SNR_{contra} is the average SNR across the electrodes in the contralateral ROI and SNR_{ipsi} is the average SNR across the electrodes in the ipsilateral ROI. The laterality index is bounded between -1 and 1, where 1 indicates only contralateral activity and -1 indicates only ipsilateral activity.

Cortical activity related to voluntary motor drive is quantified by calculating power changes in the β-band (13-30 Hz). Power changes are calculated between the active and passive task; as the joint manipulation is the same in both tasks, the main difference is expected to result from voluntary drive. The power in the β-band is calculated at each electrode, averaged over frequencies, and subsequently defined as $\beta_p^{[e]}$ and $\beta_a^{[e]}$, for the passive and active task respectively. The power change in the β-band is defined as (Pfurtscheller and Da Silva, 1999)

$$\Delta\beta^{[e]} = \frac{\beta_p^{[e]} - \beta_a^{[e]}}{\beta_p^{[e]}} \cdot 100\% \, . \qquad (6.3)$$

Consequently, a positive $\Delta\beta$ indicates a power reduction in the active task compared with the passive task; this definition is chosen as a power reduction (i.e. desynchronization) has been associated with an increase in cortical processing. The electrode within the ROI with the largest power reduction was defined as $\Delta\beta_{max}$. Similar to the lateralization index presented above, the lateralization of $\Delta\beta$ is calculated using

$$LI_{\Delta\beta} = \frac{\Delta\beta_{contra} - \Delta\beta_{ipsi}}{\Delta\beta_{contra} + \Delta\beta_{ipsi}}, \qquad (6.4)$$

where $\Delta\beta_{contra}$ is the average $\Delta\beta$ across the electrodes in the contralateral ROI, and $\Delta\beta_{ipsi}$ is the average $\Delta\beta$ across the electrodes in the ipsilateral ROI.

Anatomical damage in sensorimotor regions
The structural magnetic resonance images were analyzed to estimate the volume of the sensory and motor cortices (SMC) and tracts (SMT) affected by the stroke lesion. A participant-specific lesion mask was created from the T1-weighted volumes using the LINDA toolbox for automatic segmentation of chronic stroke lesions (Pustina et al., 2016). The volume of the SMC affected by the stroke lesion was estimated by comparing the person-specific lesion mask against a mask of the postcentral and precentral gyri (see **Figure 6.1**).

The volume of the SMT affected by the stroke lesion was estimated by comparing the person-specific lesion mask against the mask *corticospinal tract* obtained from the John Hopkins University white-matter tractography atlas (Hua et al., 2008) included in the FMRIB Software Library (Jenkinson et al., 2012); this mask incorporates both descending and ascending fibers. Only the portion of the mask which did not overlap with the SMC-mask was used (see **Figure 6.1**). The lesion volume was expressed as a percentage of the mask volume (evaluated only at the affected hemisphere).

Source level analysis

To find the generator of the signals observed at the electrodes, a source localization procedure was performed. The anatomical MR-images were processed using the Freesurfer image analysis suite (http://surfer.nmr.mgh.harvard.edu/). The extracted surfaces for scalp, skull and brain were used to create a boundary element conductivity model (BEM) with OpenMEEG (Gramfort et al., 2011). The conductivities for scalp, skull and brain were set to 0.3300, 0.0041 and 0.3300 S/m respectively. The BEM included with FieldTrip was used in case there was no anatomical MR-image available. Electrodes were aligned to the obtained volume conduction models using three anatomical landmarks, namely the nasion (NZ), and left and right pre-auricular points (LPA and RPA respectively). For one participant (ID G1), the large extent of the lesion caused the segmentation in Freesurfer to fail. To be able to obtain a proper volume conduction model, the lesion volume was replaced by anatomical information (i.e. healthy brain tissue) from the contralesional hemisphere. The resulting anatomical image was then successfully processed by Freesurfer to produce the required segmentation.

Source locations for the evoked responses were estimated by fitting a dipole with fixed location to the averaged scalp potentials $\hat{x}^{[\ell]}(n)$; dipoles were estimated on a four-millimeter grid, after which a nonlinear optimization was performed to find the dipole location which could best account for the observed variance, defined as the variance-accounted-for (VAF). Source locations are presented in CTF space (see bottom-right illustration in **Figure 6.5**). To assess changes in source location, the location for each session was presented relative to the
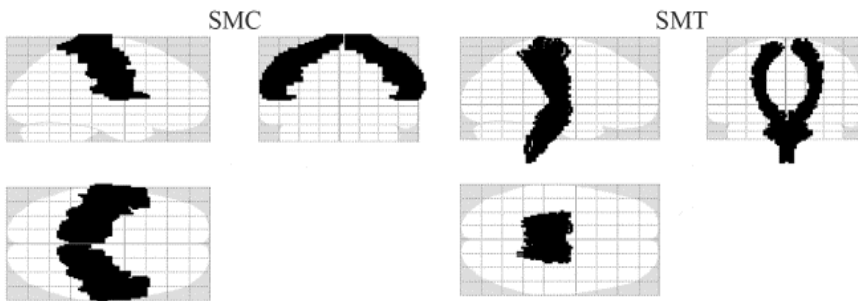

Figure 6.1. Mask for primary sensorimotor cortices (SMC) and corticospinal tract (SMT). Masks are visualized using xjView toolbox (http://www.alivelearn.net/xjview).

last recorded session. This metric, defined as d_p, may reveal a consistent shift in source location over sessions. Inter-session reproducibility of source locations has been studied before in unimpaired individuals. Using EEG and transient tactile stimulation to the finger, distance d_p was on average found to be 7 to 10 mm in seven individuals (Schaefer et al., 2002). Using MEG and electrical stimulation of the median nerve this value was on average 8 to 9 mm in nine individuals, (Wikström et al., 2000). When considering the variability across participants in these studies, a shift of more than 17 mm (mean+2.5SD) is considered abnormal. Additionally, source locations are transformed to a common anatomical space using the Statistical Parametric Mapping toolbox (SPM12 v6225) (Penny et al., 2011); this transformation facilitates comparison between participants and allows for visualization of the source locations in the same anatomical space.

List of outcome parameters

The following parameters are tracked over sessions:

SNR_{max}	- level of cortical activity related to the joint manipulation
LI_{SNR}	- lateralization of the response evoked by the joint manipulation
$\Delta\beta_{max}$	- cortical activity in voluntary drive (active task compared with the passive task)
$LI_{\Delta\beta}$	- lateralization of cortical involvement in voluntary drive
d_p	- distance from source in passive task to that of the final session
$d_{p\leftrightarrow a}$	- distance between source for passive and active task within a session

Statistical analysis

Differences across sessions within the group of all stroke participants were tested using a Friedman test, which is similar to a nonparametric repeated measures ANOVA. Mean imputation was used in the case of missing data (ID Y3, fourth session). Correlations were evaluated using Spearman's rank correlation coefficient. Differences between two groups were evaluated using a Wilcoxon rank sum test. All statistical tests were performed using a two-tailed significance level of 95% ($\alpha = 0.05$).

6.3 Results

Participant details

Four groups could be identified in the current sample based on fitting the proportional recovery model and severity of motor and sensory impairments:

- Non-fitters
    - Severe sensory and severe motor impairment in all sessions (group G, indicated with green in the figures, $n = 2$)
    - Mild to no sensory impairment and severe motor impairment in all sessions (group Y, indicated with yellow, $n = 5$)
- Fitters
    - Mild to no sensory impairment and mild motor impairment for all sessions (group B, indicated with blue, $n = 6$)
    - Mild to no sensory impairment and a substantial reduction in motor impairment over sessions (group R, indicated with red, $n = 2$).

The evolution of the clinically assessed motor and sensory impairments over time is presented in **Figure 6.2**. Other participant details are presented in **Table 6.1**. The most extensive damage to the sensorimotor cortices and tracts is found in participant ID G1, while the other participants have largely intact sensorimotor cortices and tracts.
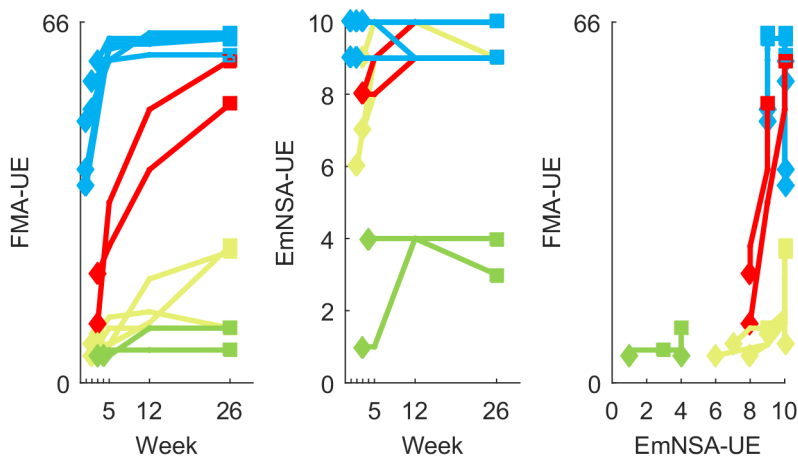

Figure 6.2. Clinical scores over time. Relations between EmNSA-UE (max score 10), FMA-UE (max score 66) and time (week) are indicated; a higher score indicates less impairment. Colors represent the different groups. The first and last recording are indicated with a diamond and a square, respectively.

Table 6.1. Participant details. No anatomical scans were available for ID: Y3 and R2. Only the first three sessions were recorded for ID Y3. *Abbreviations* Handedness/Affected side: L-left and R-right; Bamford classification: P-partial, T-total anterior circulation infarct, and L-lacunar infarct; lesioned area: SMC-sensorimotor cortices and SMT-sensorimotor tracts. Asterisk indicates participants for who the final sessions was included in a previous publication on chronic stroke.

ID	Age [years]	Sex	First session [week]	Affected side	Handed-ness	Bamford	Lesioned SMC [%]	Lesioned SMT [%]
G1*	71	F	3	L	R	T	65	13
G2*	64	M	4	R	R	T	0.8	8.8
Y1*	93	F	3	R	R	P	0.0	0.0
Y2	94	F	3	L	R	P	0.0	0.0
Y3	75	F	2	R	R	P	N/A	N/A
Y4*	77	F	2	L	R	P	0.0	2.2
Y5*	52	F	3	R	R	L	0.1	0.3
B1*	70	F	1	R	R	P	0.1	0.0
B2*	75	F	2	L	R	P	3.7	1.3
B3*	78	F	3	R	R	L	0.0	0.0
B4	86	F	1	R	R	L	0.0	0.0
B5*	73	M	2	L	R	L	0.0	0.0
B6	63	M	1	R	L	L	0.0	0.0
R1	58	M	3	R	R	P	0.0	0.0
R2	76	F	3	R	R	P	N/A	N/A

Passive task

Figure 6.3 shows the maximum SNR and lateralization index (LI) for each participant in the different sessions. Groups Y, R and B demonstrate a response at the hemisphere contralateral to the manipulated joint. The SNR in group G is low compared with the other groups and that there is no clear lateralization of the response. There was no statistically significant difference across recording sessions for SNR_{max} (p = 0.80) or LI_{SNR} (p = 0.18). **Figure 6.3** reveals a relation between SNR_{max} and EmNSA-UE for the last two sessions. A relation between SNR_{max} and FMA-UE was not demonstrated in any session. The largest differences in SNR over sessions are found in group Y: ID Y3, Y1 and Y5, who had an initial EmNSA-UE scores of 6, 7 and 8 respectively, improved their EmNSA-UE score and demonstrated an increase in SNR_{max} over sessions.

The variance-accounted-for (VAF) by the source (a single dipole) was high for all participants and sessions, with a mean VAF of around 87% (see **Table 6.2**). There was no significant difference in VAF of the source among sessions (p = 0.61). **Figure 6.4** additionally shows the source locations for the unimpaired participants. All sources are located at the contralateral sensorimotor cortex for all participants, except for the participant with the largest anatomical damage (ID: G1). **Figure 6.5** shows the location of the source for the

passive task for each session, expressed relative to the position of the source for the last recorded session. No consistent shift of source location over sessions was observed. Additionally, the Euclidian distance between the sources for each session and the last session (see **Table 6.2**), shows that the location of the source does not shift over sessions towards the final location (i.e. there is not a change in distance over sessions). There was no significant difference in Euclidian distance of the sources among subsequent sessions (p = 0.57).
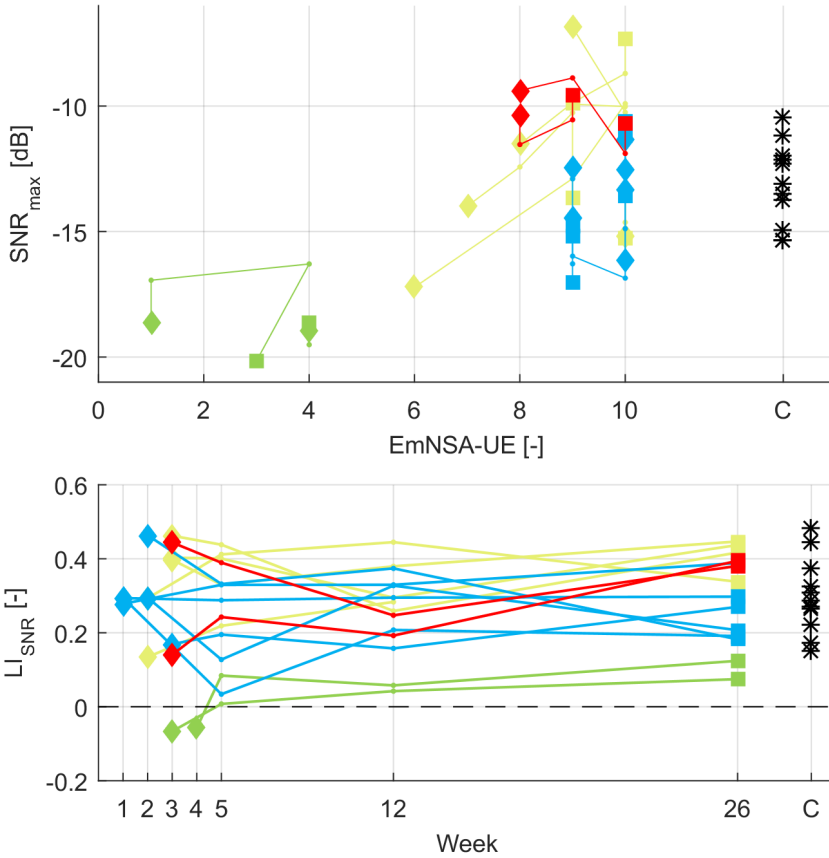

Figure 6.3. Signal-to-noise ratio and lateralization. **Top graph** shows the relation between SNR and EmNSA. Correlation between EmNSA-UE and SNR_{max} is significant for the third and fourth session (Spearman's ρ = 0.63 (p = 0.01) and ρ = 0.55 (p = 0.04), respectively). There was no significant correlation between FMA-UE and SNR_{max} in any session (0.34<p<0.75). **Bottom graph** show the lateralization of the SNR. The black dashed line indicated a laterality index of zero (i.e. no lateralization). Colors represent the different groups. The first and last recording are indicated with a diamond and a square, respectively. Black markers indicate the control participants (C).

Table 6.2. Dipole details for the passive and active task. There were no significant differences among sessions regarding VAF or distance (Friedman test).

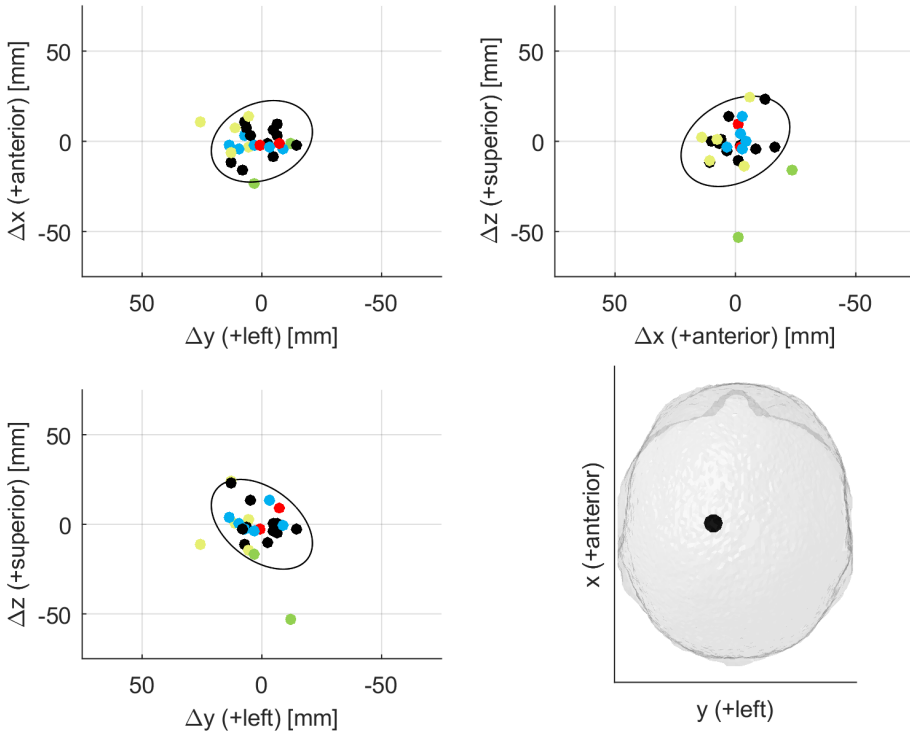| Passive task mean±standard deviation					
Session	1 (n = 15)	2 (n = 15)	3 (n = 15)	4 (n = 14)	C (n = 11)
VAF [%]	87%±5	87%±4	88%±5	87%±4	87%±3
d_p: Euclidian distance to final session [mm]	12±5	13±7	14±4	-	-
Active task mean±standard deviation					
Session	1 (n = 5)	2 (n = 6)	3 (n = 10)	4 (n = 9)	C (n = 7)
VAF [%]	90%±1	87%±2	89%±3	87%±4	88%±2
$d_{p \leftrightarrow a}$: Euclidian distance to passive task same session [mm]	7±3	8±3	6±2	6±4	9±5

Figure 6.4. Dipole locations for the passive task for all participants in standard anatomical space (source location of the last session is shown). Results presented in three planes. Source locations are expressed relative to the average location for the control participants (n = *11*, individually indicated by the black markers). The ellipsoid indicates the 90% confidence interval based on the covariance matrix of the dipole locations for the control participants. Bottom-right figure shows a top view of the standard anatomical space and the black dot shows the average source location for the control participants. Colors represent the different groups. The results are flipped with respect to the sagittal plane for participants who performed the task with the left hand.

Figure 6.5. Shift of passive dipole over sessions. Results presented in CTF space (see bottom right illustration). Solid dot is dipole location at first recording session. The dipole location for the last session is set to (0,0,0). Colors represent the different groups. The results are flipped along the y-axis for participants who performed the task with the left hand. The first and last recording are indicated with a diamond and a square, respectively.
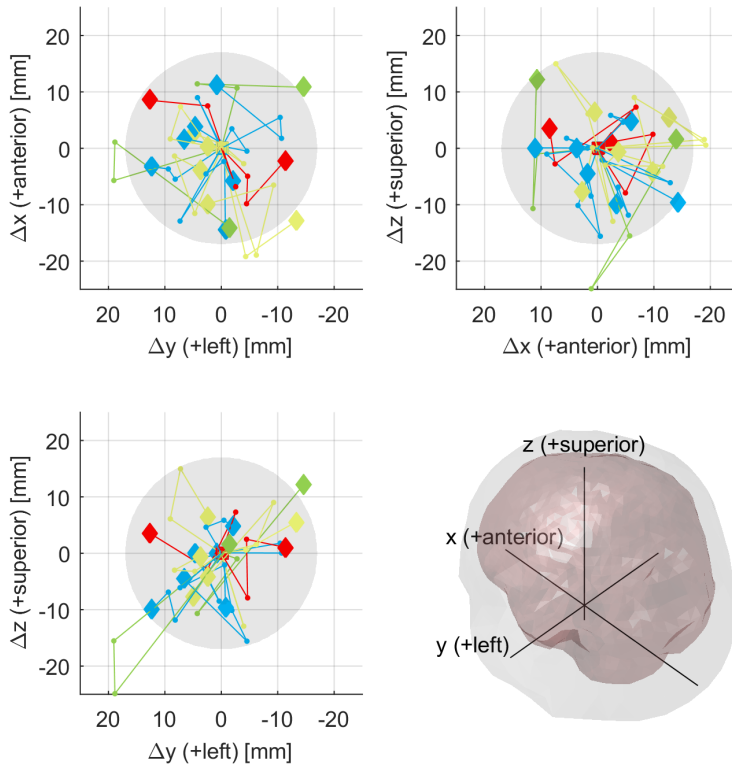
Alterations in the active task

In the first two sessions only few participants were able to perform the task (see **Table 6.2**); these were either in group B or R (i.e. fitters to the proportional recovery model). The absence of mirror movements was ensured during the experiment as well as during post-processing of the EMG signals recorded from the unaffected wrist. The VAF for the source obtained during the active task was not significantly different from the VAF obtained during the passive task in the same participants within the same session (Wilcoxon signed rank tests, $p > 0.39$ for the four sessions, $p = 0.62$ for the control participants). **Figure 6.6** and **Table 6.2** reveal the location of the source for the active task is in each session close to the source of the passive task.
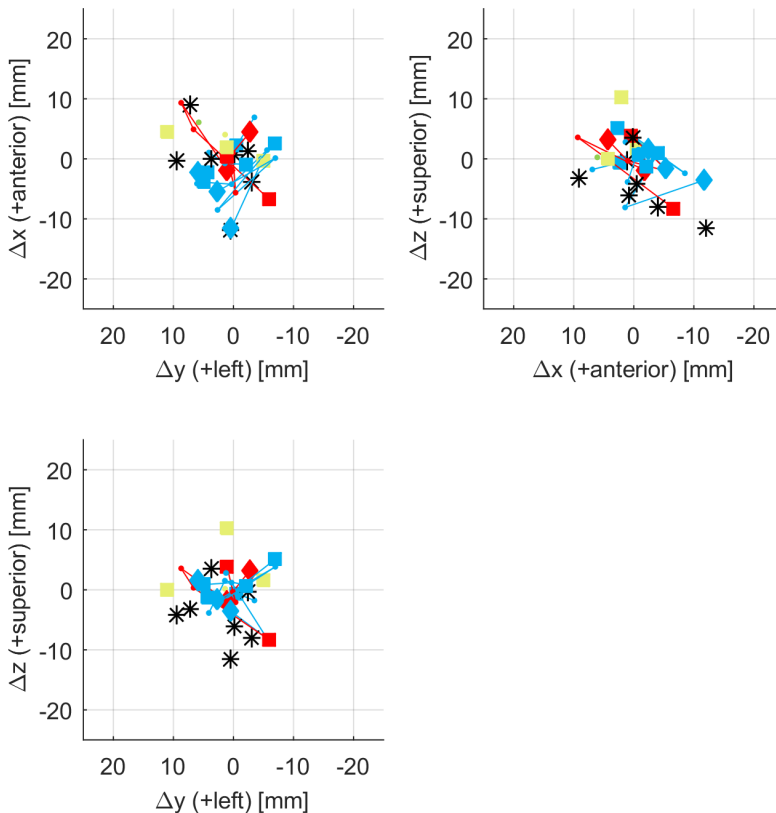

Figure 6.6. Active task dipole position relative to passive task dipole position in the same session. Dot: first recording; square: last recording. The results are flipped along the y-axis for participants who performed the task with the left hand. The first and last recording are indicated with a diamond and a square, respectively. Control participants indicated with black asterisk.

Figure 6.7 demonstrates that performing an active task results in changes in cortical activity, specifically a decrease of power in the β-band (indicates here with a positive $\Delta\beta$). In the control group no strong lateralization is observed (i.e. $LI_{\Delta\beta}$ is close to 0). For most participants who suffered a stroke $\Delta\beta$ is smaller compared with controls and its lateralization is in some case negative; there is a significant difference (Wilcoxon rank sum test) between the last measurement for participants who suffered a stroke ($n = 9$) and controls ($n = 7$), for both $\Delta\beta_{max}$ (p = 0.02) and $LI_{\Delta\beta}$ (p = 0.02). One participant (ID G2) demonstrated a LI_{SNR} of 0 for the active task. This finding is likely due to the very low SNR; the source location for the active task was 6 mm more left compared to the active task for this participant (see **Figure 6.6**), indicating that the source did not shift to the ipsilateral hemisphere.
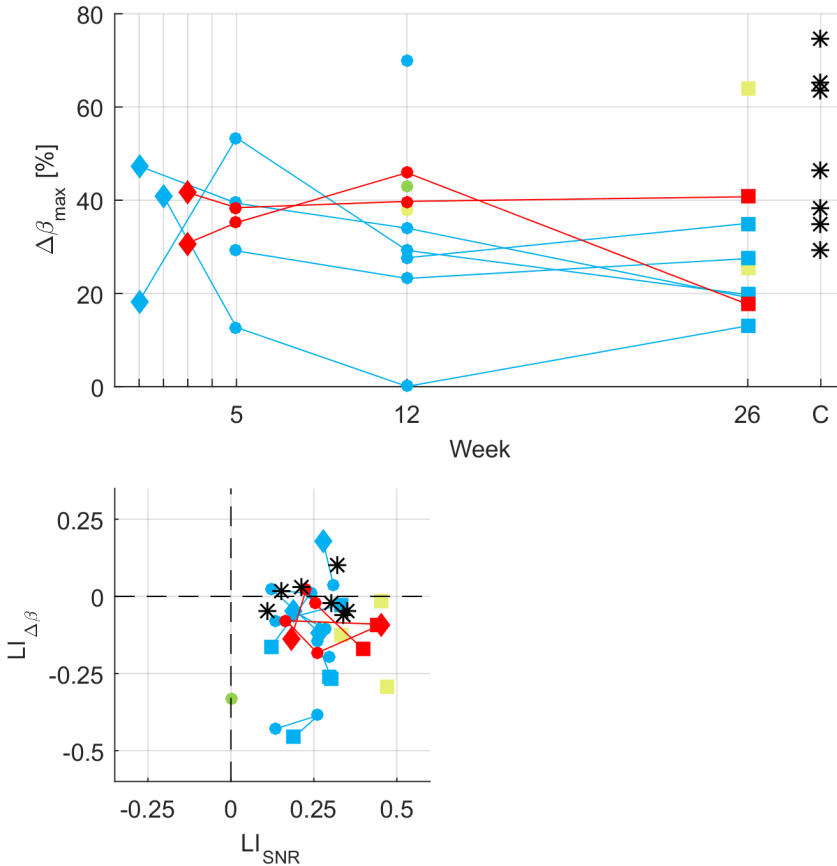
Figure 6.7. $\Delta\beta$ and its lateralization. **Top graph** shows the maximum $\Delta\beta$ within the region of interest. **Bottom graph** shows the lateralization index for the SNR in the active task related to the lateralization index for $\Delta\beta$ ($LI_{\Delta\beta}$ is only evaluated if $\Delta\beta$ is at least 10%). The first and last recording are indicated with a diamond and a square, respectively. Control participants indicated with black asterisk.

6.4 Discussion

The current study presents a protocol to track somatosensory evoked cortical activations during recovery after stroke. Studying neuroplasticity is of specific interest in individuals with poor initial upper limb function, as their recovery is poorly predicted using existing recovery models (Byblow et al., 2015, Ward, 2015, Winters et al., 2015b). The participants in this study can be split in fitters ($n = 8$) and non-fitters ($n = 7$) to the proportional recovery model (Prabhakaran et al., 2008). The fitters (participants who recovered the predicted 70% of their lost upper limb function) could be further split in participants with initial mild to moderate motor impairment (group B, $n = 6$) and participants with severe motor impairment (group R, $n = 2$). The non-fitters (participants who do not recover as predicted) all have initial severe motor impairment and could be further split in participants with severe sensory impairment in all session (group G, $n = 2$) and participants with mild, none or decreasing sensory impairment over sessions (group Y, $n = 5$). The following points address the research questions during recovery after stroke:

    i.   **Afferent connectivity**: Reduced cortical evoked responses were associated with reduced sensory function.

    ii.   **Location of the evoked response**: Participants with intact contralateral sensorimotor cortices (all except one) demonstrated an evoked response within that region.

    iii.   **Voluntary motor drive**: Participants who suffered a stroke demonstrated a decrease and altered lateralization of cortical activity related to voluntary motor drive compared with unimpaired controls. The participants with most severe motor impairment (group G and Y) were unable to perform the active task in the first sessions

    iv.   **Sensory information during the active task**: the cortical evoked response was generated by the same cortical generator in the contralateral sensorimotor cortices under passive and active conditions and no altered lateralization was observed in any session.

This is the first longitudinal study after stroke which evokes cortical responses using proprioceptive stimuli. Evoked responses as quantified by their signal-to-noise ratio (SNR) correlated with sensory impairment in the last two sessions and did not correlate with motor impairment in any session. Integrity of the sensory pathways can be quantified using the evoked responses and integrity of the sensory pathways seems to be prerequisite for motor recovery.

Afferent connectivity

Altered evoked response have been previously linked to levels of sensory (Wikström et al., 2000) and motor (Campfens et al., 2015b) impairments. In the current study, EmNSA-UE positively correlated to SNR in the last recording session, indicating that participants with more sensory impairment demonstrated a lower SNR. SNR did not correlate to FMA-UE in any session, suggesting that SNR reveals information about the status of the sensory system

rather than the motor system. These findings are in line with our previous work on responses evoked by joint manipulation in the chronic phase after stroke (Vlaar et al., 2017a; Chapter 5). Both participants in group G (severe sensory impairment) have a low SNR in all sessions. These participants also have the most extensive damage to SMC and SMT compared with the other participants, which is likely to cause less sensory information to reach the cortex. Inter-session reliability of the SSR evoked by tactile stimulation in unimpaired individuals has been previously confirmed by Pang and Mueller (2014). For all participants, the SNR is quite constant over sessions. Largest changes in SNR over sessions were found in group Y (ID Y1, Y3 and Y5), which was accompanied by substantial improvement of sensory function as measured using EmNSA-UE. Hence, the quantitatively obtained parameters reveal information related to the status of the somatosensory system.

Location of the evoked response

The evoked cortical response at the electrodes could be modeled by one dominant source. The source locations in the final session reveal a cortical source around the contralateral primary sensorimotor cortices for the unimpaired participants and for participants with largely intact sensorimotor cortices. These findings are in line with a previous longitudinal study during recovery after stroke using tactile stimulation: if a response was registered it was located in the contralateral sensorimotor areas (Roiha et al., 2011). For one participant (ID G1) the estimated source was located subcortically. The lesion of this participant damaged large parts of the primary somatosensory and motor cortices, explaining the lack of a cortical source, the low SNR, and probably the severe impairments. Nevertheless, the VAF was still high across sessions (88 to 95%). Deep cortical sources could originate from input to the dorsal column or thalamic relay neurons, as found and proposed before in an experiment with transient joint manipulation (MacKinnon et al., 2000); such a source is expected to have a low SNR and is possibly drowned out by the cortical response in the other participants.

Source locations over sessions did not shift towards the location in the chronic phase. This is in line with previous findings, where source locations changed substantially for some individuals, yet not in any recognizable pattern and were still located in contralateral sensorimotor areas (Wikström et al., 2000). The changes in source location relative to the last session was for all participants (except for two sessions of ID G1 and the first session of ID G2) less than 20 mm. These shifts are probably partially related to less accurate localization due to the poor SNR. Other participants for whom there was a shift of more than 17 mm were ID Y3 (session 1 and 2), Y4 (session 2), and Y5 (session 3). ID Y3 and Y5 demonstrated the strongest increase in SNR_{max} (and an increase in EmNSA-UE). Possibly, the difference in source locations can be explained by the increased SNR, which allows for more accurate localization (Jamali and Ross, 2012).

At no point during recovery did any participant show strong ipsilateral responses. From all recordings, the only participants for whom the responses were not lateralized to the contralateral hemisphere were the participants in the group G; the absence of a response results in a lateralization index close to zero. In a previous study on 29 individuals in the

chronic phase after stroke, no altered lateralization of the response evoked by joint manipulation was found (Vlaar et al., 2017a; Chapter 5). Wikström et al. (2000) recorded electrically evoked cortical responses during recovery after stroke and did not observe altered lateralization. In the current study, the cortical source was localized to the contralateral sensorimotor cortices for participants with largely intact sensorimotor cortices (all except ID G1) in all sessions and with high VAF. This finding is also in line with anatomy; proprioceptive and tactile information from the mechanoreceptors in the periphery is mainly mediated by the dorsal column-medial lemniscus pathways, which convey somatosensory information directly to the contralateral sensorimotor cortices. Overall, small changes in source locations were observed among recording sessions. Cortical representations within the primary sensorimotor cortices can be altered though learning in animals (Nudo et al., 1996) and unimpaired individuals (Elbert et al., 1995). Reorganization of perilesional cortical areas within the sensorimotor cortices has also been found in animal studies (Jenkins and Merzenich, 1987, Nudo and Milliken, 1996) and in individuals who suffered a stroke (Roiha et al., 2011). Changes are typically in the order of a few millimeters and such changes are not detectable on an individual level using the current approach. From the preliminary results it is hypothesized that if there is return of sensory function, it is associated with return of contralateral cortical responses and not with the (transient) emergence of ipsilateral cortical responses.

Although afferent fibers conveying proprioceptive information are known to relay to the primary sensory cortex, evoked responses to transient joint manipulation have also been found in the primary motor cortex (MacKinnon et al., 2000, Seiss et al., 2002, Onishi et al., 2013). Perhaps, both the primary motor and sensory motor cortex are involved in generating the response evoked by joint manipulation in unimpaired individuals. The source location of electrically evoked responses in the sensory cortex are found approximately slightly left and posterior of movement evoked potentials found in the motor cortex (Huang et al., 2004, Onishi et al., 2013). The participants in group B and R do not show a markedly different final source location as compared to the average location for unimpaired participants. A potentially interesting finding is that the source locations for the participants with severe initial motor impairment, demonstrate differences in source locations depending on the occurrence of motor recovery. In the last sessions, the source location for all participants in group Y is left of the average location in the control participants, which is not the case for the participants in group R (see **Figure 6.4**). In the first session, most participants in group Y seem to have a source posterior to that of the final session (see **Figure 6.5**). Possibly, the evoked response for participants in group Y originates mainly from the primary sensory cortex in the first sessions, with increasing involvement of the primary motor cortex during recovery. This difference between group Y and R might help distinguishing between individuals with severe initial motor impairment early after stroke.

Voluntary motor drive

Desynchronization of β-band activity indicates activation of the sensorimotor cortices (Pfurtscheller and Da Silva, 1999) and correlates to cortical activation as recorded during fMRI (Ritter et al., 2009). Inter-session repeatability of changes in β-band activity during voluntary wrist drive has been established (Espenhahn et al., 2016). Stimulating the somatosensory system also results in desynchronization in β-band activity, as is shown during passive limb movement (Müller et al., 2003, Parkkonen et al., 2015, Tacchino et al., 2016). In the current study, the change in β-band activity is determined by comparing the passive and active task, in which the main difference is task instruction; in both tasks the same wrist manipulation was applied. Thus, observed changes in β-band activity are assumed to result mainly from changes in voluntary motor drive.

Unimpaired participants demonstrated bilateral desynchronization in β-band activity during voluntary wrist flexion, which is in line with results from previous studies (Espenhahn et al., 2016). The contralateral hemisphere is assumed to directly innervate alpha motor neurons in the spinal cord to generate the required muscle activation. The role of the ipsilateral hemisphere is less clear and has been related to processes related to inhibition as well as facilitation (Van Wijk et al., 2012) (Espenhahn et al., 2016). The desynchronization in β-band activity of the participants who suffered a stroke was at six months significantly lower and significantly more lateralized to the ipsilateral hemisphere compared with controls. Both these findings have been reported before (Rossiter et al., 2014). The authors suggested a role for the ipsilateral (i.e. contralesional) sensorimotor cortices in movement generation in individuals with more impairment. Altered cortical lateralization of voluntary upper limb motor drive has been proposed before from fMRI studies (Buma et al., 2010). The mechanisms of this altered lateralization are not well understood (Buma et al., 2010, Rossiter et al., 2014), yet abnormal cortical lateralization of voluntary motor drive is a common finding which is also established in the current study.

Afferent information during the active task

A novelty of the current study is the attempt to distinguish between cortical activity due to voluntary motor drive and somatosensory evoked cortical activity, recorded during a motor control task. The location of the source generating the evoked response did not change compared to the passive task in unimpaired participants. Similar observations were made before in unimpaired individuals (MacKinnon et al., 2000, Piitulainen et al., 2013). This similarity in source location between tasks was also found in participants who suffered a stroke. Additionally, the VAF did not differ between passive and active task. Therefore, it is concluded that under both passive and active conditions the cortical evoked response is generated by the same dominant source as in the passive task, which explains most of the signal recorded at the electrodes. In our previous work we found no altered lateralization under active conditions in individuals during the chronic phase after stroke (Vlaar et al., 2017a; Chapter 5).

Interestingly, abnormal lateralization of cortical activity related to voluntary motor drive is not accompanied by abnormal lateralization of cortical activity related to somatosensory information for any participant, possibly due to anatomical constraints. This finding holds for the observations in the chronic phase as well as for observations during recovery. If motor drive is indeed controlled from the ipsilateral hemisphere, a lack of sensory information in that hemisphere would likely be detrimental for motor function, which relies on sensory information for proper control.

Relation between sensory impairment and motor impairment

Several previous longitudinal studies related characteristics of somatosensory evoked responses to motor impairments after stroke and have demonstrated some predictive value: if there is no evoked response in the subacute phase after stroke, recovery of motor function is not expected. (Feys et al., 2000, Rollnik, 2015). The sensorimotor system is a closed loop control system that relies on somatosensory information for control. Therefore, we hypothesize that an unaffected somatosensory system after stroke does not guarantee recovery, yet is a prerequisite for proper motor control. This hypothesis explains the lack of strong correlation between clinically assessed sensory and motor impairment (Meyer et al., 2016a), and the fact that absence of somatosensory evoked response is an indicator of poor motor recovery (Feys et al., 2000, Rollnik, 2015). Reporting the time course of motor and sensory impairment separately (as shown in **Figure 6.2**), demonstrates –albeit in a small sample- that there is indeed no motor recovery without sensory function. A similar conclusion can be drawn from our previous study on individuals in the chronic phase after stroke (Vlaar et al., 2017a; Chapter 5): severe sensory impairment is strongly linked to severe motor impairment, yet the opposite is not true. A recent longitudinal study also suggested that somatosensory impairments prevent upper limb recovery (Winters et al., 2016b). Further research will have to reveal if lack of sensory function will result in non-fitting of the proportional recovery model.

Evaluation of the protocol and analysis

Early post stroke, clinical assessments can be difficult as they rely on cognitive and motor capabilities. Hence, in this time window, functional neuroimaging might aid prediction of motor recovery. The ability to study the sensorimotor system using stimulation signals relevant to motor control is a merit of the approach presented in this study. Importantly, the passive task can be performed by individuals with severe impairments. As there is a specific interest to increase prediction accuracy for individuals with severe initial impairments, it is necessary to search for metrics which can provide discriminative power in the lower end of clinical scales. Neurological biomarkers obtained through EEG could be adopted in a clinical setting, as EEG is often readily available, relatively low cost, and safe.

The longitudinal EEG study is performed using a mobile experimental setup, limiting patient-effort for participating in the study. Out of the 15 participants who were scheduled to finish the longitudinal study before this preliminary analysis was performed, only one individual (ID

Y3) withdrew from the study after at least one EEG recording was performed. Considering the substantial time required to participate and the absence of direct patient benefits, the number of withdrawing participants can be considered low; the low preliminary dropout-rate is likely a merit of the mobile experimental setup.

Only a limited number of participants was able to perform the active task; the FMA-UE score was at least 10 for the participants who performed the task. Interestingly, the participants who demonstrated substantial recovery (group R, n = 2) were able to perform the active task in the first session (FMA-UE score of 11 and 20, both with a wrist flexion MVC of 2 Nm). The participants who did not recover the predicted upper limb function (group Y and G) did not demonstrate any voluntary wrist flexion in the first sessions and therefore did not perform the active task. Thus, the protocol did not allow for studying cortical activations in this group, hindering the use of the active task for improving prognostic models of stroke recovery.

Several longitudinal studies have set strict inclusion criteria, for example by including individuals with no sensory impairment (Tombari et al., 2004, Loubinoux et al., 2007), or by only including individuals who show improvement of clinical state (Tecchio et al., 2006). The advantage of such an approach is that a more homogenous patient sample is obtained, facilitating grouping of the individuals. The importance of focusing on a wide and representative range of recovery was recently emphasized by Ward (2015). The current study included patients with a wide range of functional impairments, which is reflected in the results of the clinical assessments as well as in the obtained EEG parameters. A larger number of patients needs to be analyzed to allow for more accurate definition of groups and to increase the number of individuals in each group.

There exists a wide range of stroke rehabilitation therapies, including physical therapy, electromyography-triggered neuromuscular stimulation (EMG-NMS), and brain stimulation such as transcranial magnetic stimulation and transcranial current stimulation. However the evidence of the effectiveness of physical therapy (Byblow et al., 2015), EMG-NMS (Kwakkel et al., 2016), or brain stimulation (Ward, 2015) is yet to be established; effect sizes of interventions account for only 5 to 15% of the differences in outcomes (Kwakkel et al., 2015, Winters et al., 2016a). An increased understanding of the (cortical) mechanisms involved in functional recovery of the upper limb, will further enable the development of rehabilitation programs (Veerbeek et al., 2014, Ward, 2015).

Future work
This paper demonstrates the feasibility of the proposed protocol to investigate cortical activation related to sensorimotor control of the affected upper limb from the subacute to the chronic phase after stroke. The relation between afferent connectivity and somatosensory impairments as observed in the current study suggests that the outcome parameters can inform on the status of the somatosensory system. The observed changes in cortical sources might aid predicting recovery in individuals with severe initial motor impairment. To further

investigate these outcome parameters, more individuals need to be added to each group. The next step is to finish recording a large cohort of stroke survivors. The influence of the outcome parameters on predicted outcome will be tested by developing a prognostic model including results from all clinical assessments as well as the outcome parameters derived from EEG recordings; the latter will include results from electrical somatosensory stimulation, resting state analysis as well as the metrics obtained for joint manipulation as presented in the current study.

6.5 4D-EEG consortium

In addition to the authors of the present study, the consortium consists of Jan de Munck, Carel Meskers, Mique Saes*, Luuk Haring*, Caroline Winters*, Aukje Andringa*, Dirk Hoevenaars*, Ines de Castro Fernandes, and Sarah Zandvliet from VU University Medical Centre; Andreas Daffertshofer from MOVE Research Institute Amsterdam; Jun Yao from Northwestern University; Yuan Yang, Mark van de Ruit, Konstantina Kalogianni, and Lena Filatova from Delft University of Technology.

*These consortium members performed the measurements.

Chapter 7

General Discussion

Chapter 7

The overall objective of this thesis was to enhance the understanding of the sensorimotor system in both unimpaired individuals and individuals who have suffered a stroke. For this, we characterized the cortical responses evoked by robotic joint manipulation in unimpaired individuals, and established how they are altered after stroke and during stroke recovery.

Several conclusions can be drawn based on the work in this thesis, which are divided into conclusion based on methodology (M), results obtained from unimpaired individuals (U), and results obtained from individuals who suffered a stroke (S). A novel approach was developed to study the characteristics of the cortical evoked responses to continuous joint manipulation (conclusions M.1 and M.2). The approach was applied to unimpaired individuals, and the nonlinear contributions to cortical evoked response were quantified (conclusion U.1) and modeled (conclusion U.2). Finally, an experimental protocol was developed to study alterations in cortical evoked responses (conclusion S.1) and their lateralization (conclusion S.2) during recovery after stroke.

- M.1 Proprioceptive information is essential to movement control and its cortical representation is well studied using continuous joint manipulation.
- M.2 Multisine perturbation signals evoke a cortical response which is rich in information: carefully designed signals allow for the detection and quantification of noise, nonlinear distortions, and slow time variations.
- U.1 The evoked cortical response is periodic with the applied joint manipulation and is highly nonlinear: over 80% of the power in the response originates from nonlinear behavior.
- U.2 A nonparametric nonlinear model describes 46% of the cortical evoked response, which is substantially better than the 8% described by a linear model.
- S.1 Reduced contralateral evoked responses are associated with somatosensory impairment after stroke. Individuals with severe somatosensory impairment also have severe motor impairment.
- S.2 Ipsilateral responses are not enhanced when contralateral responses are reduced.

The following sections discuss these conclusions in more detail. Finally, recommendations for future work are given.

M.1 Proprioceptive information is essential to movement control and its cortical representation is well studied using continuous joint manipulation

The impact of sensory impairments on recovery of motor function after stroke is not well understood (Dukelow et al., 2012). Motor impairments directly limit independence during activities of daily living (ADL), and are therefore a conspicuous consequence of stroke. Rehabilitation therapies and research into recovery after stroke mainly focus on motor impairments (Bolognini et al., 2016). Importantly, a recent study revealed that around 84% of stroke survivors have somatosensory impairments, and around 56% have impaired proprioceptive abilities (Meyer et al., 2016b). Sensory information is vital for feedback (i.e. reflexes) and feedforward (i.e. voluntary motor drive) control. Increasing our understanding of impaired control after stroke requires studying the role of sensory impairments in movement control.

Sensory impairments after stroke are generally qualitatively assessed by a clinician. Impairments are assessed on an ordinal scale, indicating no function, impaired function or unimpaired function. Consequently, the resolution of such an assessment is limited and might not reveal small differences in impairment (Simo et al., 2014). Proprioceptive impairments can be assessed in a more quantitative way and with increase resolution through the use of robotics (Dukelow et al., 2010, Simo et al., 2014, Gurari et al., 2017). The focus in these studies is on proprioceptive position sense, which is investigated by matching for example elbow joint angles across arms or within the same arm. Although allowing for well-controlled assessments, these robot-assisted assessments of sensory impairment are performed in the absence of a control task and often depend on self-reporting, making the assessment susceptible to problems with attention, comprehension and memory. Moreover, these tests focus on the capability to report static joint position, whereas movements are dynamic. Interestingly, Simo et al. (2014) additionally explored the individuals' capability to detect motion by applying small joint torque perturbations, thus acknowledging the relevance of the velocity-sensitive muscle spindles for proprioception.

As stroke-related impairments are a consequence of damage to the brain, it is of great interest to, besides looking at clinical presentation, study alterations to cortical processing (i.e. neuroplasticity). Herein lies a role for neuroimaging to provide quantitative metrics reflecting the status of the somatosensory system after stroke. The cortical evoked response to a somatosensory stimulus recorded using electroencephalography (EEG) is called an event related potential (ERP). The most commonly applied type of sensory stimulation is electrical stimulation of, for example, the median nerve. Electrical stimulation activates a large number of fibers, which originate from different layers in the underlying tissue, have varying conduction velocities and sense different somatosensory information (Forss et al., 1994b). Hence, the evoked cortical responses to stimulation of these different fibers will arrive at the cortex at different time points and possibly different locations, resulting in a mix of multiple responses which are not easily discriminated. Furthermore, electrical stimulation also

bypasses the dynamics of the sensors by directly innervating the nerves. As an alternative to electrical stimulation, the tactile system can be studied using mechanical stimuli such as vibrations (Snyder, 1992) or air puffs (Forss et al., 1994b). Such a natural stimulation allows for selectively studying the tactile system. As the sensor is stimulated instead of the fiber, the cortical evoked response to such a stimulus will also depend on the dynamics of the sensor. Both electrical and tactile stimulation generate an somatosensory evoked response, yet the type of stimulation is not specifically related to movement control, for which proprioceptive information is highly relevant (Simo et al., 2014). Importantly, proprioceptive information arrives in a different part of the primary somatosensory cortex (Brodmann area 3a) compared with information from cutaneous sensors (Brodmann area 3b). Thus, when studying movement control it is important to focus on the proprioceptive system.

The proprioceptive system can be specifically studied by recording the cortical responses evoked by applying joint manipulation. Joint manipulation can be applied as a transient stimulus (e.g. MacKinnon et al., 2000, Seiss et al., 2002, Campfens et al., 2015a) or as continuous stimulation (e.g. Campfens et al., 2013, Piitulainen et al., 2013, Yang et al., 2016b). The characteristics of the cortical response evoked by transient joint manipulation, defined here as intermittently applied stimuli, are sensitive to the inter-stimulus interval (Custead et al., 2015) and attention (Pang and Mueller, 2014). This suggests that the response is sensitive to the specific state of the system at the time when the stimulus is applied; hence, the obtained cortical response depends on the initial conditions of the system. Cortical responses evoked by continuous joint manipulation allow for studying the sensorimotor system while it is constantly and consistently engaged in control. The effects of initial conditions vanish after stimulus onset and can therefore easily be excluded from the data.

At the time of writing this discussion, there are several publications which evoked a cortical response using continuous joint manipulation and studied the coherence between stimulus and response (see previous paragraph). However, when the 4D-EEG project started in 2012, there was limited literature or data available and it was unclear to what extent small periodic joint manipulation would result in a discernible evoked cortical response. This thesis established that continuous joint manipulation evokes a cortical response in the contralateral sensorimotor cortices, which is highly nonlinear (i.e. over 80% of the response), yet is periodic with the applied periodic joint manipulation signal. As the cortical evoked response is directly associated with the manipulation signal, it is concluded that proprioceptive information generated by sensors in the periphery arrives in the contralateral sensorimotor cortices. This finding enables the study of cortical involvement in movement control tasks, in which the joint manipulation signal can serve both as a sensory stimulus to excite and study the afferent pathways, as well as a disturbance which engages the sensorimotor system in active control.

This thesis focuses on characteristics of the evoked cortical response, such as its intensity, cortical location and dynamic relation with joint manipulation signal. The role of this proprioceptive information arriving in the cortex is a question which remains unaddressed.

One important purpose is the forming of internal models for generating motor commands (Sainburg et al., 1995). Proprioceptive information also facilitates cortical feedback control, for example by selecting a control strategy (e.g. the modulation of spinal reflexes) based on external disturbances (Pruszynski and Scott, 2012). Sensorimotor networks in the cerebral cortex, basal ganglia and cerebellum facilitate highly skilled motor actions. How the brain uses sensory feedback for online control remains poorly understood (Scott, 2016). The insights obtained from this thesis can aid the design of experimental paradigms to further explore cortical involvement in feedback control.

M.2 Multisine perturbation signals evoke a cortical response which is rich in information

Evoked cortical signals recorded using EEG generally have a very poor signal-to-noise ratio (SNR). Here, signal is defined as the evoked response (i.e. the response to the joint manipulation). The noise is defined as all other activity, such as cortical background activity, ocular movements, and activity originating from jaw and neck muscles. Throughout this thesis, the SNR was found to be around -10 to -15 dB, indicating that the noise power is approximately 10 to 30 times larger than the signal power. Hence, to obtain an estimate of the response evoked by somatosensory stimulation, the stimulus should be applied many times such that the influence of noise can be reduced by averaging; parts of the response related to the stimulus will remain, while all activity originating from unrelated processes (i.e. the 'noise') will vanish with an increased number of repetitions. However, when investigating the behavior of the sensorimotor system (i.e. performing system identification), this approach should be applied with care.

The relation between input and output of a linear system can be studied by applying a continuous random perturbation signal (e.g. white noise) and the cross-correlation between input and output will reveal the dynamics of the system. When recording signals with poor SNR, a recording can be divided into multiple segments and averaging across these different segments of data will increase the SNR (Welch, 1967). Importantly, when applying random perturbation signals to a nonlinear system, averaging over different segments of data would remove not only the noise but also any stochastic nonlinear distortions; stochastic nonlinear distortions and noise have very similar properties (see **Box 7.1**). To be able to distinguish the response of a nonlinear system from the noise, it is necessary to repeatedly apply the same perturbation signal; the stochastic nonlinear distortions are not random once the perturbation signal is fixed (Pintelon and Schoukens, 2012).

Box 7.1. The best linear approximation of a nonlinear system.
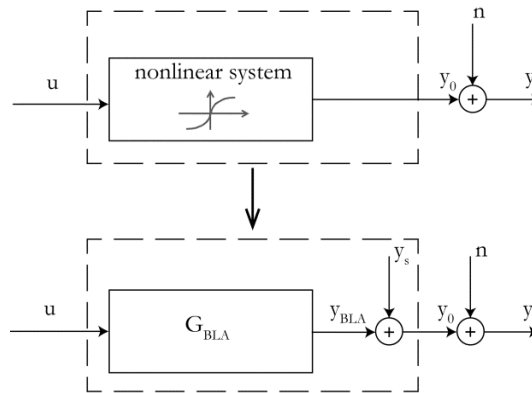
Top diagram shows a nonlinear system excited by random input *u* and with recorded output *y*. The recorded output is the true output (y_0) contaminated with noise (*n*). An equivalent representation is given in the bottom diagram. The nonlinear system is replaced by its best linear approximation (G_{BLA}) and the stochastic nonlinear distortions (y_s) are added to the output (y_{BLA}). The stochastic nonlinear distortions have properties very similar to those of the noise and are therefore hard to distinguish in the recorded output. Both the noise and the stochastic nonlinear distortions are reduced by averaging.

When using a periodic perturbation signal (e.g. a multisine signal) the stochastic nonlinear distortions are not random anymore and will be periodic with the perturbation. Hence, averaging over periods will reduce the effect of noise, yet the stochastic nonlinear distortions will not be removed. Note that because the stochastics nonlinear distortions are fixed for a fixed perturbation signal, a linear coherence analysis fails to detect nonlinear distortions and the distortions will bias the coherence (Maki, 1986). Furthermore, a linear model estimated using a fixed perturbation signal might not be valid for another perturbation signal with the exact same power spectrum and amplitude distribution; validity depends on the level of stochastic nonlinear distortions. Techniques using multisine signals can be employed to detect and quantify these stochastic nonlinear distortions (Pintelon and Schoukens, 2012) (Box 7.4), which are used in Chapter 2 and 3. Figure adapted from Schoukens et al. (2016).

Box 7.2. Exciting the system with a perturbation signal
rich enough to reveal all relevant characteristics.

The continuous stimulation used in most neuroimaging studies consists of a single or a few sinusoids. A complete representation of the system's behavior can only be obtained if the perturbation signal is rich enough (i.e. excites all the relevant characteristics of the system). An example is found in the identification of an (ideal) linear mass-spring-damper system: if the perturbation signal does not excite the natural frequency of the system (e.g. a slow or low-frequent signal), an important part of the dynamic behavior cannot be observed from the response. When stimulating the system with a richer signal, the response might drastically alter and the model identified before is not valid anymore.

When investigating a nonlinear system, its behavior can be studied in a specific operating range, which facilitates linear analysis: in a small operating range the systems behavior can possibly be linearized. Again, to obtain a proper representation of the system (within the operating range), the perturbation signal must be rich enough to reveal all characteristics of the system within that range. In contrast to a system description (i.e. model) obtained from a linear system, the model obtained from a nonlinear system is only valid within the investigated operating range; model extrapolation outside this range will likely fail.

Repeatedly applying the exact same stimulation signal to reduce the effect of noise is a common approach in neuroimaging studies on evoked responses. When these studies investigate the temporal characteristics (i.e. dynamics) of the sensorimotor system, the following points should be taken into consideration:

1. As for a nonlinear system the superposition principle does not hold, a slight change in stimulation signal could substantially alter the evoked response, and thus the interpretation of the relation between stimulus and response.
    a. When repeatedly applying the same stimulus, the observed relation between stimulus and evoked response is only valid for that very specific (yet quite arbitrary) stimulus. As nonlinear distortions are easily overlooked, linearity might be wrongfully assumed.
    b. For identification of a linear system, the amplitude distribution of the perturbation signal is trivial. In contrast, the response of a nonlinear system does depend on the amplitude distribution of the perturbation signal (see **Box 7.3**).
2. The perturbation signal should be rich enough to reveal all the relevant characteristics of the system (see **Box 7.2**).

Insight in linear and nonlinear contributions to the evoked response can be obtained by carefully designing a random phase multisine signal, which is a periodic perturbation signal consisting over several summed sinusoids (see Eq 2.1 for a definition). A multisine signal has a fully customizable frequency content, which enables the detection of time-variant behavior and nonlinear distortions. An illustration of the use of multisine perturbation signals is presented in Chapter 2. By the virtue of recording long segments (i.e. 55 s), it was possible to check for slow time variations during a segment. The results of Chapter 2 revealed no substantial time variant (i.e. non-stationary) behavior. Additionally, no subharmonics were detected in the recorded responses. These findings are important for all other chapters: the evoked response is periodic with the perturbation, indicating it is valid to segment the recorded data into individual periods and further benefit from the advantages of multisine perturbation signals. As specific frequencies were included in the perturbation signal in Chapter 2, it was possible to distinguish between linear and nonlinear responses. By designing a multisine signal including only odd harmonics of the fundamental frequency (equal to 1 over the duration of the period), it is possible to distinguish between odd and even nonlinear distortions (see **Box 7.4**).

The signal-to-noise ratio (SNR) is used throughout this thesis as a metric to determine which cortical signal (at electrodes or independent components) shows a response associated with the perturbation signal. In Chapter 5 and 6, the SNR is also used to study the integrity of the somatosensory pathways, by comparing the SNR across individuals. Note that the estimated SNR strongly depends on the number of recorded periods (see **Box 7.5**). The advantage of comparing the SNR as opposed to the power in the evoked response, is that it is a dimensionless metric which has less dependence on anatomical differences across individuals. A weakness of this approach is that from an altered SNR it is unclear if the power in the signal, the power in the noise, or both are altered. Intra-individual changes in power in the evoked cortical responses across measurement sessions could be assessed by expressing the power relative to the first or last session. However, comparison between individuals is hindered by such an approach. In Chapter 5, comparison of the evoked response in the active task was enabled by calculating the difference in power between the passive and active task, which also results in a dimensionless metric which is less sensitive to alterations in noise. A combination of the various metrics will provide most information on alterations to cortical

Box 7.3. Output of a nonlinear system depends on the amplitude distribution of the input signal.
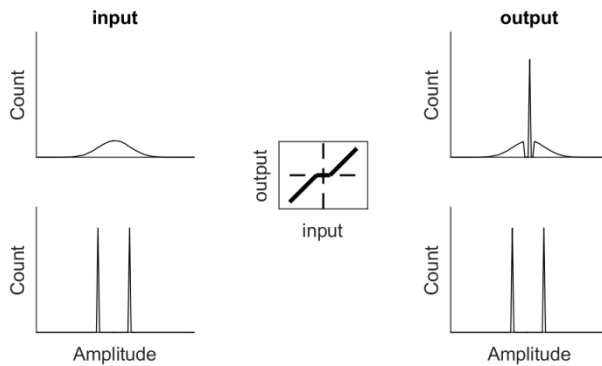
Two graphs on the left show the amplitude distribution (i.e. histogram) of a normally distributed random input signal (top) and a random binary signal (bottom). The graph in the center shows the input-output relation for a dead-zone operator: small amplitude signals cannot pass through the system. The two graphs on the right show the amplitude distribution of the output signal corresponding to the input signal in the same row. The response to an input signal with an amplitude distribution concentrated around zero (e.g. normally distributed noise) will clearly show the effect of the dead-zone. In contrast, the response to a perturbation signal with an amplitude distribution concentrated in the extremes (e.g. random binary signal) will pass through the nonlinear operator unaltered; any subsequent system identification will be blind to the nonlinearity. Therefore, when studying a nonlinear system it is important to do so using a specific class of input signals, as the observed relation might not be valid for a different class. For the class of input signals with a Gaussian distribution the properties of the best linear approximation and the stochastic nonlinear distortions are well known (see Box 7.1) (Schoukens et al., 2016). Random-phase multisine perturbation signals have such a distribution, given that enough frequencies are excited. Note that shifting the phases of the sinusoids to reduce the crest factor, allows for an increase of power in the input signal, which is a powerful tool for identification of linear dynamic systems. However, this process substantially alters the amplitude distribution of the multisine signal towards a signal with a binary distribution and should therefore be avoided when linearizing a nonlinear system.

evoked responses after stroke. The SNR metric has demonstrated to be a reliable metric to find evoked responses associated with the manipulation signal, even in the presence of strong noise sources such as ocular and muscle activity. Furthermore, while coherence metrics only focus on a small part of the response, the SNR quantifies the complete nonlinear response of the sensorimotor system.

Box 7.4. Example of a frequency domain response of a nonlinear system to a multisine perturbation.
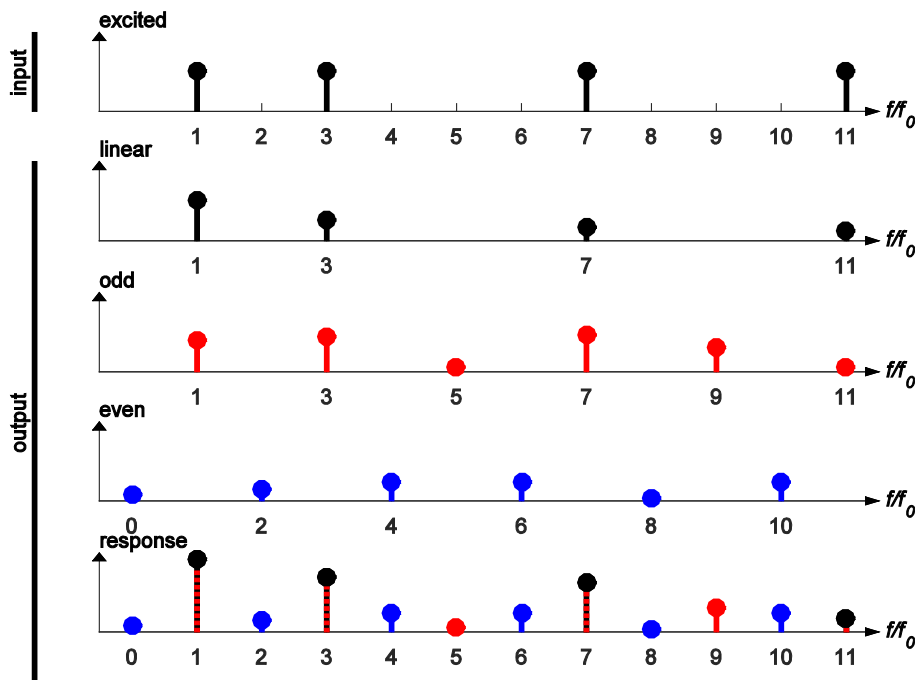

Only magnitude is shown. Noise is not considered here. **Top row** shows that only odd frequency lines in the multisine signal are excited (f is frequency and f_0 is the fundamental frequency, i.e. one over the period duration). **Rows two, three and four** show the linear, odd nonlinear and even nonlinear contributions to the output, respectively. These contributions are generated by intermodulation of the excited frequencies in the input. **Bottom row** shows the response, which is a mix of the linear, odd and even contributions. Note that at the unexcited frequency lines in the response odd and even nonlinear contributions can be distinguished, yet the signal at the excited frequency lines in the output is a mix of linear and odd nonlinear contributions. Thus, the signal at the excited frequencies should not be considered as the linear part of the response, since it may contain odd nonlinear distortions. Note that in a linear system the response can only contain signal at the frequencies excited in the input. Figure adapted from Schoukens et al. (2016).

U.1 The evoked cortical response is periodic with the applied joint manipulation and is highly nonlinear

The characteristics of the cortical responses evoked by continuous wrist manipulation in unimpaired individuals were investigated in Chapter 2 and 3. Chapter 2 revealed the cortical evoked responses to periodic with the applied manipulation; there were no detectable slow time variant dynamics or subharmonics. However, strong responses were observed at frequencies which were not excited in the input, indicating nonlinear behavior. Systems with

Box 7.5. SNR depends on number of periods included for estimation.
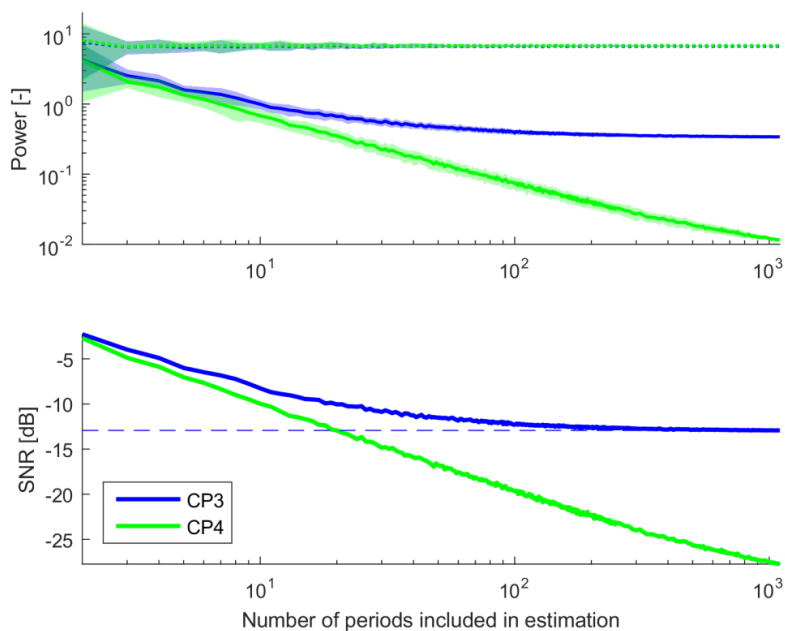
Top graph: solid line and dotted line represent the estimated signal and noise power, respectively. Estimates are obtained by randomly selecting a number of periods out of the available number of 1100 (electrode level data from Chapter 2), and repeating this 50 times. Lines indicate the average and shaded areas indicate the standard deviation. **Bottom graph**: signal-to-noise ratio (SNR) estimated from the results in the top graph. Dashed blue line indicates the estimated SNR for electrode CP3 when including all available data. Electrode CP3 is located over the contralateral sensorimotor cortices, while CP4 is located over the ipsilateral sensorimotor cortices.

The noise level can be accurately estimated using a small number of periods. A good estimate of the power in the evoked response, and consequently of the SNR, requires around 100 periods at an electrode over the contralateral sensorimotor cortices (CP3). The initial decrease in estimated SNR is due to the very poor true SNR (dashed blue line at around -13 dB), in which the power of the signal is approximately 20 times smaller than the power in the noise. Interestingly, the power in the evoked response on an electrode over the ipsilateral sensorimotor cortices (CP4) keeps decreasing when more periods are included; therefore, the discriminative ability of the SNR-metric increases when more periods are included.

weak nonlinear behavior can be studied in a specific operating range, facilitating linear analysis. Compared with nonlinear system identification techniques, linear system identification techniques are matured, computationally undemanding, require little a priori knowledge and can reveal many characteristics of the system under study.

The possibility of applying linear system identification techniques was investigated in Chapter 3. A nonparametric linear model (the best linear approximation) was estimated between the recorded wrist joint angle and wrist joint torque, wrist flexor and extensor muscle activity and the cortical response which was most associated with the perturbation signal (i.e. with the highest SNR). The relation between wrist joint angle and torque could be linearized well, as the nonparametric linear model explained 99% of the recorded signal. The relation between wrist angle and muscle activity was weakly nonlinear: the observed nonlinear behavior mainly originated from an odd nonlinearity and a nonparametric linear model could explain around 70% of the recorded muscle activity. Under both passive ("relax and ignore the perturbation signal") as active ("maintain joint angle and resist perturbation signal"), only a very small portion of the cortical evoked response could be explained by the linear model (10%). A detailed analysis of the power spectrum of the evoked response revealed that there were strong nonlinear distortions in all participants, which mainly (>75%) originated from an even nonlinearity.

Quantification of the response preferably separates linear and nonlinear contributions. This can be achieved by using multiple realizations of a multisine signal, as performed in Chapter 3. Alternatively, nonlinear distortions can be detected by leaving some frequencies unexcited, as done in Chapter 2 and 3. In Chapter 5 and 6 a perturbation signal was used which did not allow for separating linear and nonlinear contributions. The ability of detecting nonlinear distortions comes at the price of extra measurement time. As it was already known that the cortical response to joint manipulation is dominated by nonlinear distortions, it was decided to design a relatively rich perturbation signal (i.e. many excited frequencies) to reduce measurement time and increase unpredictability of the signal. The metrics used in Chapter 5 and 6 therefore quantify the full response to a rich joint manipulation signal.

Linear coherence is a metric used in neuroimaging to quantify the coupling between joint manipulation and evoked response (position-cortico coherence; Campfens et al., 2013, corticokinematic coherence; Piitulainen et al., 2013). Based on the findings in this thesis, such linear coupling metrics can only capture a small part of the response. Moreover, as these studies use one fixed periodic perturbation signal (to reduce the effect of noise), linear coherence is biased by the nonlinear distortions (Maki, 1986). Overall, linear coherence is not suitable to quantify the cortical evoked response or to make interpretations about the dynamics of the sensorimotor system. As an alternative, higher order cross-spectral coherence can be used to study nonlinear coupling (Shils et al., 1996, Yang et al., 2016a). Such an approach allows for the detection of nonlinear coupling. However, these coherence metrics create limited insight in dynamic behavior. To further investigate the nonlinear

dynamic relation between joint manipulation and evoked cortical response, a nonlinear system identification technique is required.

U.2 A nonparametric nonlinear model can describe the cortical evoked response substantially better than a linear model

The relation between joint manipulation and cortical evoked response could not be described using a nonparametric linear model (VAF: 10%), as established in Chapter 3. In search of a model which could better capture this relation, several parametric and nonparametric nonlinear modeling techniques were explored. The main advantage of a nonparametric nonlinear modeling approach, is that it requires little a priori knowledge or assumptions. The drawback is that often many parameters need to be estimated compared with parametric models.

A possible nonparametric nonlinear modeling approach is a Volterra series (Schetzen, 1980). A Volterra series is similar to a Taylor series, yet it includes dynamics. A disadvantage of estimating a Volterra series is that it requires many data, and the amount of data needed increases drastically for higher order Volterra kernels. Regularization can reduce this problem by incorporating some prior information about the system. Here, the regularization promotes correlation of kernel coefficients (i.e. a smooth kernel) and decay of the kernel (i.e. the models impulse response is finite) (Birpoutsoukis et al., 2017a). Note that the regularization is applied as a penalty, such that correlation and decay are encouraged but not imposed. Chapter 3 had revealed strong even nonlinear behavior and therefore a 2nd order (i.e. even) Volterra kernel was estimated to investigate the feasibility of the approach. An independent component analysis was applied to the data of Chapter 3 to obtain for each participant on one signal representing one cortical source, as opposed to a mix of multiple sources as seen on the EEG electrodes (Makeig et al., 1996b). Here, the component most associated with the perturbation signal was used for modeling. However, the approach could be applied to the signal of any component.

The nonlinear model estimated in Chapter 4 was able to explain a substantially larger portion of the evoked cortical response than a linear model (46% compared to 8%, respectively). The dynamics of the obtained 2nd order kernels were similar across all participants and revealed high-pass dynamics. These high-pass dynamics were linked to velocity sensitivity of the muscle spindles. This high-frequent behavior of the obtained models is associated with low correlation of the model parameters, even though there was a penalty encouraging smoothness of the kernel (which could be considered low-pass behavior). This reveals the strength of the regularization, which steers towards, but does not enforce certain behavior.

Several studies investigated the cortical evoked response due to transient joint manipulation (Mima et al., 1996, MacKinnon et al., 2000, Seiss et al., 2002, Campfens et al., 2015a). When varying amplitude of the transient perturbation while keeping velocity the same, very similar responses were evoked which differed mainly in duration and not in amplitude (Seiss et al., 2002, Campfens et al., 2015a). Exploring the cortical evoked response to stimuli with

different amplitude can also reveal nonlinear behavior. Similar responses when varying stimulus amplitude and not velocity, could be a sign of strong velocity sensitivity, which would be in line with the findings of this thesis. For both finger (Seiss et al., 2002) and wrist (Campfens et al., 2015a) manipulation, joint flexion and extension result in a very similar evoked response. Insensitivity to the sign of the input is common to an even nonlinear system (e.g. $y=u^2$), and is therefore in agreement with the findings based on continuous joint manipulation in this thesis.

To further strengthen the confidence in the modeled dynamics of the sensorimotor system, experiments with richer perturbation signals could be performed. By designing a multisine signal with a longer period (i.e. increase frequency resolution), more sinusoids can be accommodated. Such an experiment can reveal if there are dynamics in the system which are not being excited using the perturbation signal of Chapter 3 and 4. A pilot experiment using a richer perturbation signal was performed (see **Box 7.6**). From this experiment very similar

---

Box 7.6. Nonlinear model obtain using a richer perturbation signal.
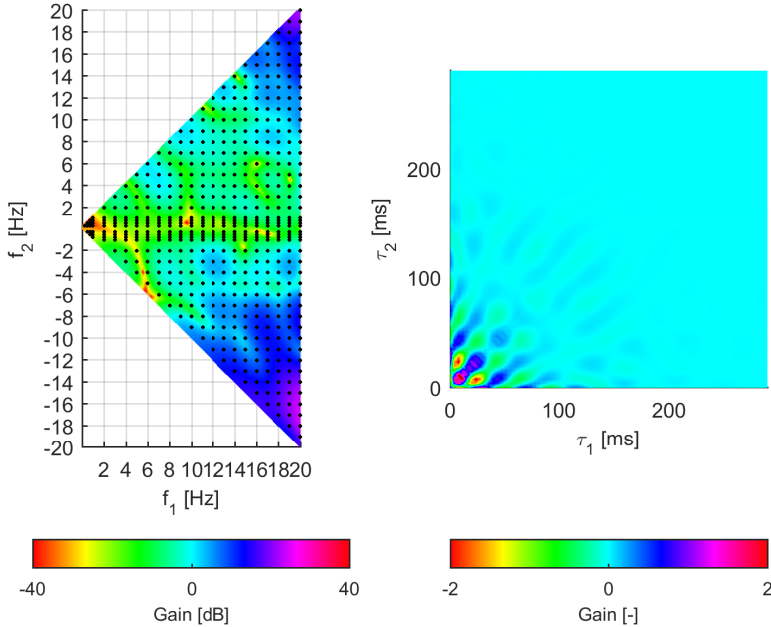
In an additional experiment with one young healthy participant a perturbation signal with a period of 4 s was used (Birpoutsoukis et al., 2017b). Excited frequencies included: 0.25, 0.5, 0.75, 1, 2, 3 ... 20 Hz (after 4 Hz, -20dB/dec). The same rms of 0.02 rad was used. The number of recorded periods was 105 and 7 different realizations were recorded (average noise level of 7%). Note that no distinction can be made between even and odd nonlinear contributions in the output using such a perturbation signal. Processing of the data was similar as in Chapter 4; however, here only a second order Volterra kernel was estimated. The VAF achieved in this experiment was around 45% on the validation data. **Left graph** shows the frequency domain representation of the obtained model; the obtained model is comparable to the models obtained in Chapter 4. **Right graph** shows the time domain representation of the same model. The decay is clearly visible in this graph.

---

results to those of Chapter 4 were obtained, further increasing the confidence in the approach and the interpretation given to the dynamics of the sensorimotor system.

S.1 Reduced contralateral evoked responses are associated with somatosensory impairment after stroke.

In the chronic phase after stroke (Chapter 5), the group of individuals with severe sensory impairment had significantly reduced responses compared with the group of unimpaired age-matched individuals, as assessed under passive conditions. Reduced responses were also found during recovery after stroke (Chapter 6) in the participants with severe sensory impairment. Interestingly, participants who regained sensory function, also showed an increase of evoked responses. Hence, functional neuroimaging using continuous joint manipulation can quantitatively inform on the status of the sensorimotor system.
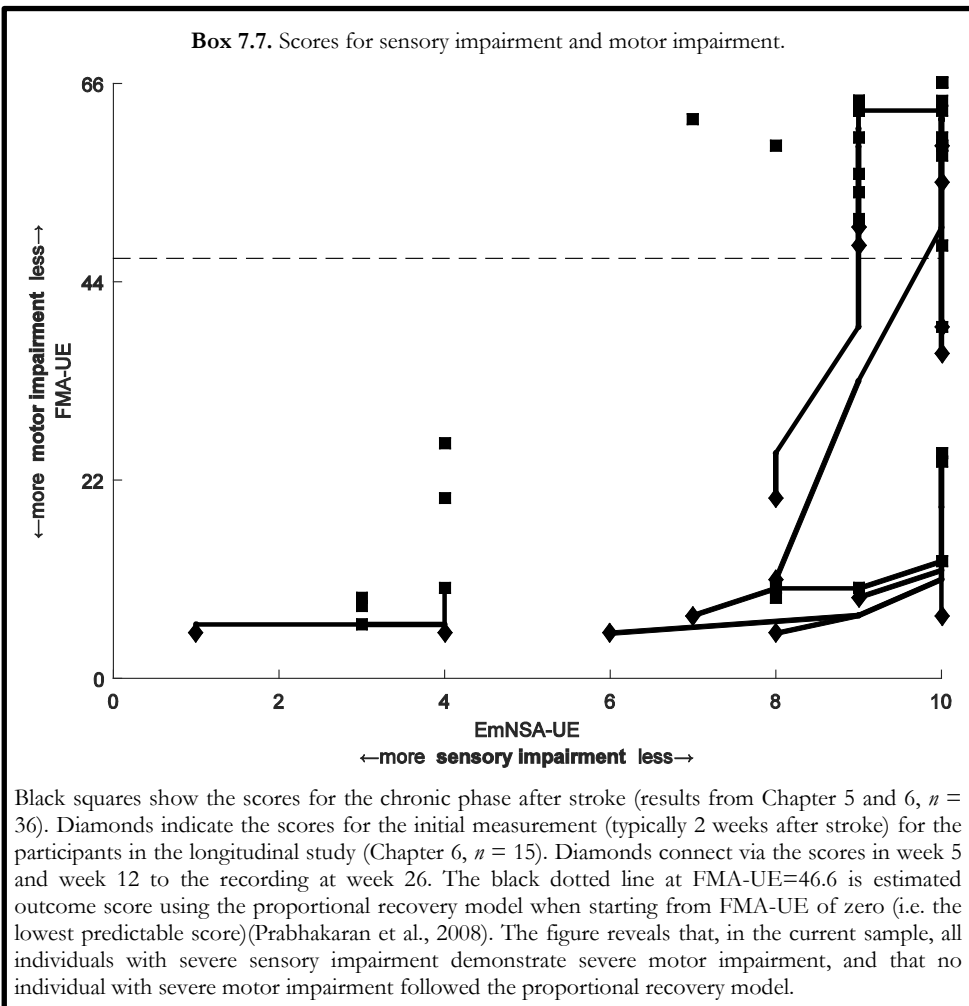
Existing models which predict motor outcome after stroke do so based on initial motor impairment (Prabhakaran et al., 2008, Nijland et al., 2010). The proportional recovery model (Prabhakaran et al., 2008) can predict motor outcome after stroke quite accurately; however, for stroke survivors with severe initial motor impairment (e.g. FMA-UE scores lower than 31), the recovery is much less predictable and outcome varies greatly (Byblow et al., 2015, Ward, 2015, Winters et al., 2015b), resulting in fitters and non-fitters to the model. The non-fitters are the individuals who do not demonstrate the expected (proportional) recovery. Limited recovery has been associated with severe initial motor impairment (Zarahn et al., 2011, Winters et al., 2015a), aphasia (Lazar et al., 2010) and visuospatial neglect (Winters et al., 2016c).

Based on the findings in this thesis it is hypothesized that there is also an association with sensory impairment: individuals with severe sensory impairment might not fit the proportional recovery model and thus not show the expected spontaneous recovery. Argumentation for this is found in the relation between motor impairment and sensory impairment for the participants in this thesis (see **Box 7.7**); there is no recovery of motor function in the absence of sensory function. The proposed hypothesis is further supported by another recent study, which did not find a strong correlation between clinically assessed somatosensory and motor impairments in the first week after stroke, in the chronic phase after stroke, or between the somatosensory impairment in the first week and the motor impairment in the chronic phase after stroke (Meyer et al., 2016a). Additionally, previous neuroimaging studies which attempted to predict motor outcome based on cortical responses evoked by electrical somatosensory stimulation only found an association between absence of the response and poor motor recovery (Feys et al., 2000, Rollnik, 2015); the characteristics of the evoked response (if present) did not aid prediction of motor outcome in a large cohort study with 449 stroke survivors (Rollnik, 2015). The lack of correlation between levels of sensory impairment (assessed clinically or using neuroimaging) and motor impairment supports the proposed hypothesis: sensory function is a prerequisite but no guarantee for motor recovery.

S.2 Ipsilateral responses are not enhanced when contralateral responses are reduced

For the evoked cortical signals recorded from unimpaired individuals, the highest SNR was always around the contralateral sensorimotor cortices. This finding is in line with previous literature on somatosensory evoked responses evoked by tactile stimulation of the hand (Snyder, 1992) and by wrist joint manipulation (Campfens et al., 2013), and is also expected based on where afferent fibers carrying proprioceptive and tactile information reach the cortex (Kandel et al., 2000).

This thesis specifically investigated if there is a disbalance in representation of somatosensory information between hemispheres after stroke, which was investigated using the lateralization index. Participants with severe sensory impairment demonstrated absent or reduced cortical evoked responses, resulting in an absence of lateralization; however, increased ipsilateral (i.e.

Box 7.7. Scores for sensory impairment and motor impairment.

Black squares show the scores for the chronic phase after stroke (results from Chapter 5 and 6, $n = 36$). Diamonds indicate the scores for the initial measurement (typically 2 weeks after stroke) for the participants in the longitudinal study (Chapter 6, $n = 15$). Diamonds connect via the scores in week 5 and week 12 to the recording at week 26. The black dotted line at FMA-UE=46.6 is estimated outcome score using the proportional recovery model when starting from FMA-UE of zero (i.e. the lowest predictable score)(Prabhakaran et al., 2008). The figure reveals that, in the current sample, all individuals with severe sensory impairment demonstrate severe motor impairment, and that no individual with severe motor impairment followed the proportional recovery model.

contralesional) responses were not found in the chronic phase after stroke (Chapter 5), nor during recovery after stroke (Chapter 6). All participants who suffered a stroke showed an evoked response around the contralateral sensorimotor cortices. One exception was found in a participant for whom most of the contralateral sensorimotor cortices were damaged as a consequence of the stroke. In agreement with existing literature, differences in source locations over time were small and no consistent shifts were observed. Any alterations to the evoked response were linked to changes in strength of the response and not in location.

Several studies have reported altered lateralization of voluntary motor drive after stroke, indicating a disbalance between activity in contralateral and ipsilateral hemisphere compared with unimpaired individuals. The mechanisms of this altered lateralization are not well understood (Buma et al., 2010, Rossiter et al., 2014), yet abnormal cortical lateralization of voluntary motor drive is a common finding which is also established in the Chapter 6. In the active conditions in Chapter 5 and 6, we studied voluntary motor drive while applying continuous joint manipulation. This allowed for quantifying cortical activity related to voluntary motor drive as well as the sensory representation of proprioceptive information by studying the cortical evoked response. No altered involvement of the ipsilateral hemisphere in processing proprioceptive information was found during recovery after stroke, suggesting that the unaffected hemisphere does not take over this role when processing in the affected hemisphere is reduced, possibly due to anatomical constraints. From the results in this thesis it is concluded that if there is return of sensory function it is associated with the return of function in the contralateral (i.e. ipsilesional) sensorimotor cortices. Thus, damage to the contralateral sensorimotor cortices is likely indicative of poor changes of sensory -and perhaps also- motor recovery.

Future directions

Further improving the model between wrist movement and cortical response
The modeling approach used in this thesis can explain approximately 46% of the observed data. As the noise level was estimated to be around 8%, there is another 46% of data which is currently unmodeled. A next step in investigating the dynamics between imposed wrist movement and evoked cortical response using nonparametric modeling techniques, would be to include a 4th order Volterra kernel. As the even frequency lines in Chapter 4 contained the largest portion of unmodeled data, the inclusion of higher order odd kernels will not yield a large increase of model performance. When including more Volterra kernels in the estimation, the amount of data needed for estimation increases. The experimental protocol used to obtained data presented in **Box 7.6** would be more suitable for this than the data used in Chapter 4, due to the extra information (i.e. more excited frequencies) in the perturbation signal. Experimental protocols which excite more frequencies in the region 10 to 20 Hz could also be explored, as it seems that most of the dynamics are within that region. Accurate execution of the perturbations at these higher frequencies cannot be guaranteed with the robotic manipulator used in this thesis and should be performed on a more capable manipulator (Schouten et al., 2006).

The nonparametric modeling approach created insights into the dynamics of the sensorimotor system, which could be used when moving towards a parametric model representation. Both the 1st order (linear) and 2nd order (nonlinear) nonparametric models obtained in Chapter 4 revealed strong high-pass behavior. Several studies used anesthesia to reveal that under passive conditions the cortical response evoked by joint manipulation is largely generated by the muscle spindles (Starr et al., 1981, Abbruzzese et al., 1985, Mima et al., 1996). Therefore, the observed high-pass behavior was linked to the velocity sensitivity of the muscle spindles, which is conveyed to the cortex via Ia afferent fibers. When developing a parametric model representation, a possibility would be to incorporate an existing model of the muscle spindles (Mileusnic et al., 2006). Furthermore, the obtained 2nd order kernels reveal that the nonlinear dynamics cannot be fully described by a single Hammerstein branch, as the off-diagonal elements in the 2nd order kernel are not zero (Westwick and Kearney, 2003). Several other guidelines for relating the Volterra kernels to cascades of various Wiener and Hammerstein structures exist (Westwick and Kearney, 2003). Before investigating this more deeply, it is important to obtain more confidence in the truncated Volterra series expansion by estimating multiple kernels (at least 1st and 2nd order) on data from experiments with richer and more informative perturbation signals.

To further increase insight in the dynamic relation between wrist movement and cortical evoked response anesthesia or microneurography can be considered. Anesthesia of selected mechanoreceptors (e.g. tactile sensors) could help identify the source of the cortical evoked response, as similarly done before in the studies mentioned in the previous paragraph. This approach allows the relation between proprioceptors and cortical response to be studied in isolation. Microneurography could be employed to add a measurement point in-between the wrist movement and the cortical evoked response, which allows the study of the dynamic relation between wrist movement and mechanoreceptors, and between mechanoreceptors and cortical evoked response separately. The advantage is that the dynamics of the mechanoreceptors can be estimated and modeled separately. Such measurements during joint manipulation are challenging due to the required precision in placing the electrodes combined with the movements of the tissue due to the manipulation (De Gooijer-van de Groep et al., 2011). Additionally, an experimental paradigm with separate tactile stimulation and joint manipulation could be employed to separate the cortical sources responsible for processing the respective somatosensory stimuli. Optimized multisine stimulation signals with for example different (non-integer multiple) fundamental frequencies would enable the separation of the temporal responses.

Identifying cortical areas involved in processing proprioceptive information
Cortical generators of responses evoked by joint manipulation are expected in part of the primary somatosensory cortex which processes proprioceptive input (Brodmann area 3a). Interestingly, several studies using transient joint manipulation reported a strong evoked responses originating from the contralateral primary motor cortex (Brodmann area 4) (MacKinnon et al., 2000, Seiss et al., 2002). In the literature it is not entirely clear which region generates the response; it is likely that both contralateral primary sensory and motor

cortex are involved in generating the response to a transient proprioceptive stimulus (Onishi et al., 2013), which could depend on movement parameters (Seiss et al., 2002). In this thesis a single dipole could explain most of the observed cortical response evoked by continuous joint manipulation. With the current experimental setup and analysis techniques it was not possible to differentiate between the two locations, as they are spaced only few millimeters apart. An increase in the number of electrodes combined with the use of signal-separation techniques (e.g. independent component analysis) can aid in distinguishing between these proximal cortical sources. Small differences were observed in source locations between the groups with different recovery patterns (see Chapter 6). It would be interesting to investigate if these differences facilitate distinguishing between individuals early after stroke.

Studying the cortical network involved in movement control

It would be of interest to investigate the network of cortical regions involved in sensory processing and how this network is altered after stroke (Grefkes and Fink, 2014). In this thesis, the strongest responses were obtained at the contralateral sensorimotor cortices. Similarly, previous studies on transient joint manipulation obtained a strong evoked response around the contralateral central sulcus for all their participants (MacKinnon et al., 2000, Seiss et al., 2002, Onishi et al., 2013). Some of these participants also had an identifiably evoked response in the contralateral supplementary motor area (SMA) and posterior parietal cortex (PPC), and in contralateral and ipsilateral secondary somatosensory cortices (Onishi et al., 2013). The independent component analysis performed in Chapter 2, 4, 5 and 6, revealed multiple cortical sources with a response associated with the perturbation. In all cases, the response located around the contralateral sensorimotor cortices was the response with the highest SNR. Interestingly, in many participants components were identified which could be associated with cortical areas such as SMA and PPC. A future step is to study the dynamic relation between the cortical regions involved in processing sensory information, and the planning and generation of motor commands. A multitude of linear and nonlinear connectivity measures exist, such as measures based on Granger causality (e.g. partial directed coherence), dynamic causal modeling and phase locking index. Further research will prove which techniques are suitable to study the connectivity between cortical areas specifically involved in generating evoked responses to continuous periodic perturbation. Combining functional connectivity measures with anatomical imaging methods such as diffusion tensor imaging (e.g. Fukushima et al., 2015), has the potential to uncover accurate maps of pathways conveying information related to feedback and feedforward control.

Studying the impaired sensorimotor system

Robotic joint manipulation under passive conditions can inform on the status of the somatosensory systems relevant to movement control, even in severely impaired individuals. As such, the focus in this thesis was on passive tasks. The results obtained from these passive tasks revealed that cortical evoked responses were associated with severe sensory impairments in Chapter 5 and 6, and that there was no increase in evoked responses in the ipsilateral hemisphere. Future efforts on modeling the relation between joint movement and cortical response, as well as uncovering the cortical networks involved in processing

proprioceptive information, could create insight into abnormal cortical activity during recovery after stroke. Modeling cortical evoked responses in patients and stroke survivors first requires further investigation in unimpaired individuals. The experimental protocols used in this thesis were quite long due to the large number of data being collected. By optimizing the joint manipulation signals and analysis techniques, more concise experiments can be designed to study the relevant aspects of the cortical evoked response, resulting in a smaller burden on impaired individuals.

Control tasks with an active component, such as performed in Chapter 3, 5 and 6, require higher mental and physical efforts. Studying cortical involvement in active movement control is challenging in a very interesting group of stroke survivors, i.e. individuals with initially severe motor impairments. To study the sensorimotor system under active conditions in participants who were mentally and physically able to sustain longer experiments, but who could not voluntarily flex their wrist, other experimental paradigms could be investigated. The use of a robotic joint manipulator for more proximal upper limb joints would allow to study cortical activity in individuals with more severe motor impairments, as proximal joints demonstrate faster return of function compared with distal joints (Colebatch and Gandevia, 1989). When thinking about the use of robotic joint manipulation for use in a clinical setting, a more distal joint is recorded more easily, as the required robotic manipulator could be much smaller.

Besides movement impairments associated with stroke, there exists a wide range of movement disorders, such as Parkinson's disease and many types of tremor. These disorders cause erroneous control and often have an unknown pathophysiology (Obeso et al., 2014, Smith et al., 2014b). Diagnosis of movement disorders can be hindered by the similarity of their symptoms (Benamer et al., 2000). By studying movement control in individuals with these disorders using experimental protocols such as presented and suggested in this thesis, we can increase our understanding of the associated pathophysiologies, with the aim of expediting diagnosis and ultimately improving treatment.

Applying the proposed techniques to other modalities

The approaches presented in this thesis for the quantification and modeling of the nonlinear sensorimotor system can be translated to other modalities. Linearity of the visual system was investigated by Herrmann (2001), who investigated presence of higher harmonics to stimulation with a single sinusoid. Modeling of the nonlinear relation between visual stimuli retinal response was undertaken by Victor and Shapley (1980). Current work on the visual system in the Leiden University Medical Centre investigates the relation between the evoked cortical response and neurological diseases such as migraine using a multisine approach (Perenboom et al., 2016). Similarly, a project within the recently started NeuroCIMT program (www.neurocimt.nl) identifies dynamic cortical relations within the auditory system, with the aim of reducing hearing impairments.

Concluding remarks

Stroke is the leading cause of acquired disability in the developed world (Feigin et al., 2014). Stroke incidence was estimated to be around 1.5 million in 2015 in Europe, which is associated with a large burden to society and economy (Wilkins et al., 2017). Reducing the impact of stroke can be achieved through prevention, improving acute treatments and improving post-stroke rehabilitation. Stroke is the leading preventable cause of disability and effective prevention methods should be explored (Frieden and Berwick, 2011). Major developments in the treatment of acute stroke, such as thrombolysis within six hours after onset, increases the fraction of stroke survivors and independence during activities of daily living (Wardlaw et al., 2014). In the sub-acute phase after stroke, spontaneous recovery is currently the largest contributor to reduction of impairments (Kwakkel et al., 2016); rehabilitation therapies can at present only account for 5 to 15% of observed improvement (Kwakkel et al., 2015, Winters et al., 2016a). Research into recovery mechanisms of stroke may lead to the development of more effective rehabilitation programs. Neuroimaging can facilitate this by investigating anatomical and functional changes inside the brain during recovery after stroke. The methodologies and insights presented in this thesis can hopefully be employed to deepen our understanding of the recovery mechanisms of stroke, with the ultimate goal of minimizing impairments and maximizing independence of stroke survivors.

References

References

Abbruzzese G, Berardelli A, Rothwell JC, Day BL, Marsden CD (1985) Cerebral potentials and electromyographic responses evoked by stretch of wrist muscles in man. Experimental Brain Research 58:544-551.

Adler J, Giabbiconi C-M, Müller MM (2009) Shift of attention to the body location of distracters is mediated by perceptual load in sustained somatosensory attention. Biological Psychology 81:77-85.

Ahn S, Ahn M, Cho H, Jun SC (2014) Achieving a hybrid brain–computer interface with tactile selective attention and motor imagery. Journal of neural engineering 11:066004.

Angelini L, De Tommaso M, Guido M, Hu K, Ivanov PC, Marinazzo D, Nardulli G, Nitti L, Pellicoro M, Pierro C (2004) Steady-state visual evoked potentials and phase synchronization in migraine patients. Physical review letters 93:038103.

Appenteng K, Prochazka A, Proske U, Wand P (1982) Effect of fusimotor stimulation on Ia discharge during shortening of cat soleus muscle at different speeds. J Physiol 329:509.

Ashworth B (1964) Preliminary trial of carisoprodol in multiple sclerosis. The practitioner 192:540.

Bai E-W, Cai Z, Dudley-Javorosk S, Shields RK (2009) Identification of a modified Wiener–Hammerstein system and its application in electrically stimulated paralyzed skeletal muscle modeling. Automatica 45:736-743.

Bardouille T, Picton T, Ross B (2010) Attention modulates beta oscillations during prolonged tactile stimulation. European Journal of Neuroscience 31:761-769.

Bardouille T, Ross B (2008) MEG imaging of sensorimotor areas using inter-trial coherence in vibrotactile steady-state responses. NeuroImage 42:323-331.

Bell AJ, Sejnowski TJ (1995) An information-maximization approach to blind separation and blind deconvolution. Neural computation 7:1129-1159.

Benamer HTS, Patterson J, Grosset DG, Booij J, de Bruin K, van Royen E, Speelman JD, Horstink MHIM, Sips HJWA, Dierckx RA, Versijpt J, Decoo D, Van Der Linden C, Hadley DM, Doder M, Lees AJ, Costa DC, Gacinovic S, Oertel WH, Pogarell O, Hoeffken H, Joseph K, Tatsch K, Schwarz J, Ries V (2000) Accurate differentiation of parkinsonism and essential tremor using visual assessment of [123I]-FP-CIT SPECT imaging: The [123I]-FP-CIT study group. Mov Disord 15:503-510.

Benjamin EJ, Blaha MJ, Chiuve SE, Cushman M, Das SR, Deo R, de Ferranti SD, Floyd J, Fornage M, Gillespie C, Isasi CR, Jiménez MC, Jordan LC, Judd SE, Lackland D, Lichtman JH, Lisabeth L, Liu S, Longenecker CT, Mackey RH, Matsushita K, Mozaffarian D, Mussolino ME, Nasir K, Neumar RW, Palaniappan L, Pandey DK, Thiagarajan RR, Reeves MJ, Ritchey M, Rodriguez CJ, Roth GA, Rosamond WD, Sasson C, Towfighi A, Tsao CW, Turner MB, Virani SS, Voeks JH, Willey JZ, Wilkins JT, Wu JH, Alger HM, Wong SS, Muntner P (2017) Heart Disease and Stroke Statistics—2017 Update: A Report From the American Heart Association. Circulation.

Bernhardt J, Borschmann K, Boyd L, Carmichael ST, Corbett D, Cramer SC, Hoffmann T, Kwakkel G, Savitz SI, Saposnik G (2016) Moving rehabilitation research forward: Developing consensus statements for rehabilitation and recovery research. International Journal of Stroke 11:454-458.

Birpoutsoukis G, Marconato A, Lataire J, Schoukens J (2017a) Regularized Nonparametric Volterra Kernel Estimation. Automatica (accepted for publication).

Birpoutsoukis G, Vlaar MP, Lataire J, Schoukens M, Schouten AC, Schoukens J, Van der Helm FCT (2017b) Volterra series model of the brain response to imposed wrist motion. In: 36th Benelux Meeting on Systems and Control.

Bolognini N, Russo C, Edwards DJ (2016) The sensory side of post-stroke motor rehabilitation. Restor Neurol Neurosci.

Breitwieser C, Kaiser V, Neuper C, Müller-Putz GR (2012) Stability and distribution of steady-state somatosensory evoked potentials elicited by vibro-tactile stimulation. Medical & biological engineering & computing 50:347-357.

Breitwieser C, Pokorny C, Neuper C, Muller-Putz G (2011) Somatosensory evoked potentials elicited by stimulating two fingers from one hand—Usable for BCI? In: Engineering in Medicine and Biology Society, EMBC, 2011 Annual International Conference of the IEEE, pp 6373-6376: IEEE.

Brenner CA, Krishnan GP, Vohs JL, Ahn W-Y, Hetrick WP, Morzorati SL, O'Donnell BF (2009) Steady state responses: electrophysiological assessment of sensory function in schizophrenia. Schizophrenia bulletin 35:1065-1077.

Briggs WL, Henson V (1995) The DFT: An Owner's Manual for the Discrete Fourier Transform.

Buch ER, Rizk S, Nicolo P, Cohen LG, Schnider A, Guggisberg AG (2016) Predicting motor improvement after stroke with clinical assessment and diffusion tensor imaging. Neurology 86:1924-1925.

Budd TW, Timora JR (2013) Steady state responses to temporally congruent and incongruent auditory and vibrotactile amplitude modulated stimulation. International Journal of Psychophysiology 89:419-432.

Buma F, Kwakkel G, Ramsey N (2013) Understanding upper limb recovery after stroke. Restorative neurology and neuroscience 31:707-722.

Buma FE, Lindeman E, Ramsey NF, Kwakkel G (2010) Functional neuroimaging studies of early upper limb recovery after stroke: a systematic review of the literature. Neurorehabilitation and neural repair.

Byblow WD, Stinear CM, Barber PA, Petoe MA, Ackerley SJ (2015) Proportional recovery after stroke depends on corticomotor integrity. Annals of neurology 78:848-859.

Campfens SF, Meskers CGM, Schouten AC, van Putten MJAM, Van der Kooij H (2015a) Stretch evoked potentials in healthy subjects and after stroke: a potential measure for proprioceptive sensorimotor function. IEEE Transactions on Neural Systems and Rehabilitation Engineering 23:643-654.

Campfens SF, Schouten AC, van Putten MJAM, van der Kooij H (2013) Quantifying connectivity via efferent and afferent pathways in motor control using coherence measures and joint position perturbations. Experimental brain research 228:141-153.

Campfens SF, Zandvliet SB, Meskers CG, Schouten AC, van Putten MJ, van der Kooij H (2015b) Poor motor function is associated with reduced sensory processing after stroke. Experimental brain research 233:1339-1349.

Canizales DL, Voisin JIA, Michon P-E, Roy M-A, Jackson PL (2013) The influence of visual perspective on the somatosensory steady-state response during pain observation. Frontiers in Human Neuroscience 7:849.

Capilla A, Pazo-Alvarez P, Darriba A, Campo P, Gross J (2011) Steady-state visual evoked potentials can be explained by temporal superposition of transient event-related responses. PLoS One 6:e14543.

Chang MC, Ahn SH, Cho YW, Son SM, Kwon YH, Lee MY, Byun WM, Jang SH (2009) The comparison of cortical activation patterns by active exercise, proprioceptive input,

References

and touch stimulation in the human brain: a functional MRI study. NeuroRehabilitation 25:87-92.

Chen T, Ohlsson H, Ljung L (2012) On the estimation of transfer functions, regularizations and Gaussian processes—revisited. Automatica 48:1525-1535.

Clementz BA, Keil A, Kissler J (2004) Aberrant brain dynamics in schizophrenia: delayed buildup and prolonged decay of the visual steady-state response. Cognitive brain research 18:121-129.

Colebatch JG, Gandevia S (1989) The distribution of muscular weakness in upper motor neuron lesions affecting the arm. Brain 112:749-763.

Connell LA, Lincoln N, Radford K (2008) Somatosensory impairment after stroke: frequency of different deficits and their recovery. Clinical Rehabilitation 22:758-767.

Connell LA, Tyson SF (2012) Clinical reality of measuring upper-limb ability in neurologic conditions: a systematic review. Archives of physical medicine and rehabilitation 93:221-228.

Coupar F, Pollock A, Rowe P, Weir C, Langhorne P (2012) Predictors of upper limb recovery after stroke: a systematic review and meta-analysis. Clinical rehabilitation 26:291-313.

Crago PE, Houk JC, Rymer WZ (1982) Sampling of total muscle force by tendon organs. Journal of neurophysiology 47:1069-1083.

Cramer SC (2008) Repairing the human brain after stroke: I. Mechanisms of spontaneous recovery. Annals of neurology 63:272-287.

Cruccu G, Aminoff MJ, Curio G, Guerit JM, Kakigi R, Mauguiere F, Rossini PM, Treede R-D, Garcia-Larrea L (2008) Recommendations for the clinical use of somatosensory-evoked potentials. Clinical neurophysiology 119:1705-1719.

Custead R, Oh H, Rosner AO, Barlow S (2015) Adaptation of the cortical somatosensory evoked potential following pulsed pneumatic stimulation of the lower face in adults. Brain research 1622:81-90.

De Gooijer-van de Groep K, Van Schelven L, Van der Kooij H, Oey L, Van der Helm FCT (2011) Comparison of multi-unit microneurography and model simulations of the muscle spindle. In: 3rd Dutch Biomedical Engineering Conference The Netherlands.

Delorme A, Makeig S (2004) EEGLAB: an open source toolbox for analysis of single-trial EEG dynamics including independent component analysis. Journal of neuroscience methods 134:9-21.

Dimitriou M (2014) Human Muscle Spindle Sensitivity Reflects the Balance of Activity between Antagonistic Muscles. The Journal of Neuroscience 34:13644-13655.

Dimyan MA, Cohen LG (2011) Neuroplasticity in the context of motor rehabilitation after stroke. Nature Reviews Neurology 7:76-85.

Dobkin BH (2005) Rehabilitation after stroke. New England Journal of Medicine 352:1677-1684.

Dukelow SP, Herter TM, Bagg SD, Scott SH (2012) The independence of deficits in position sense and visually guided reaching following stroke. Journal of neuroengineering and rehabilitation 9:72.

Dukelow SP, Herter TM, Moore KD, Demers MJ, Glasgow JI, Bagg SD, Norman KE, Scott SH (2010) Quantitative assessment of limb position sense following stroke. Neurorehabilitation and neural repair 24:178-187.

Elbert T, Pantev C, Wienbruch C, Rockstroh B, Taub E (1995) Increased cortical representation of the fingers of the left hand in string players. Science 270:305.

Espenhahn S, de Berker AO, van Wijk BC, Rossiter HE, Ward NS (2016) Movement-related beta oscillations show high intra-individual reliability. NeuroImage.

Faisal AA, Selen LP, Wolpert DM (2008) Noise in the nervous system. Nature reviews neuroscience 9:292-303.

Feigin VL, Forouzanfar MH, Krishnamurthi R, Mensah GA, Connor M, Bennett DA, Moran AE, Sacco RL, Anderson L, Truelsen T (2014) Global and regional burden of stroke during 1990–2010: findings from the Global Burden of Disease Study 2010. The Lancet 383:245-255.

Feys H, Van Hees J, Bruyninckx F, Mercelis R, De Weerdt W (2000) Value of somatosensory and motor evoked potentials in predicting arm recovery after a stroke. Journal of Neurology, Neurosurgery & Psychiatry 68:323-331.

Folstein MF, Robins LN, Helzer JE (1983) The mini-mental state examination. Archives of general psychiatry 40:812-812.

Forbes PA, Dakin CJ, Geers AM, Vlaar MP, Happee R, Siegmund GP, Schouten AC, Blouin J-S (2014) Electrical Vestibular Stimuli to Enhance Vestibulo-Motor Output and Improve Subject Comfort. PLoS ONE 9:e84385.

Forss N, Hari R, Salmelin R, Ahonen A, Hämäläinen M, Kajola M, Knuutila J, Simola J (1994a) Activation of the human posterior parietal cortex by median nerve stimulation. Experimental Brain Research 99:309-315.

Forss N, Salmelin R, Hari R (1994b) Comparison of somatosensory evoked fields to airpuff and electric stimuli. Electroencephalography and Clinical Neurophysiology/Evoked Potentials Section 92:510-517.

Franklin DW, Wolpert DM (2011) Computational mechanisms of sensorimotor control. Neuron 72:425-442.

Franzén O, Offenloch K (1969) Evoked response correlates of psychophysical magnitude estimates for tactile stimulation in man. Experimental brain research 8:1-18.

Frieden TR, Berwick DM (2011) The "Million Hearts" Initiative — Preventing Heart Attacks and Strokes. New England Journal of Medicine 365:e27.

Fugl-Meyer AR, Jääskö L, Leyman I, Olsson S, Steglind S (1974) The post-stroke hemiplegic patient. 1. a method for evaluation of physical performance. Scandinavian journal of rehabilitation medicine 7:13-31.

Fukushima M, Yamashita O, Knösche TR, Sato M-a (2015) MEG source reconstruction based on identification of directed source interactions on whole-brain anatomical networks. NeuroImage 105:408-427.

Giabbiconi CM, Dancer C, Zopf R, Gruber T, Müller MM (2004) Selective spatial attention to left or right hand flutter sensation modulates the steady-state somatosensory evoked potential. Cognitive brain research 20:58-66.

Giabbiconi CM, Trujillo-Barreto NJ, Gruber T, Müller MM (2007) Sustained spatial attention to vibration is mediated in primary somatosensory cortex. NeuroImage 35:255-262.

Goto Y, Taniwaki T, Yamashita K-i, Kinukawa N, Tobimatsu S (2003) Interhemispheric functional desynchronization in the human vibratory system. Brain Research 980:249-254.

Gramfort A, Papadopoulo T, Olivi E, Clerc M (2011) Forward Field Computation with OpenMEEG. Computational Intelligence and Neuroscience 2011:13.

Grefkes C, Fink GR (2014) Connectivity-based approaches in stroke and recovery of function. Lancet Neurol 13:206-216.

Gurari N, Drogos JM, Dewald JP (2017) Individuals with chronic hemiparetic stroke can correctly match forearm positions within a single arm. Clinical Neurophysiology 128:18-30.

References

Hasan Z (1983) A model of spindle afferent response to muscle stretch. Journal of Neurophysiology 49:989-1006.

Hashimoto I, Gatayama T, Yoshikawa K, Sasaki M, Nomura M (1992) Input-output relation of the somatosensory system for mechanical air-puff stimulation of the index finger in man. Experimental brain research 88:645-650.

Hayward KS, Schmidt J, Lohse KR, Peters S, Bernhardt J, Lannin NA, Boyd LA (2017) Are we armed with the right data? Pooled individual data review of biomarkers in people with severe upper limb impairment after stroke. NeuroImage: Clinical 13:310-319.

Herrmann CS (2001) Human EEG responses to 1–100 Hz flicker: resonance phenomena in visual cortex and their potential correlation to cognitive phenomena. Experimental brain research 137:346-353.

Holloway V, Gadian DG, Vargha-Khadem F, Porter DA, Boyd SG, Connelly A (2000) The reorganization of sensorimotor function in children after hemispherectomy. Brain 123:2432-2444.

Houk JC, Rymer WZ, Crago PE (1981) Dependence of dynamic response of spindle receptors on muscle length and velocity. Journal of Neurophysiology 46:143-166.

Hua K, Zhang J, Wakana S, Jiang H, Li X, Reich DS, Calabresi PA, Pekar JJ, van Zijl PC, Mori S (2008) Tract probability maps in stereotaxic spaces: analyses of white matter anatomy and tract-specific quantification. Neuroimage 39:336-347.

Huang M, Davis L, Aine C, Weisend M, Harrington D, Christner R, Stephen J, Edgar J, Herman M, Meyer J (2004) MEG response to median nerve stimulation correlates with recovery of sensory and motor function after stroke. Clinical neurophysiology 115:820-833.

Jamali S, Ross B (2012) Precise mapping of the somatotopic hand area using neuromagnetic steady-state responses. Brain research 1455:28-39.

Jamali S, Ross B (2013) Somatotopic finger mapping using MEG: Toward an optimal stimulation paradigm. Clinical Neurophysiology 124:1659-1670.

Jenkins WM, Merzenich MM (1987) Reorganization of neocortical representations after brain injury: a neurophysiological model of the bases of recovery from stroke. Progress in brain research 71:249-266.

Jenkinson M, Beckmann CF, Behrens TE, Woolrich MW, Smith SM (2012) Fsl. Neuroimage 62:782-790.

Johnson D, Jürgens R, Kornhuber HH (1980) Somatosensory-evoked potentials and vibration. Archiv für Psychiatrie und Nervenkrankheiten 228:101-107.

Jung P, Baumgärtner U, Bauermann T, Magerl W, Gawehn J, Stoeter P, Treede R-D (2003) Asymmetry in the human primary somatosensory cortex and handedness. NeuroImage 19:913-923.

Kandel E, Schwartz J, Jessell T (2000) Principles of Neural Science, Fourth Edition: McGraw-Hill Companies,Incorporated.

Kearney RE, Hunter IW (1990) System identification of human joint dynamics. Critical reviews in biomedical engineering 18:55-87.

Kearney RE, Stein RB, Parameswaran L (1997) Identification of intrinsic and reflex contributions to human ankle stiffness dynamics. IEEE Transactions on Biomedical Engineering 44:493-504.

Kelly EF, Folger SE (1999) EEG evidence of stimulus-directed response dynamics in human somatosensory cortex. Brain research 815:326-336.

Kim B, Winstein C (2017) Can Neurological Biomarkers of Brain Impairment Be Used to Predict Poststroke Motor Recovery? A Systematic Review. Neurorehabilitation and Neural Repair 31:3-24.

Krakauer JW (2005) Arm function after stroke: from physiology to recovery: Copyright© 2005 by Thieme Medical Publishers, Inc., 333 Seventh Avenue, New York, NY 10001, USA.

Krakauer JW (2006) Motor learning: its relevance to stroke recovery and neurorehabilitation. Current opinion in neurology 19:84-90.

Krakauer JW, Marshall RS (2015) The proportional recovery rule for stroke revisited. Annals of neurology 78:845-847.

Kwakkel G, Kollen B (2013) Predicting activities after stroke: what is clinically relevant? International Journal of Stroke 8:25-32.

Kwakkel G, Kollen BJ, van der Grond J, Prevo AJH (2003) Probability of Regaining Dexterity in the Flaccid Upper Limb. Impact of Severity of Paresis and Time Since Onset in Acute Stroke 34:2181-2186.

Kwakkel G, Veerbeek JM, Wegen EE, Wolf SL (2015) Constraint-induced movement therapy after stroke. Lancet Neurol 14.

Kwakkel G, Winters C, Van Wegen EE, Nijland RH, Van Kuijk AA, Visser-Meily A, De Groot J, De Vlugt E, Arendzen JH, Geurts AC (2016) Effects of unilateral upper limb training in two distinct prognostic groups early after stroke: the EXPLICIT-stroke randomized clinical trial. Neurorehabilitation and neural repair 30:804-816.

Laaksonen K, Kirveskari E, Mäkelä JP, Kaste M, Mustanoja S, Nummenmaa L, Tatlisumak T, Forss N (2012) Effect of afferent input on motor cortex excitability during stroke recovery. Clinical Neurophysiology 123:2429-2436.

Langdon AJ, Boonstra TW, Breakspear M (2011) Multi-frequency phase locking in human somatosensory cortex. Progress in biophysics and molecular biology 105:58-66.

Langhorne P, Bernhardt J, Kwakkel G (2011) Stroke rehabilitation. The Lancet 377:1693-1702.

Langhorne P, Coupar F, Pollock A (2009) Motor recovery after stroke: a systematic review. Lancet Neurol 8.

Lataire J, Chen T (2016) Transfer function and transient estimation by Gaussian process regression in the frequency domain. Automatica 72:217-229.

Lataire J, Pintelon R (2009) Estimating a nonparametric colored-noise model for linear slowly time-varying systems. Instrumentation and Measurement, IEEE Transactions on 58:1535-1545.

Lazar RM, Minzer B, Antoniello D, Festa JR, Krakauer JW, Marshall RS (2010) Improvement in aphasia scores after stroke is well predicted by initial severity. Stroke 41.

Lazar RM, Speizer AE, Festa JR, Krakauer JW, Marshall RS (2008) Variability in language recovery after first-time stroke. Journal of Neurology, Neurosurgery & Psychiatry 79:530-534.

Lewis GN, MacKinnon CD, Trumbower R, Perreault EJ (2010) Co-contraction modifies the stretch reflex elicited in muscles shortened by a joint perturbation. Experimental brain research 207:39-48.

Lin Y-Y, Kajola M (2003) Neuromagnetic somatosensory responses to natural moving tactile stimulation. The Canadian Journal of Neurological Sciences 30:31-35.

Loubinoux I, Dechaumont-Palacin S, Castel-Lacanal E, De Boissezon X, Marque P, Pariente J, Albucher J-F, Berry I, Chollet F (2007) Prognostic value of FMRI in recovery of hand function in subcortical stroke patients. Cerebral cortex 17:2980-2987.

Ludvig D, Cathers I, Kearney RE (2007) Voluntary modulation of human stretch reflexes. Experimental brain research 183:201-213.

References

Lyle RC (1981) A performance test for assessment of upper limb function in physical rehabilitation treatment and research. International Journal of Rehabilitation Research 4:483-492.

MacKinnon CD, Verrier MC, Tatton WG (2000) Motor cortical potentials precede long-latency EMG activity evoked by imposed displacements of the human wrist. Experimental Brain Research 131:477-490.

Makeig S, Bell AJ, Jung T-P, Sejnowski TJ (1996a) Independent Component Analysis of Electroencephalographic Data. Advances in Neural Information Processing Systems 8:145-151.

Makeig S, Bell AJ, Jung T-P, Sejnowski TJ (1996b) Independent component analysis of electroencephalographic data. Advances in neural information processing systems 145-151.

Maki BE (1986) Interpretation of the coherence function when using pseudorandom inputs to identify nonlinear systems. IEEE transactions on biomedical engineering 8:775-779.

Marcoux L-A, Michon P-E, Lemelin S, Voisin JA, Vachon-Presseau E, Jackson PL (2014) Feeling but not caring: Empathic alteration in narcissistic men with high psychopathic traits. Psychiatry Research: Neuroimaging 224:341-348.

Matthews PB (1964) Muscle spindles and their motor control. Physiological reviews 44:219-288.

Matthews PB (1991) The human stretch reflex and the motor cortex. Trends in neurosciences 14:87-91.

Mendis S (2013) Stroke disability and rehabilitation of stroke: World Health Organization perspective. International Journal of Stroke 8:3-4.

Meskers CG, Schouten AC, de Groot JH, de Vlugt E, van Hilten BJ, Van der Helm FC, Arendzen HJ (2009) Muscle weakness and lack of reflex gain adaptation predominate during post-stroke posture control of the wrist. Journal of neuroengineering and rehabilitation 6:1.

Meyer S, De Bruyn N, Krumlinde-Sundholm L, Peeters A, Feys H, Thijs V, Verheyden G (2016a) Associations Between Sensorimotor Impairments in the Upper Limb at 1 Week and 6 Months After Stroke. Journal of Neurologic Physical Therapy 40:186-195.

Meyer S, De Bruyn N, Lafosse C, Van Dijk M, Michielsen M, Thijs L, Truyens V, Oostra K, Krumlinde-Sundholm L, Peeters A (2016b) Somatosensory impairments in the upper limb poststroke: distribution and association with motor function and visuospatial neglect. Neurorehabilitation and neural repair 30:731-742.

Mileusnic MP, Brown IE, Lan N, Loeb GE (2006) Mathematical models of proprioceptors. I. Control and transduction in the muscle spindle. Journal of neurophysiology 96:1772-1788.

Miller LC, Dewald JP (2012) Involuntary paretic wrist/finger flexion forces and EMG increase with shoulder abduction load in individuals with chronic stroke. Clinical Neurophysiology 123:1216-1225.

Mima T, Terada K, Maekawa M, Nagamine T, Ikeda A, Shibasaki H (1996) Somatosensory evoked potentials following proprioceptive stimulation of finger in man. Experimental Brain Research 111:233-245.

Mirbagheri M, Barbeau H, Kearney R (2000) Intrinsic and reflex contributions to human ankle stiffness: variation with activation level and position. Experimental Brain Research 135:423-436.

Mirbagheri M, Barbeau H, Ladouceur M, Kearney R (2001) Intrinsic and reflex stiffness in normal and spastic, spinal cord injured subjects. Experimental Brain Research 141:446-459.

Mortimer JA, Webster DD (1979) Evidence for a quantitative association between EMG stretch responses and parkinsonian rigidity. Brain research 162:169-173.

Mugge W, Abbink DA, Schouten AC, Dewald JPA, van der Helm FCT (2010) A rigorous model of reflex function indicates that position and force feedback are flexibly tuned to position and force tasks. Experimental brain research 200:325-340.

Mugge W, Schouten AC, van Hilten JJ, van der Helm FC (2016) Impaired inhibitory force feedback in fixed dystonia. IEEE Transactions on Neural Systems and Rehabilitation Engineering 24:475-484.

Müller-Putz G, Scherer R, Neuper C, Pfurtscheller G (2006) Steady-state somatosensory evoked potentials: suitable brain signals for brain-computer interfaces? Neural Systems and Rehabilitation Engineering, IEEE Transactions on 14:30-37.

Müller G, Neuper C, Pfurtscheller G (2001) " Resonance-like" frequencies of sensorimotor areas evoked by repetitive tactile stimulation. Biomedizinische Technik Biomedical engineering 46:186-190.

Müller G, Neuper C, Rupp R, Keinrath C, Gerner H, Pfurtscheller G (2003) Event-related beta EEG changes during wrist movements induced by functional electrical stimulation of forearm muscles in man. Neuroscience letters 340:143-147.

Murphy TH, Corbett D (2009) Plasticity during stroke recovery: from synapse to behaviour. Nat Rev Neurosci 10:861-872.

Nangini C, Ross B, Tam F, Graham S (2006) Magnetoencephalographic study of vibrotactile evoked transient and steady-state responses in human somatosensory cortex. Neuroimage 33:252-262.

Narici L, Portin K, Salmelin R, Hari R (1998) Responsiveness of human cortical activity to rhythmical stimulation: a three-modality, whole-cortex neuromagnetic investigation. NeuroImage 7:209-223.

Nijland R, Kwakkel G, Bakers J, van Wegen E (2011) Constraint-induced movement therapy for the upper paretic limb in acute or sub-acute stroke: a systematic review. International Journal of Stroke 6:425-433.

Nijland RH, Wegen EE, Harmeling-van der Wel BC, Kwakkel G (2010) Presence of finger extension and shoulder abduction within 72 hours after stroke predicts functional recovery: early prediction of functional outcome after stroke: the EPOS cohort study. Stroke 41.

Nudo RJ, Milliken G, Jenkins WM, Merzenich MM (1996) Use-dependent alterations of movement representations in primary motor cortex of adult squirrel monkeys. Journal of Neuroscience 16:785-807.

Nudo RJ, Milliken GW (1996) Reorganization of movement representations in primary motor cortex following focal ischemic infarcts in adult squirrel monkeys. Journal of Neurophysiology 75:2144-2149.

Obeso JA, Rodriguez-Oroz MC, Stamelou M, Bhatia KP, Burn DJ (2014) The expanding universe of disorders of the basal ganglia. The Lancet 384:523-531.

Oldfield RC (1971) The assessment and analysis of handedness: The Edinburgh inventory. Neuropsychologia 9:97-113.

Onishi H, Oyama M, Soma T, Kubo M, Kirimoto H, Murakami H, Kameyama S (2010) Neuromagnetic activation of primary and secondary somatosensory cortex

following tactile-on and tactile-off stimulation. Clinical Neurophysiology 121:588-593.

Onishi H, Sugawara K, Yamashiro K, Sato D, Suzuki M, Kirimoto H, Tamaki H, Murakami H, Kameyama S (2013) Neuromagnetic activation following active and passive finger movements. Brain and Behavior 3:178-192.

Oostenveld R, Fries P, Maris E, Schoffelen J-M (2011) FieldTrip: Open Source Software for Advanced Analysis of MEG, EEG, and Invasive Electrophysiological Data. Computational Intelligence and Neuroscience 2011:9.

Oostenveld R, Praamstra P (2001) The five percent electrode system for high-resolution EEG and ERP measurements. Clinical Neurophysiology 112:713-719.

Pang CY, Mueller MM (2014) Test–retest reliability of concurrently recorded steady-state and somatosensory evoked potentials in somatosensory sustained spatial attention. Biological psychology 100:86-96.

Park C-h, Kou N, Ward NS (2016) The contribution of lesion location to upper limb deficit after stroke. Journal of Neurology, Neurosurgery & Psychiatry 87:1283-1286.

Parkkonen E, Laaksonen K, Piitulainen H, Parkkonen L, Forss N (2015) Modulation of the~ 20‐Hz motor‐cortex rhythm to passive movement and tactile stimulation. Brain and behavior 5.

Patel N, Jankovic J, Hallett M (2014) Sensory aspects of movement disorders. The Lancet Neurology 13:100-112.

Penny WD, Friston KJ, Ashburner JT, Kiebel SJ, Nichols TE (2011) Statistical parametric mapping: the analysis of functional brain images: Academic press.

Perenboom MJ, Yang Y, van der Helm FC, Ferrari MD, Schouten AC, Tolner EA (2016) Nonlinearity of the visual system assessed by cross-frequency phase coupling. In: International Pharmaco-EEG society, p 86 Nijmegen, The Netherlands.

Perreault EJ, Chen K, Trumbower RD, Lewis G (2008) Interactions With Compliant Loads Alter Stretch Reflex Gains But Not Intermuscular Coordination. Journal of Neurophysiology 99:2101-2113.

Pfurtscheller G, Da Silva FL (1999) Event-related EEG/MEG synchronization and desynchronization: basic principles. Clinical neurophysiology 110:1842-1857.

Piitulainen H, Bourguignon M, De Tiège X, Hari R, Jousmäki V (2013) Corticokinematic coherence during active and passive finger movements. Neuroscience 238:361-370.

Pillonetto G, Quang MH, Chiuso A (2011) A new kernel-based approach for nonlinear system identification. IEEE Transactions on Automatic Control 56:2825-2840.

Pintelon R, Schoukens J (2012) System Identification: A Frequency Domain Approach: Wiley.

Pisano F, Miscio G, Del Conte C, Pianca D, Candeloro E, Colombo R (2000) Quantitative measures of spasticity in post-stroke patients. Clinical Neurophysiology 111:1015-1022.

Pokorny C, Breitwieser C, Muller-Putz GR (2014) A Tactile Stimulation Device for EEG Measurements in Clinical Use. Biomedical Circuits and Systems, IEEE Transactions on 8:305-312.

Porcu E, Keitel C, Müller MM (2013) Concurrent visual and tactile steady-state evoked potentials index allocation of inter-modal attention: A frequency-tagging study. Neuroscience Letters 556:113-117.

Prabhakaran S, Zarahn E, Riley C, Speizer A, Chong JY, Lazar RM, Marshall RS, Krakauer JW (2008) Inter-individual variability in the capacity for motor recovery after ischemic stroke. Neurorehabilitation and neural repair 22:64-71.

Prochazka A, Gorassini M (1998) Models of ensemble firing of muscle spindle afferents recorded during normal locomotion in cats. J Physiol 507 (Pt 1):277-291.

Prochazka A, Hulliger M, Zangger P, Appenteng K (1985) 'Fusimotor set': new evidence for α-independent control of γ-motoneurones during movement in the awake cat. Brain research 339:136-140.

Pruszynski JA, Kurtzer I, Scott SH (2011) The long-latency reflex is composed of at least two functionally independent processes. Journal of neurophysiology 106:449-459.

Pruszynski JA, Scott SH (2012) Optimal feedback control and the long-latency stretch response. Experimental brain research 218:341-359.

Pujol J, Deus J, Losilla JM, Capdevila A (1999) Cerebral lateralization of language in normal left-handed people studied by functional MRI. Neurology 52:1038-1038.

Pustina D, Coslett HB, Turkeltaub PE, Tustison N, Schwartz MF, Avants B (2016) Automated segmentation of chronic stroke lesions using LINDA: Lesion identification with neighborhood data analysis. Human Brain Mapping 37:1405-1421.

Raghavan P (2015) Upper Limb Motor Impairment After Stroke. Physical medicine and rehabilitation clinics of North America 26:599-610.

Raimondo F, Kamienkowski JE, Sigman M, Slezak DF (2012) CUDAICA: GPU optimization of infomax-ICA EEG analysis. Computational intelligence and neuroscience 2012:2.

Rasmussen CE, Williams CK (2006) Gaussian processes for machine learning. 2006. The MIT Press, Cambridge, MA, USA 38:715-719.

Regan D (1966) Some characteristics of average steady-state and transient responses evoked by modulated light. Electroencephalography and Clinical Neurophysiology 20:238-248.

Reinkensmeyer DJ, Burdet E, Casadio M, Krakauer JW, Kwakkel G, Lang CE, Swinnen SP, Ward NS, Schweighofer N (2016) Computational neurorehabilitation: modeling plasticity and learning to predict recovery. Journal of neuroengineering and rehabilitation 13:1.

Reis J, Swayne OB, Vandermeeren Y, Camus M, Dimyan MA, Harris-Love M, Perez MA, Ragert P, Rothwell JC, Cohen LG (2008) Contribution of transcranial magnetic stimulation to the understanding of cortical mechanisms involved in motor control. J Physiol 586:325-351.

Risuleo RS, Bottegal G, Hjalmarsson H (2015) A kernel-based approach to Hammerstein system identication. IFAC-PapersOnLine 48:1011-1016.

Ritter P, Moosmann M, Villringer A (2009) Rolandic alpha and beta EEG rhythms' strengths are inversely related to fMRI-BOLD signal in primary somatosensory and motor cortex. Human brain mapping 30:1168-1187.

Roiha K, Kirveskari E, Kaste M, Mustanoja S, Mäkelä JP, Salonen O, Tatlisumak T, Forss N (2011) Reorganization of the primary somatosensory cortex during stroke recovery. Clinical neurophysiology 122:339-345.

Rollnik JD (2015) May clinical neurophysiology help to predict the recovery of neurological early rehabilitation patients? BMC neurology 15:239.

Ross B, Jamali S, Miyazaki T, Fujioka T (2013) Synchronization of beta and gamma oscillations in the somatosensory evoked neuromagnetic steady-state response. Experimental Neurology 245:40-51.

References

Rossini PM, Tecchio F, Pizzella V, Lupoi D, Cassetta E, Paqualetti P (2001) Interhemispheric differences of sensory hand areas after monohemispheric stroke: MEG/MRI integrative study. Neuroimage 14:474-485.

Rossiter HE, Boudrias M-H, Ward NS (2014) Do movement-related beta oscillations change after stroke? Journal of neurophysiology 112:2053-2058.

Sainburg RL, Ghilardi MF, Poizner H, Ghez C (1995) Control of limb dynamics in normal subjects and patients without proprioception. Journal of neurophysiology 73:820-835.

Schaefer M, Mühlnickel W, Grüsser SM, Flor H (2002) Reproducibility and Stability of Neuroelectric Source Imaging in Primary Somatosensory Cortex. Brain Topography 14:179-189.

Schetzen M (1980) The Volterra and Wiener theories of nonlinear systems.

Schoukens J, Pintelon R, Rolain Y (2012) Mastering System Identification in 100 Exercises: Wiley.

Schoukens J, Vaes M, Pintelon R (2016) Linear System Identification in a Nonlinear Setting: Nonparametric Analysis of the Nonlinear Distortions and Their Impact on the Best Linear Approximation. IEEE Control Systems 36:38-69.

Schouten AC (2004) Proprioceptive reflexes and neurological disorders.

Schouten AC, de Vlught E, Van der Helm FCT (2004) Quantification of spinal reflexes in neurological disorders. In: Systems, Man and Cybernetics, 2004 IEEE International Conference on, vol. 3, pp 2492-2499 vol.2493.

Schouten AC, de Vlugt E, van Hilten JB, van der Helm FC (2006) Design of a torque-controlled manipulator to analyse the admittance of the wrist joint. Journal of neuroscience methods 154:134-141.

Schouten AC, de Vlugt E, van Hilten JJB, Van der Helm FCT (2008a) Quantifying Proprioceptive Reflexes During Position Control of the Human Arm. Biomedical Engineering, IEEE Transactions on 55:311-321.

Schouten AC, Mugge W, van der Helm FCT (2008b) NMClab, a model to assess the contributions of muscle visco-elasticity and afferent feedback to joint dynamics. Journal of biomechanics 41:1659-1667.

Schwerin S, Dewald JP, Haztl M, Jovanovich S, Nickeas M, MacKinnon C (2008) Ipsilateral versus contralateral cortical motor projections to a shoulder adductor in chronic hemiparetic stroke: implications for the expression of arm synergies. Exp Brain Res 185:509-519.

Scott SH (2012) The computational and neural basis of voluntary motor control and planning. Trends in cognitive sciences 16:541-549.

Scott SH (2016) A functional taxonomy of bottom-up sensory feedback processing for motor actions. Trends in Neurosciences 39:512-526.

Seiss E, Hesse CW, Drane S, Oostenveld R, Wing AM, Praamstra P (2002) Proprioception-Related Evoked Potentials: Origin and Sensitivity to Movement Parameters. NeuroImage 17:461-468.

Serrien DJ, Strens LH, Cassidy MJ, Thompson AJ, Brown P (2004) Functional significance of the ipsilateral hemisphere during movement of the affected hand after stroke. Experimental neurology 190:425-432.

Severens M, Farquhar J, Desain P, Duysens J, Gielen C (2010) Transient and steady-state responses to mechanical stimulation of different fingers reveal interactions based on lateral inhibition. Clinical Neurophysiology 121:2090-2096.

Severens M, Farquhar J, Duysens J, Desain P (2013) A multi-signature brain–computer interface: use of transient and steady-state responses. Journal of neural engineering 10:026005.

Shils J, Litt M, Skolnick B, Stecker M (1996) Bispectral analysis of visual interactions in humans. Electroencephalography and clinical neurophysiology 98:113-125.

Simo L, Botzer L, Ghez C, Scheidt RA (2014) A robotic test of proprioception within the hemiparetic arm post-stroke. Journal of NeuroEngineering and Rehabilitation 11:77.

Smith DJ, Varghese LA, Stepp CE, Guenther FH (2014a) Comparison of steady-state visual and somatosensory evoked potentials for brain-computer interface control. Conference proceedings: Engineering in Medicine and Biology Society (EMBC) 2014:1234-1237.

Smith Y, Galvan A, Ellender TJ, Doig N, Villalba RM, Huerta-Ocampo I, Wichmann T, Bolam JP (2014b) The thalamostriatal system in normal and diseased states. Frontiers in Systems Neuroscience 8:5.

Snyder AZ (1992) Steady-state vibration evoked potentials: description of technique and characterization of responses. Electroencephalography and Clinical Neurophysiology/Evoked potentials Section 84:257-268.

Spitzer B, Blankenburg F (2011) Stimulus-dependent EEG activity reflects internal updating of tactile working memory in humans. Proceedings of the National Academy of Sciences 108:8444-8449.

Spitzer B, Wacker E, Blankenburg F (2010) Oscillatory correlates of vibrotactile frequency processing in human working memory. The Journal of Neuroscience 30:4496-4502.

Stapells DR, Linden D, Suffield JB, Hamel G, Picton TW (1984) Human auditory steady state potentials. Ear and hearing 5:105-113.

Starr A, McKeon B, Skuse N, Burke D (1981) Cerebral potentials evoked by muscle stretch in man. Brain 104:149-166.

Stinear C (2010) Prediction of recovery of motor function after stroke. The Lancet Neurology 9:1228-1232.

Stolk-Hornsveld F, Crow J, Hendriks E, Van Der Baan R, Harmeling-Van der Wel B (2006) The Erasmus MC modifications to the (revised) Nottingham Sensory Assessment: a reliable somatosensory assessment measure for patients with intracranial disorders. Clinical rehabilitation 20:160-172.

Tacchino G, Gandolla M, Coelli S, Barbieri R, Pedrocchi A, Bianchi AM (2016) EEG Analysis During Active and Assisted Repetitive Movements: Evidence for Differences in Neural Engagement. IEEE Transactions on Neural Systems and Rehabilitation Engineering PP:1-1.

Teale P, Pasko B, Collins D, Rojas D, Reite M (2013) Somatosensory timing deficits in schizophrenia. Psychiatry Research: Neuroimaging 212:73-78.

Tecchio F, Zappasodi F, Tombini M, Oliviero A, Pasqualetti P, Vernieri F, Ercolani M, Pizzella V, Rossini PM (2006) Brain plasticity in recovery from stroke: an MEG assessment. Neuroimage 32:1326-1334.

Teng F, Chen Y, Choong AM, Gustafson S, Reichley C, Lawhead P, Waddell D (2011) Square or sine: Finding a waveform with high success rate of eliciting SSVEP. Computational intelligence and neuroscience 2011:2.

Tibshirani R (1996) Regression shrinkage and selection via the lasso. Journal of the Royal Statistical Society Series B (Methodological) 58:267-288.

Timora JR, Budd TW (2013) Dissociation of psychophysical and EEG steady-state response measures of cross-modal temporal correspondence for amplitude modulated

acoustic and vibrotactile stimulation. International Journal of Psychophysiology 89:433-443.

Tobimatsu S, Zhang YM, Kato M (1999) Steady-state vibration somatosensory evoked potentials: physiological characteristics and tuning function. Clinical neurophysiology 110:1953-1958.

Tobimatsu S, Zhang YM, Suga R, Kato M (2000) Differential temporal coding of the vibratory sense in the hand and foot in man. Clinical neurophysiology 111:398-404.

Tombari D, Loubinoux I, Pariente J, Gerdelat A, Albucher J-F, Tardy J, Cassol E, Chollet F (2004) A longitudinal fMRI study: in recovering and then in clinically stable sub-cortical stroke patients. Neuroimage 23:827-839.

Truelsen T, Piechowski-Jóźwiak B, Bonita R, Mathers C, Bogousslavsky J, Boysen G (2006) Stroke incidence and prevalence in Europe: a review of available data. European journal of neurology 13:581-598.

Vakorin VA, Ross B, Krakovska O, Bardouille T, Cheyne D, McIntosh AR (2010) Complexity analysis of source activity underlying the neuromagnetic somatosensory steady-state response. NeuroImage 51:83-90.

van der Kooij H, van Asseldonk E, van der Helm FC (2005) Comparison of different methods to identify and quantify balance control. Journal of neuroscience methods 145:175-203.

van Drunen P, Maaswinkel E, van der Helm FCT, van Dieeen JH, Happee R (2013) Identifying intrinsic and reflexive contributions to low-back stabilization. Journal of biomechanics 46:1440-1446.

Van Wijk B, Beek P, Daffertshofer A (2012) Differential modulations of ipsilateral and contralateral beta (de) synchronization during unimanual force production. European Journal of Neuroscience 36:2088-2097.

Veerbeek JM, Kwakkel G, van Wegen EE, Ket JC, Heymans MW (2011) Early prediction of outcome of activities of daily living after stroke a systematic review. Stroke 42:1482-1488.

Veerbeek JM, van Wegen E, van Peppen R, van der Wees PJ, Hendriks E, Rietberg M, Kwakkel G (2014) What is the evidence for physical therapy poststroke? A systematic review and meta-analysis. PloS one 9:e87987.

Victor J, Shapley R (1980) A method of nonlinear analysis in the frequency domain. Biophysical Journal 29:459-483.

Vlaar MP, Solis-Escalante T, Dewald JPA, van Wegen EEH, Schouten AC, Kwakkel G, van der Helm FCT (2017a) Quantification of task-dependent cortical activation evoked by robotic continuous wrist joint manipulation in chronic hemiparetic stroke. Journal of NeuroEngineering and Rehabilitation 14:30.

Vlaar MP, Solis-Escalante T, Vardy AN, Van der Helm FCT, Schouten AC (2017b) Quantifying Nonlinear Contributions to Cortical Responses Evoked by Continuous Wrist Manipulation. IEEE Transactions on Neural Systems and Rehabilitation Engineering 25:481-491.

Vlaar MP, van der Helm FCT, Schouten AC (2015) Frequency Domain Characterization of the Somatosensory Steady State Response in Electroencephalography. In: 17th IFAC Symposium on System Identification SYSID 2015, vol. 48, pp 1391-1396 Beijing, China.

Voisin JI, Rodrigues EC, Hétu S, Jackson PL, Vargas CD, Malouin F, Chapman CE, Mercier C (2011a) Modulation of the response to a somatosensory stimulation of the hand during the observation of manual actions. Experimental brain research 208:11-19.

Voisin JIA, Marcoux L-A, Canizales DL, Mercier C, Jackson PL (2011b) I Am Touched by Your Pain: Limb-Specific Modulation of the Cortical Response to a Tactile Stimulation During Pain Observation. The Journal of Pain 12:1182-1189.

Ward N (2011) Assessment of cortical reorganisation for hand function after stroke. J Physiol 589:5625-5632.

Ward NS (2015) Does neuroimaging help to deliver better recovery of movement after stroke? Curr Opin Neurol 28:323-329.

Wardlaw JM, Murray V, Berge E, del Zoppo GJ (2014) Thrombolysis for acute ischaemic stroke. The Cochrane Library.

Weinberg H, Johnson B, Cohen P, Crisp D, Robertson A (1989) Functional imaging of brain responses to repetitive sensory stimulation: sources estimated from EEG and SPECT. Brain topography 2:171-180.

Welch P (1967) The use of fast Fourier transform for the estimation of power spectra: a method based on time averaging over short, modified periodograms. IEEE Transactions on audio and electroacoustics 15:70-73.

Welniarz Q, Dusart I, Gallea C, Roze E (2015) One hand clapping: lateralization of motor control. Frontiers in neuroanatomy 9.

Westwick DT, Kearney RE (2000) Identification of a Hammerstein model of the stretch reflex EMG using separable least squares. In: Proceedings of the 22nd Annual International Conference of the IEEE Engineering in Medicine and Biology Society (Cat No00CH37143), vol. 3, pp 1901-1904 vol.1903.

Westwick DT, Kearney RE (2003) Identification of nonlinear physiological systems: John Wiley & Sons.

Wikström H, Roine RO, Aronen HJ, Salonen O, Sinkkonen J, Ilmoniemi RJ, Huttunen J (2000) Specific changes in somatosensory evoked magnetic fields during recovery from sensorimotor stroke. Annals of neurology 47:353-360.

Wilkins E, Wilson L, Wickramasinghe K, Bhatnagar P, Leal J, Luengo-Fernandez R, Burns R, Rayner M, Townsend N (2017) European Cardiovascular Disease Statistics 2017. Brussels: European Heart Network.

Winters C, Heymans MW, van Wegen EEH, Kwakkel G (2016a) How to design clinical rehabilitation trials for the upper paretic limb early post stroke? Trials 17:468.

Winters C, Kwakkel G, Nijland R, van Wegen E, consortium E-s (2016b) When does return of voluntary finger extension occur post-stroke? A prospective cohort study. PloS one 11:e0160528.

Winters C, van Wegen EE, Daffertshofer A, Kwakkel G (2016c) Generalizability of the Maximum Proportional Recovery Rule to Visuospatial Neglect Early Poststroke. Neurorehabilitation and Neural Repair 31:334-342.

Winters C, Wegen EE, Daffertshofer A, Kwakkel G (2015a) Generalizability of the Proportional Recovery Model for the upper extremity after an ischemic stroke. Neurorehabil Neural Repair 29.

Winters C, Wegen EEHv, Daffertshofer A, Kwakkel G (2015b) Generalizability of the Proportional Recovery Model for the Upper Extremity After an Ischemic Stroke. Neurorehabilitation and Neural Repair 29:614-622.

Winward CE, Halligan PW, Wade DT (1999) Current practice and clinical relevance of somatosensory assessment after stroke. Clinical rehabilitation 13:48-55.

Witham CL, Riddle CN, Baker MR, Baker SN (2011) Contributions of descending and ascending pathways to corticomuscular coherence in humans. J Physiol 589:3789-3800.

References

Yang Y, Schouten AC, Solis-Escalante T, Van der Helm FCT (2015) Probing the Nonlinearity in Neural Systems Using Cross-frequency Coherence Framework. 17th IFAC Symposium on System Identifiction.

Yang Y, Solis-Escalante T, van der Helm FC, Schouten AC (2016a) A generalized coherence framework for detecting and characterizing nonlinear interactions in the nervous system. IEEE Transactions on Biomedical Engineering 63:2629-2637.

Yang Y, Solis-Escalante T, Yao J, Daffertshofer A, Schouten AC, van der Helm FC (2016b) A General Approach for Quantifying Nonlinear Connectivity in the Nervous System Based on Phase Coupling. International Journal of Neural Systems 26:1550031.

Yao N, Qiao H, Shu N, Wang Z, Chen D, Wu L, Deng X, Xu Y (2013) Cortex mapping of ipsilateral somatosensory area following anatomical hemispherectomy: a MEG study. Brain and Development 35:331-339.

Zarahn E, Alon L, Ryan SL, Lazar RM, Vry M-S, Weiller C, Marshall RS, Krakauer JW (2011) Prediction of motor recovery using initial impairment and fMRI 48 h poststroke. Cerebral Cortex 21:2712-2721.

Summary

Cortical damage after a stroke often affects movement control, resulting in impairments such as paresis and synergies. Although some recover, most stroke survivors are left with reduced function of the upper limb, which has a severe impact on their activities of daily living. People who have suffered a stroke demonstrate heterogeneous impairments due to large variability in lesion location and extent; thus, rehabilitation should be tailored to each individual. Design and evaluation of rehabilitation programs requires a thorough understanding of the healthy and impaired sensorimotor system. Impairments to the motor system have been extensively investigated. On the contrary, the sensory aspects of impaired motor control have received less attention. This thesis intends to characterize the relation between somatosensory information from the periphery and the corresponding cortical responses using electroencephalography (EEG).

Throughout this thesis, a robotic manipulator is used to apply stimulation to the wrist joint. Joint manipulation elicits a response from the mechanoreceptors in the periphery which, via the spinal cord, arrives in the cortex. When applied continuously, such stimulation evokes a steady state response (SSR) in the cortex, which can be measured using EEG. Previous studies reported a cortical response with power at frequencies that were not in the stimulation signal, indicating nonlinear behavior. The goal of Chapter 2 is to characterize the cortical response evoked by continuous wrist manipulation, and establishes the type of system identification tools that can be used to study the relation between applied stimulus and evoked response. Continuous joint manipulation using a multisine signal (i.e. the sum of several sinusoids) was applied to unimpaired individuals, to investigate the properties of the SSR in the frequency domain. The results showed a response in the contralateral sensorimotor cortex at the stimulated frequencies, yet with more power at their even harmonics, indicating substantial nonlinear behavior. Chapter 2 concludes that the SSR evoked by continuous joint manipulation is nonlinear; however, shows no time-variant behavior or subharmonics, allowing for the application of a broad range of (non)linear system identification tools.

Even though the selection of analysis techniques depends on the linearity of the system under study, the importance of nonlinear contributions to evoked cortical responses has not been formally addressed. The goal of Chapter 3 is to quantify the nonlinear contributions to the cortical evoked response. Multisine stimulation signals elicited a periodic cortical response and enabled assessment of nonlinear contributions to the response. Wrist dynamics (relation

between joint angle and torque) were successfully linearized, explaining 99% of the recorded response. In contrast, the cortical evoked response revealed a highly nonlinear relation; most power (~80%) occurred at non-stimulated frequencies. Moreover, only 10% of the response could be explained using a nonparametric linear model. These results indicate that the recorded evoked cortical responses are governed by nonlinearities and that linear methods do not suffice when describing the relation between mechanical stimulus and cortical response. The characteristics of this relationship are further explored in Chapter 4.

The goal of Chapter 4 is to obtain a nonparametric nonlinear dynamic model, which can consistently explain the recorded cortical response requiring little a priori assumptions about model structure. Wrist joint manipulation was applied in ten unimpaired participants during which their cortical activity was recorded and modeled using a truncated Volterra series. The obtained models explain 46% of the cortical response, thereby demonstrating the relevance of nonlinear modeling. The high similarity of the obtained models across participants indicates that the models reveal common characteristics of the underlying system. The models show predominantly high-pass behavior, suggesting that velocity-related information originating from the muscle spindles governs the cortical response. Chapter 4 concludes that the nonlinear modeling approach using a truncated Volterra series with regularization provides a quantitative way of investigating the sensorimotor system, offering insight into the underlying physiology.

Stroke is a leading cause of long-term disability in the developed world: cortical damage after stroke can drastically impair sensory and motor function of the upper limb, affecting the execution of activities of daily living and quality of life. The goal of Chapter 5 is to assess the integrity of the somatosensory system in individuals with chronic hemiparetic stroke with different levels of sensory impairment. Continuous robotic joint manipulation was applied during a passive and active task, defined as 'relaxed wrist' and 'maintaining 20% maximum wrist flexion', respectively. The evoked cortical responses in the EEG were quantified using the power in the averaged responses and their signal-to-noise ratio. Thirty individuals with chronic hemiparetic stroke and ten unimpaired individuals without stroke participated in this study. Participants with stroke were classified as having severe, mild, or no sensory impairment, based on clinical assessment. Under passive conditions, wrist manipulation resulted in contralateral cortical responses in unimpaired and chronic stroke participants with mild and no sensory impairment. In participants with severe sensory impairment the cortical responses were strongly reduced in amplitude, which related to anatomical damage. Under active conditions, participants with mild sensory impairment showed reduced responses compared with the passive condition, whereas unimpaired and chronic stroke participants without sensory impairment did not show this reduction. Robotic continuous joint manipulation enables studying somatosensory cortical evoked responses during the execution of meaningful upper limb control tasks. This particular approach allows the quantitative assessment of the integrity of sensory pathways; in the context of movement control this provides additional information required to develop more effective neurorehabilitation therapies.

Prediction of recovery of upper limb function in stroke survivors is important for stroke management, yet is challenging in individuals with severe initial impairments. The understanding of stroke recovery and accuracy of prediction may be enhanced by using functional neuroimaging to measure cortical mechanisms of neurological recovery (i.e. neuroplasticity). Chapter 6 presents preliminary results of a protocol that tracks time-dependent neuroplasticity from the subacute to the chronic phase after stroke, focusing on the sensorimotor system. Cortical activity of hemiparetic stroke survivors was recorded at four fixed time points during recovery after stroke using EEG. Participants performed passive and active wrist control tasks with the affected wrist, as in Chapter 5. The intensity and location of the response evoked by the robotic joint manipulation were studied. Preliminary results are presented for the fifteen participants who completed the four recording sessions. Eleven unimpaired participants performed the same protocol. Cortical responses evoked by joint manipulation were less strong in participants with severe sensory impairment and increased over time in participants who regained sensory function. The cortical sources generating the evoked responses were in all participants with intact contralateral primary sensorimotor cortices located within this region (all participants except one). No altered balance between contralateral and ipsilateral cortical evoked responses was observed under passive and active conditions. Recovery of sensory function was associated with return of responses to the contralateral hemisphere; we observed no compensatory mechanism for processing sensory information involving the ipsilateral hemisphere. Sensory information is essential to movement control and the results suggest that severe sensory impairment hinders recovery of motor function after stroke.

The overall objective of this thesis is to enhance the understanding of the sensorimotor system in both unimpaired individuals and individuals who have suffered a stroke. Cortical responses evoked by joint manipulation contain information about the functioning of the sensorimotor system. This thesis concludes that multisine stimulation signals evoke a cortical response that is rich in information. The evoked cortical response is periodic with the applied joint manipulation and is highly nonlinear: over 80% of the power in the response originates from nonlinear behavior. A nonparametric nonlinear model describes 46% of the cortical evoked response, a substantial improvement compared with the 8% described by a linear model. After stroke, the intensity of contralateral evoked responses is associated with somatosensory impairment, and ipsilateral responses are not enhanced when contralateral responses are reduced. The methodologies and insights presented in this thesis can be employed to deepen our understanding of the recovery mechanisms of stroke, with the ultimate goal of minimizing impairments and maximizing independence of stroke survivors.

Samenvatting

Hersenschade na een beroerte tast vaak bewegingssturing aan, wat resulteert in beperkingen zoals parese en synergiën. Hoewel sommigen volledig herstellen, houdt het merendeel van de personen die een beroerte hebben gehad beperkingen aan de bovenste ledematen, wat een negatieve invloed heeft op hun dagelijkse activiteiten. Mensen die een beroerte hebben gehad hebben heterogene beperkingen door de grote variabiliteit in de locatie en omvang van de laesie, waardoor rehabilitatietherapie op elk individu worden aangepast. Het ontwikkelen en evalueren van rehabilitatietherapieën vereist een gedegen inzicht in het gezonde en aangedane sensorische-motorische systeem. Beperkingen van het motorisch systeem na een beroerte zijn uitvoerig bestudeerd. De invloed van sensorische beperkingen op bewegingssturing heeft echter minder aandacht gekregen. Dit proefschrift wil de relatie tussen somatosensorische informatie uit het perifere zenuwstelsel en de bijbehorende corticale responsen kwantificeren met behulp van elektro-encefalografie (EEG).

In dit proefschrift wordt een gerobotiseerde gewrichtsmanipulator gebruikt om het polsgewricht te stimuleren. Gewrichtsmanipulatie wekt een respons op van de mechanoreceptoren in het perifere zenuwstelsel, die via het ruggenmerg in de cortex terechtkomt. Als een dergelijke stimulus continu aangeboden wordt, wekt deze een steady state respons (SSR) op in de cortex, welke gemeten kan worden met EEG. Verschillende studies hebben een corticale respons gerapporteerd met vermogen op frequenties die niet in het stimulatiesignaal aanwezig waren, wat wijst op niet-lineair gedrag. Het doel van Hoofdstuk 2 is het karakteriseren van de corticale respons opgewekt door continue pols manipulatie en vast te stellen welke systeemidentificatietechnieken gebruikt kunnen worden om de relatie tussen aangeboden stimulus en opgewekte respons te bestuderen. Continue gewrichtsmanipulatie met behulp van een multisinus-signaal (d.w.z. de som van meerdere sinusoïden) werd toegepast op personen zonder beperkingen om de eigenschappen van de SSR in het frequentiedomein te onderzoeken. De resultaten laten een respons zien in de contralaterale sensorische-motorische cortex op de gestimuleerde frequenties, maar met meer vermogen op hun even hogere harmonischen, wat aanzienlijk niet-lineair gedrag aangeeft. De conclusie is dat de SSR opgewekt door continue gewrichtsmanipulatie niet-lineair is, maar geen tijdvariant gedrag of subharmonischen laat zien, waardoor de toepassing van een groot aantal (niet)-lineaire systeemidentificatietechnieken mogelijk is.

Hoewel de keuze voor een analysetechniek afhangt van de lineariteit van het onderzochte systeem, is het belang van niet-lineaire bijdragen aan de opgewekte corticale respons niet

formeel onderzocht. Het doel van Hoofdstuk 3 is het kwantificeren van deze niet-lineaire bijdragen aan de opgewekte corticale respons. Multisinus-stimulatiesignalen wekten een periodieke corticale respons op en maakten het mogelijk om de niet-lineaire bijdragen aan de respons te bestuderen in tien personen zonder beperkingen. De mechanische dynamica van de pols (de relatie tussen gewrichtshoek en gewrichtsmoment) kon succesvol worden gelineariseerd, waarbij 99% van de respons verklaard kan worden. Daarentegen onthulde de opgewekte corticale respons een zeer niet-lineaire relatie; het meeste vermogen (~80%) werd gevonden op niet-gestimuleerde frequenties. Bovendien kan slechts 10% van de respons worden verklaard door een niet-parametrisch lineair model. Deze resultaten wijzen erop dat de opgenomen corticale responsen worden overheerst door niet-lineariteiten en dat lineaire methoden niet volstaan bij het beschrijven van de relatie tussen mechanische stimulus en corticale respons. De kenmerken van deze relatie worden verder onderzocht in Hoofdstuk 4.

Het doel van hoofdstuk 4 is het verkrijgen van een niet-parametrisch niet-lineair dynamisch model dat de opgenomen corticale respons consistent kan beschrijven en daarbij weinig veronderstellingen over de modelstructuur vereist. Polsgewrichtsmanipulatie werd toegepast bij tien personen zonder beperkingen waarbij hun corticale activiteit werd gemeten met EEG en gemodelleerd met behulp van een Volterra-serie. De verkregen modellen verklaren 46% van de corticale respons, waarmee de relevantie van het schatten van niet-lineaire modellen wordt aangetoond. De grote gelijkenis van de verkregen modellen voor de verschillende personen geeft aan dat de modellen gemeenschappelijke kenmerken van het onderliggende fysiologische systeem onthullen. De modellen tonen hoog-doorlaat gedrag, wat suggereert dat snelheid-gerelateerde informatie afkomstig van de spierspoeltjes een groot deel van de corticale respons bepaalt. De niet-lineaire modelleerbenadering met behulp van een Volterra-serie met regularisatie geeft een kwantitatieve manier om het sensorische-motorische systeem te bestuderen en biedt inzicht in de onderliggende fysiologie.

Beroertes zijn een belangrijke oorzaak van langdurige beperkingen in de ontwikkelde landen: corticale schade na beroerte kan de sensorische en motorische functie van de bovenste ledematen drastisch verminderen, hetgeen de uitvoering van dagelijkse activiteiten vermoeilijkt en levenskwaliteit negatief beïnvloedt. Het doel van Hoofdstuk 5 is het vaststellen van de integriteit van het somatosensorische systeem bij personen in de chronische fase na een hemiparetische beroerte met verschillende niveaus van sensorische beperkingen. Continue gewrichtsmanipulatie werd toegepast tijdens een passieve en actieve taak, respectievelijk gedefinieerd als 'ontspannen pols' en '20% van maximale pols flexie'. De opgewekte corticale responsen in het EEG werden gekwantificeerd met behulp van het vermogen in de gemiddelde responsen en hun signaal-ruisverhouding. Dertig personen in de chronische fase na een hemiparetische beroerte en tien personen zonder beperkingen namen deel aan deze studie. Deelnemers met een beroerte werden geclassificeerd als hebbende ernstige, milde of geen sensorische beperkingen, op basis van een klinische beoordeling. Onder passieve condities resulteerde polsmanipulatie in contralaterale corticale responsen bij deelnemers zonder beperkingen en deelnemers met milde en geen sensorische beperkingen na een beroerte. Bij deelnemers met ernstige sensorische beperkingen waren de corticale

responsen sterk verlaagd in amplitude, wat gerelateerd was aan anatomische schade. Onder actieve condities lieten deelnemers met milde sensorische beperkingen verminderde responsen zien in vergelijking met de passieve conditie, terwijl deelnemers zonder beperkingen en deelnemers zonder sensorische beperkingen na een beroerte deze reductie niet lieten zien. Continue gewrichtsmanipulatie maakt het mogelijk om somatosensorische corticale responsen te bestuderen tijdens de uitvoering van betekenisvolle taken met de bovenste ledematen. Met behulp van een deze specifieke aanpak is het mogelijk om de integriteit van de sensorische paden kwantitatief te beoordelen. Dit biedt belangrijke aanvullende informatie over bewegingssturing, welke nodig is om effectievere rehabilitatietherapieën te ontwikkelen.

Het voorspellen van herstel van functie in de bovenste ledematen bij personen die een beroerte hebben gehad is belangrijk voor het opstellen van een behandelplan, maar is complex bij personen met ernstige initiële beperkingen. Begrip van herstel na een beroerte en nauwkeurigheid van voorspelling kan worden verbeterd door functionele hersenmetingen om corticale mechanismen van neurologisch herstel te meten (d.w.z. neuroplasticiteit). Hoofdstuk 6 presenteert de voorlopige resultaten van een protocol dat het verloop van neuroplasticiteit bestudeert van de subacute tot de chronische fase na een beroerte en dat zich richt op het sensorische-motorische systeem. Corticale activiteit van personen die een hemiparetische beroerte hebben gehad werd gemeten op vier vaste tijdspunten tijdens herstel met behulp van EEG. Deelnemers hebben passieve en actieve bewegingssturingstaken uitgevoerd met de aangedane pols zoals in Hoofdstuk 5. De intensiteit en de locatie van de responsen opgewekt in de cortex door polsgewrichtmanipulatie werden onderzocht. Voorlopige resultaten werden gepresenteerd voor vijftien deelnemers die de vier opnamesessies hebben afgerond. Elf deelnemers zonder beperkingen hebben hetzelfde protocol uitgevoerd. Door gewrichtsmanipulatie opgewekte corticale responsen waren minder sterk bij deelnemers met een ernstige sensorische beperking en namen mettertijd toe bij deelnemers bij wie sensorische functie terugkeerde. De corticale bronnen die de opgewekte responsen genereerden waren in alle deelnemers met intacte contralaterale primaire sensorische-motorische cortex in dit deel van de cortex (alle deelnemers behalve één). Er werd geen veranderde balans waargenomen tussen contralaterale en ipsilaterale corticale responsen onder passieve en actieve omstandigheden. Herstel van de sensorische functie ging gepaard met terugkeer van responsen in de contralaterale hemisfeer. Er werd ook geen compenserend mechanisme gevonden voor het verwerken van sensorische informatie waarbij de ipsilaterale hemisfeer betrokken was. Sensorische informatie is essentieel voor bewegingssturing en deze resultaten suggereren dat ernstige sensorische beperkingen het herstel van de motorfunctie na beroerte verhinderen.

Het algemene doel van dit proefschrift is om het begrip van het sensorische-motorische systeem te verbeteren bij personen zonder beperkingen en personen die een beroerte hebben gehad. Corticale responsen die door gewrichtsmanipulatie worden opgewekt bevatten informatie over het functioneren van het sensorische-motorische systeem. Er wordt geconcludeerd dat multisinus-stimulatiesignalen een corticale respons veroorzaken die rijk is

aan informatie. De opgewekte corticale respons is periodiek met de toegepaste gewrichtsmanipulatie en is zeer niet-lineair: meer dan 80% van het vermogen in de respons komt voort uit niet-lineair gedrag. Een niet-parametrisch niet-lineair model kan 46% van de corticale respons beschrijven, wat aanzienlijk beter is dan de 8% beschreven door een lineair model. Na een beroerte is de intensiteit van contralaterale responsen verbonden met somatosensorische beperkingen. Ipsilaterale responsen worden niet sterker wanneer contralaterale responsen verminderd zijn door anatomische schade. De methodologieën en inzichten die in dit proefschrift worden gepresenteerd, kunnen worden gebruikt om ons begrip van de herstelmechanismen na een beroerte te verbeteren, om daarmee de onafhankelijkheid van mensen die een beroerte hebben gehad te maximaliseren.

List of publications

Journal articles

Vlaar, M.P., Birpoutsoukis, G., Lataire, J., Schoukens, M., Schouten, A.C., Schoukens, J., and Van der Helm, F.C.T (2017), Modeling the nonlinear cortical response in EEG evoked by continuous wrist joint manipulation. *IEEE Transactions on Neural Systems and Rehabilitation Engineering 2017, accepted*

Vlaar, M.P., Solis-Escalante, T., Dewald, J.P.A., Van Wegen, E.E.H., Schouten, A.C., Kwakkel, G., and Van der Helm, F.C.T (2017), Quantification of task-dependent cortical activation evoked by robotic continuous wrist joint manipulation in chronic hemiparetic stroke. *Journal of NeuroEngineering and Rehabilitation*, 14(1), 30.

Vlaar, M.P., Solis-Escalante, T., Vardy, A.N., Van der Helm, F.C.T., and Schouten, A.C. (2016). Quantifying nonlinear contributions to cortical responses evoked by continuous wrist manipulation. *IEEE Transactions on Neural Systems and Rehabilitation Engineering 2017, 25(5), 481-491*

Vlaar, M.P., Mugge, W., Groot, P.F.C., Sharifi, S., Bour, L.J., Van der Helm, F.C.T, Van Rootselaar, A.F., and Schouten, A.C. (2016). Targeted brain activation using an MR-compatible wrist torque measurement device and isometric motor tasks during functional magnetic resonance imaging. *Magnetic Resonance Imaging*, 34(6), 795-802.

Forbes, P.A., Dakin, C.J., Geers, A.M., **Vlaar, M.P.**, Happee, R., Siegmund, G.P., Schouten, A.C., and Blouin, J.S. (2014). Electrical vestibular stimuli to enhance vestibulo-motor output and improve subject comfort. *PloS one*, 9(1), e84385.

Conference articles

Vlaar, M.P., Van der Helm, F.C.T., and Schouten, A.C. (2015). Frequency domain characterization of the somatosensory steady state response in electroencephalography. *IFAC Symposium on System Identification*, China, 48(28), 1391-1396.

Vlaar, M.P. and Schouten, A.C. (2015). System identification for human motion control. *IEEE Instrumentation and Measurement Technology Conference (I2MTC)*, Italy, 600-605.

Curriculum Vitae

1985   Born in Rheden, the Netherlands

2010   B.Sc. Mechanical engineering at Delft University of Technology

Minor: Biomedical Engineering

2012   M.Sc. Biomedical Engineering at Delft University of Technology

Specialization: Biomechatronics

Thesis: Targeted Brain Activation Using Isometric Motor Tasks During Functional Magnetic Resonance Imaging

2012-2017   Ph. D. research at Delft University of Technology

The 4D-EEG Project: A New Tool to Investigate the Spatial and Temporal Activity Patterns in the Brain

Collaboration between Delft University of Technology, VU Medical Centre, VU University Amsterdam and Northwestern University

https://www.linkedin.com/in/martijn-vlaar-834b7432/